Crashworthy Hydrogen-Powered Aircraft

Retrofit Preliminary Design

Master of Science Thesis

Yi-Hsiu Wu

Delft University of Technology

TU Delft

Crashworthy Hydrogen-Powered Aircraft

Retrofit Preliminary Design

by

Yi-Hsiu Wu

Student Number: 5518695

Committee:	Dr. Ing. S.G.P. Castro
	Dr.ir. R.C. Alderliesten
	Dr. F. Oliviero
Supervisor:	Dr. Ing. S.G.P. Castro, TU Delft
Duration:	15/09/2023 - 4/07/2024
Faculty:	Faculty of Aerospace Engineering, Delft

Cover:	Airbus ZEROe turbofan concept art, available at https://www.airbus.com/en/innovation/low-carbon-aviation/hydrogen/zeroe
Style:	TU Delft Report Style, with modifications by Daan Zwaneveld

TU Delft

Preface

I would like to express my gratitude to my supervisor, Professor Saullo G. P. Castro, for his guidance and patience, as well as to PhD candidate Shreyas Anand for his invaluable assistance. I am also thankful to every friend I made during my three years in Delft for their academic and emotional support throughout my thesis and my time at TU Delft in general. Additionally, I want to extend my appreciation to Professor Pai Chen Guan for his motivating words.

A special thank you goes to my family, who not only stood by me for three years but also travelled to the Netherlands to share this amazing experience with me.

Lastly, I would like to honour my father, who passed away 14 years ago.

Yi-Hsiu Wu
Delft, August 2024

Acknowledgements

This research is conducted within the research and innovation programme Luchtvaart in Transitie, which is co-funded by the Netherlands National Growth Fund and in part by the European Union. It is part of the "Hydrogen Aircraft Powertrain and Storage Systems (HAPSS)" project, and part of The CrashProof Knowledge Centre (CrashProofLab) [1].

Abstract

Design methodologies for retrofitting are devised, and the retrofitted fuselage configuration designs were developed and tested for crashworthiness using finite element analysis in this thesis. These retrofits aimed to install hydrogen tanks within the fuselage, contributing to an efficient transition of the aerospace sector towards hydrogen-powered aviation.

Liquid hydrogen is chosen as the fuel source for hydrogen tanks due to its high density compared to other forms of hydrogen storage. However, storing the same amount of energy as traditional fuel still requires four times as much volume. Therefore, installing hydrogen tanks within the fuselage is necessary due to the low volumetric density and the relatively high flammability of liquid hydrogen. The retrofits were carried out on a typical fuselage, the most common tube and wing aircraft section.

The chosen aircraft type was the single-aisle/short-haul aircraft, and the typical section designed for was the F28. The designs aimed to maximize the fuel capacity within the fuselage, ensuring the retrofitted aircraft could achieve the maximum range. The design methodology was based on practical packing solutions commonly used in the logistics sector to transport as much fuel volume as possible within the constraints imposed by the available volume. This approach is especially beneficial for liquefied hydrogen tanks, considering their low volumetric density and the resulting demand for a large volume.

The design methodology is based on packing solutions popularly employed in the transportation and logistics sector to transport large containers of a specific shape in a constrained volume. Packing solutions utilize tessellation, in which a plane of a certain shape is covered or filled by another shape. This method is beneficial for hydrogen tanks since all of them will be of the same shape in a plane, namely, a circle.

Three designs were devised based on two tank orientations. Two designs are in the lateral direction, while the other is in the longitudinal direction. All three designs use different packing solutions to design the tank configuration with the fuselage, with the tank supports designed accordingly.

Some tank design choices were influenced by other fuel tanks and liquefied hydrogen tanks related to regulations such as API 620. Five crashworthiness tests were conducted based on criteria outlined in certification standards such as CS-25 or FAR-25. All designs passed the crashworthiness and fuel system criteria, indicating their ability to meet crashworthiness certification. The crashworthiness results for each design were compared and discussed, and observations were noted.

By loading the tanks onto the frames, longitudinal circle packing (LCP) can alter the load path and facilitate significant friction dissipation. This helps avoid issues with a lighter fuselage, which may not produce enough plastic deformation in the lower fuselage to correspond with the designed crash sequence. On the other hand, LHP lacks this mechanism, leading to extreme acceleration on the tanks. Lateral square packing (LSP) closely resembles the designed loading, follows the crash sequence as intended, and shows the lowest average DRI despite necessitating the highest energy dissipation.

Finally, a trade-off study was conducted to compare the designs based on the retrofitted aircraft's range, inspectability, crashworthiness, and retrofit cost estimation. LCP was selected as the best design due to its range advantage and crashworthiness.

Contents

List of Figures

List of Tables

Nomenclature

Symbols

Symbol	Definition
c	Damping Coefficient
C_D	Drag Coefficient
C_L	Lift Coefficient
d	Diameter
E	Energy
E_A	Artificial Strain Energy
E_{FD}	Frictional Dissipated Energy
E_{IE}	Internal Energy
E_{KE}	Kinetic Energy
E_P	Plastic dissipated energy
E_{SE}	Stored Strain Energy
E_{TOTAL}	Energy balance
E_V	Viscous dissipated energy
g	Gravitational Acceleration
H	Height
K	Kelvin
k	Spring Constant
L	Length
m	Mass
N	Total Number of Tanks
P_L	Permissible Length
r	Radius
v	Velocity
S	Wing Area
W	Weight
W_0	Initial Weight
W_1	Zero Fuel Weight
W_T	Tank Weight
W_{LH2}	Liquid Hydrogen Weight
w	Width
X	Number of Tanks Along Longitudinal Direction
Y	Number of Tanks Along Vertical Direction
ρ	Density
θ	Angle
Δ	Differentials

Abbreviations

Term	Definition
AIS	Abbreviated Injury Scale
API	American Petroleum Institute
ARAC	Aviation Rulemaking Advisory Committee
ASME	American Society of Mechanical Engineers

Term	Definition
ATD	Anthropomorphic Test Dummies
BWB	Blended Wing Body
CAD	Computer-aided Design
CAR	Civil Air Regulations
CERVIA	Metodi di Certificazione e Verifica Innovativi ed Avanzati
CFRP	Carbon Fiber Reinforced Plastic
CID	Controlled Impact Demonstrations
CLE	Crush Load Efficiency
CLT	Classical Laminate Theory
DRI	Dynamic Response Index
DV	Designated Volume
EASA	European Union Aviation Safety Agency
EIS	Entry Into Service
EWIS	Electrical Wiring Integrated System
FAA	Federal Aviation Administration
FEA	Finite Element Analysis
FEM	Finite Element Method
FWF	Fuel Weight Fraction
FS	Fuselage Station
GED	Gravimetric Energy Density
GFRP	Glass Fiber Reinforced Polymers
HIC	Head Injury Criterion
JSSG	Joint Services Specification Guide
LHV	Lower Heating Value
LRS	Limit of Reasonable Survivability
LSTC	Livermore Software Technology Corporation
MLI	Multi-Layer Insulation
MTOW	Maximum Takeoff Weight
NASA	National Aeronautics and Space Administration
NATO	North Atlantic Treaty Organization
NCAP	New Car Assessment Programme
OEM	Original Equipment Manufacturers
PEEQ	Plastic Strain Equivalent
SAF	Sustainable Aviation Fuel
SEA	weight-Specific Energy Absorption
SFC	Specific Fuel Consumption
TACDWG	Transport Category Airplane Ditching Standards and Requirements
TRL	Technology Readiness Level
USAF	United States Air Force
VED	Volumetric Energy Density

1

Introduction

1.1. Future of Aviation

The European aviation sector faces significant challenges due to the ambitious goal set by the European Commission to achieve net-zero greenhouse gas emissions within Europe by 2050. Although aviation currently only contributes approximately 3% to global carbon emissions, projections indicate that this figure could rise to 24% of global CO_2 emissions by 2050, a significant increase[1][2].

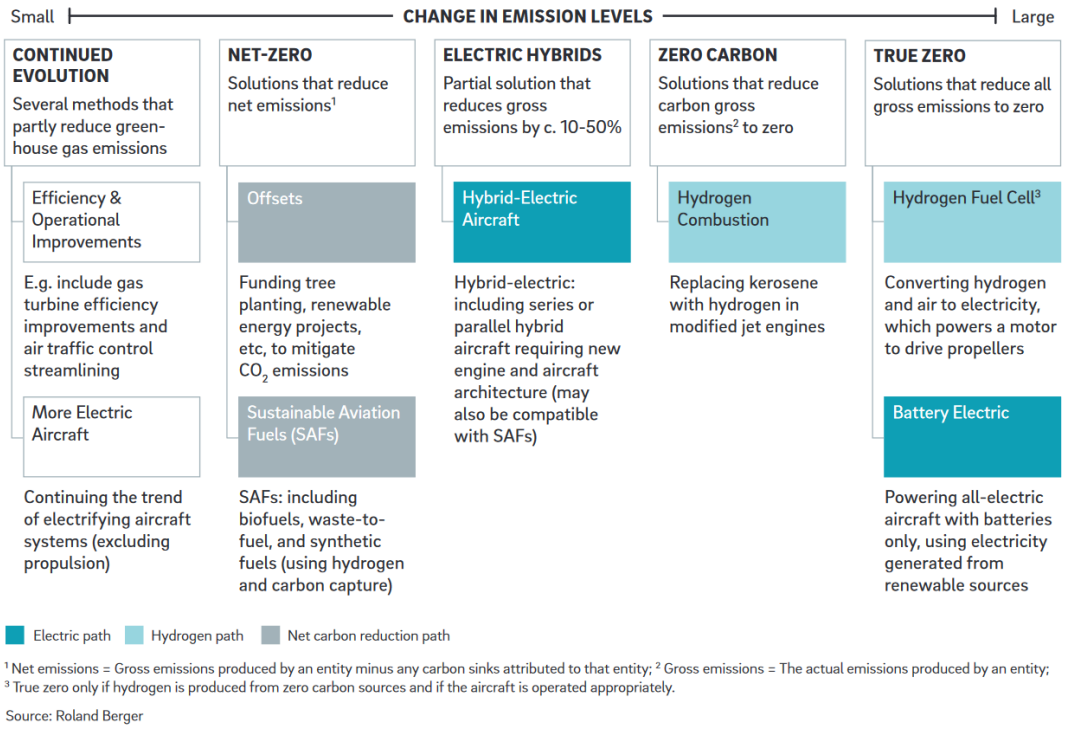

Figure 1.1: Solutions for aviation emissions[2].

This increase in CO_2 emission is attributed to a few key factors: the nonlinearity between the distance travelled and its carbon emission, aviation activity outgrowing the efficiency improvement of the aviation industry, and the influence of non-CO_2 greenhouse emissions such as CO, NO_x, SO_x, and hydrocarbon emission[3]. Various alternatives to traditional jet turbines have been proposed to mitigate carbon emissions, which can be categorized into three main approaches: electrification of aircraft propulsion,

[1] Under emission scenario representative concentration pathways (RCPs) 2.6, which is the best emission scenario, with aviation staying on the current tendency

utilization of hydrogen as the primary fuel, and implementation of carbon reduction measures, as shown in Figure 1.1. These solutions range from incremental improvements in fuel efficiency to gradually reducing emissions to eliminating crucial greenhouse gas emissions[2].

Although the European Commission's goal is net-zero greenhouse emissions, engine electrification and the adoption of hydrogen fuel are required to compensate for manufacturing emissions.

1.1.1. Hydrogen-Fuelled Aviation

Hydrogen possesses the highest energy content per unit mass among all chemical fuels, with a lower heating value (LHV) of approximately 120 MJ/kg, in contrast to kerosene's LHV of around 43 MJ/kg[4, 5]. On top of that, hydrogen-based propulsion emissions are often less polluting than conventional alternatives such as SAF (Sustainable aviation fuel).

Hydrogen, as a fuel source, emits only water vapour upon combustion, positioning it as an environmentally benign alternative to conventional jet fuel. Hydrogen also removes the carbon in the fuel source, which results in a near-total elimination of soot and sulfate emissions. Additionally, it is anticipated that the emission of nitrogen oxides (NO_x) will experience a significant reduction in hydrogen gas turbine applications and complete elimination in fuel cell implementations. This led to companies like Airbus developing their ZEROe program for short- and medium-haul flights mainly covered by regional or narrow-body aircraft. Airbus is betting on LH_2 as a viable, sustainable fuel, with the aggressive goal to reach the market by 2035[6]. Embraer with the Energia program[7], Universal Hydrogen[8], and multiple startups are also pushing for hydrogen-powered aircraft as a main alternative to current fossil fuel-based designs.

Figure 1.2: Airbus ZEROe turbofan concept[6].

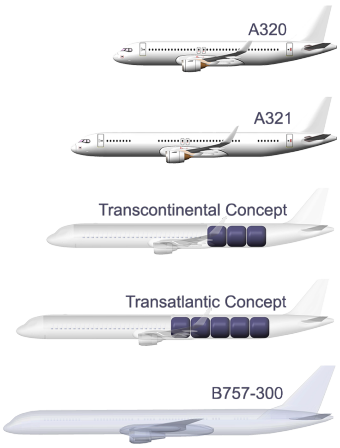

Figure 1.3: Universal Hydrogen Single Aisle / Narrow-body Concepts[8].

Figure 1.4: Embraer Energia H2 gas turbine E50-H2GT[7].

The exceptional energy density per unit mass of hydrogen is counterbalanced by its remarkably low density. Being the lightest element, hydrogen exhibits the lowest density among all known substances. Gaseous hydrogen has a merely 0.0899 g/L density at standard ambient temperature and pressure. In contrast, the air has a density of 1.225 g/L under the same conditions, while kerosene possesses a density of approximately 800 g/L. Consequently, hydrogen storage and its implications for aircraft are the main obstacles to the industry's adoption of hydrogen-based propulsion systems.

The two main solutions for this problem are either highly pressurizing the hydrogen into compressed gaseous hydrogen CGH_2 or cooling it to a cryogenic liquid state as LH_2. The aerospace industry has favoured LH_2 as an alternative fuel due to its superior energy density per unit volume compared to compressed hydrogen. This results in a reduced storage footprint and increased onboard weight for the aircraft, which are crucial factors in optimizing fuel efficiency and performance. This will be later discussed in chapter 2. LH2 requires about 4 times more volume than kerosene for the same energy. On top of that, the container of liquid hydrogen will need to be cryogenic and kept safe in specialized

storage tanks capable of insulating and preventing sloshing. Storing them in a structure that could also be a structural component is currently impossible. This presents some problems with the storage of the liquefied hydrogen[9].

Table 1.1: Comparison of energy carriers and storage solutions[2].

	Gravimetric Energy Density (kWh/kg)	Volumetric Energy Density (kWh/L)
Fuel	12.0	10.4
Jet Fuel With Storage System	~8.9	~9.5
Batteries	~0.3	~0.8
Liquid Hydrogen	~33	~2.4
Potential Future Hydrogen With Storage System	~10-21	~1.6-2.1

Airplanes must undergo a major redesign or retrofitting to accommodate on-board hydrogen storage. Research into concurrent design concepts has revealed several approaches. Firstly, a drastic change in aircraft configuration, such as a Blended Wing Body (BWB) aircraft[9], would allow for substantial storage space in the plane. Secondly, current airplanes could be retrofitted to enable aircraft segments to hold hydrogen tanks. Lastly, tube and wing aircraft could be redesigned or extended to fit in hydrogen tanks. These approaches could pave the way towards a more sustainable aviation industry, and any one of them would require significant investments and technological advancements [5, 6, 10, 11, 12, 13, 14].

Furthermore, hydrogen storage tanks still require certification due to their flammability and proneness to detonation. Liquid hydrogen fuel must be stored at cryogenic temperatures, which presents an extra danger to the operating crew, thus requiring certification of hazardous materials.

Despite these hurdles, hydrogen fuel has significant potential advantages. It promises to aid the aviation industry in achieving its sustainability targets and, in the long term, could result in economic benefits owing to its relative abundance and potential low cost.

1.2. Retrofitting

A new generation of aircraft is typically introduced every 15 to 20 years to replace older models in the same category. As the previous development cycle ended with the introduction of the Boeing 737 Max and A320 Neo family in the market from 2014 to 2020, demand decreased as the market purchased these aircraft; this resulted in a gap in innovation during the second half of the 2020s until demand recovered for the next generation of aircraft.

Furthermore, the European Commission only announced its demand for climate neutrality in 2019, which means that aircraft specifically run on hydrogen fuel are expected to finish development no earlier than 2035 [15]. This means that it will take the aviation industry exceedingly long periods of time to start switching to hydrogen fuel, let alone the investment required to start a completely new project with difficulties in certification. Adopting this new technology is also likely to be challenging due to the unpredictability of the market embracing this new fuel source and treating it as a replacement or support for their existing fleet.

In such a situation, retrofitting the aircraft with hydrogen components and systems could be attractive, bringing a rapid transition to hydrogen-powered aviation. This process can bring about the required change without the need for introducing a new aircraft generation, which can be time-consuming. By retrofitting, a fleet of aircraft can utilize these technologies, meet strict regulations, provide more comfort to passengers, and enhance the company's reputation [16].

However, the retrofitting process presents a multitude of challenges. It necessitates substantial alterations to aircraft design and infrastructure and safety considerations associated with the storage and transportation of hydrogen.

Despite these hurdles, hydrogen fuel has significant potential advantages. Owing to its relative abundance and potential low cost, it promises to aid the aviation industry in achieving its sustainability targets and economic benefits. It also promises to help the airport adapt its infrastructure to service and adapt to the new demand for hydrogen fuelling facilities.

Certain regional aircraft undergo a fuselage retrofit process that involves removing seats and installing a hydrogen tank in the cabin or at the entrance area, as shown in Figure 1.5.

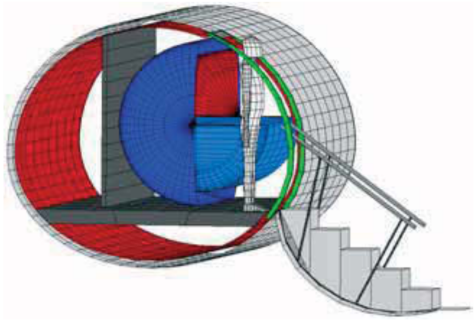

Figure 1.5: Integration of forward hydrogen tank and entrance area [5].

However, this retrofit is a complex undertaking requiring significant effort, including relocating doors [5]. Furthermore, the design cannot be easily retrofitted due to the tanks being too large to fit through the door. As a result, the fuselage must be opened, and the frames either removed or cut, significantly increasing the complexity and cost of retrofitting. This would also add to the certification effort, particularly when changing primary loading structures, since some parts of the frames would have to be cut off for the installation of the larger doors, resulting in essentially a new fuselage that would need to be recertified.

1.3. Crashworthiness

Crashworthiness has gained much traction in recent years due to the increased popularity of flying. The number of departures grew from 18 million flights in 2002 to more than 30 million flights in 2019, pre-COVID-19 pandemic. The global fleet size also grew to 28,000+ aircraft, almost double that of 2002[17]. Crashworthiness is especially important when designing a new fuselage layout since a fuselage with a crashworthiness design in mind can protect the occupants from serious harm or injury during less fatal accidents. These accidents typically happen during the aircraft's takeoff and landing when the aircraft is experiencing low speed and low altitude. During a crash, the fuselage would elastically and plastically deform and fracture to absorb the energy incurred upon the fuselage. The energy absorption should occur such that the occupants do not experience severe injuries due to high deceleration impact with the surroundings and are not exposed to toxic gases or high temperatures during and after the crash. Furthermore, during a crash, the structure should be deformed so that a survivable volume remains and evacuation routes are kept free.

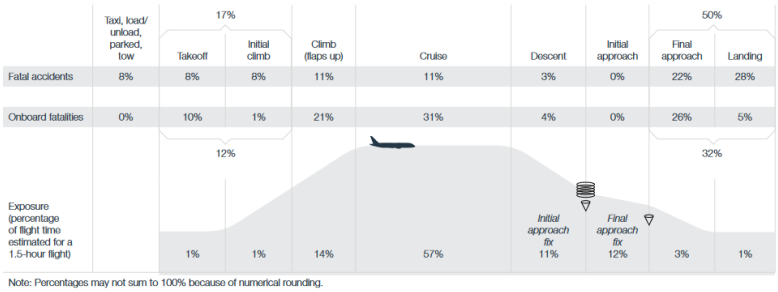

Figure 1.6: Percentage of fatal accidents and onboard fatalities | 2012 through 2021[17].

Research on crashworthiness started in the 1950s and continued until the 1980s, when commercial air travel became more widely available. In these periods, crashworthiness was based on full-scale crash tests and controlled impact demonstrations (CID), mainly conducted by the FAA and National Advisory Committee for Aeronautics (NACA), where full aircraft are tested upon. From the 1980s onward, more of these tests were conducted on fuselage sections using drop tests. Unlike CIDs, drop tests emphasise the detailed investigation of the failure behaviour of the structure to ensure the safety of occupants rather than the investigation of post-crash fire behaviour[18].

Figure 1.7: Full-scale crash test.

Figure 1.8: Fuselage section drop test.

During the 1990s, the FAA and EASA each carried out tests on their newest commercial planes, the B737 and A320. The FAA's investigation focused on passengers' safety and potential injuries, while EASA's research centred on the crash behaviour of the metal structure and sub-component failure testing.

The crashworthiness of the fuselage is critical in ensuring the safety of passengers and crew members during aircraft design. The fuselage structure is vital in minimizing injuries and providing protection in case of an accident or crash. The fuselage structure must undergo controlled deformation during such events to maintain survival space and shield occupants from secondary impacts. This is also why civil aviation safety agencies like the FAA and EASA regulate crashworthiness.

One major concern in the research of hydrogen-powered aircraft is the safety of the hydrogen tank-carrying fuselage in the event of a crash. Many current designs assume that the entire fuselage can be used to house the hydrogen tanks[10, 12, 13, 14, 19], as shown in the figures below. With the entire fuselage being designated for hydrogen fuel, the tanks could easily be damaged during the event of a crash. This could cause significant leakage and danger of both fire and explosion. This would make these designs unable to survive a conventionally survivable crash, making the designed aircraft exceedingly dangerous to operate and difficult to certify.

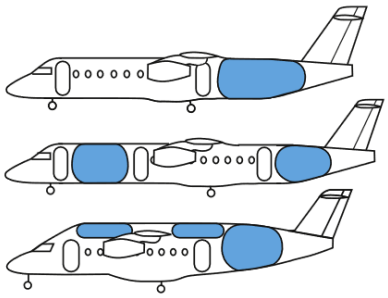

Figure 1.9: The different tank arrangements for the regional airliner[12].

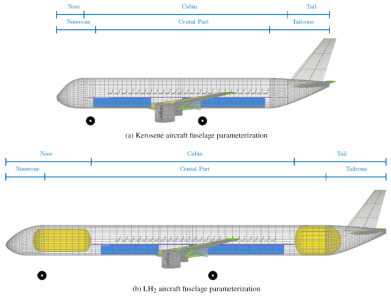

Figure 1.10: Fuselage sections and location of LH_2 tanks, fuel tanks in yellow[10].

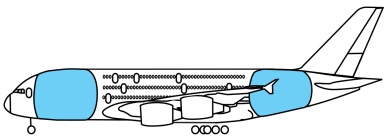

Figure 1.11: Fuselage tanks for large long-range transport aircraft[19].

1.4. Research Objective

With the newly designed aircraft far from being developed, the current market not yet adapted to new types of fuel, and aircraft unable to be certified, retrofitting, which operates on already certified aircraft's structural design, could prove useful. Retrofitting has gained significant traction recently, especially in conducting aircraft retrofits for hydrogen fuel operating in short to mid-haul range, such as the project HAPSS[2] [3], and by the company Universal Hydrogen, which already has a working concept for regional aircraft.

Retrofitting the tanks within the fuselage, however, comes with its own set of challenges. These challenges encompass storage and safety requirements associated with hydrogen, limitations imposed by the dimensions of the aircraft, the retrofitted aircraft's performance in terms of range and continued airworthiness, constraints on retrofit operations due to restrictions on major structural changes, safety concerns when transporting hazardous materials, compliance with crashworthiness regulations for the tanks, as well as related structural support. Additionally, the lack of information on the tank designs and related data due to their confidential nature adds to the complexity.

Currently, there are no high-accuracy and efficient retrofit design methodologies to assess crashworthiness compatible with the iterations needed in the preliminary design of fuselage structures. This presents a scientific challenge that must be addressed before achieving more efficient hydrogen-powered aircraft.

This thesis aims to establish a preliminary design methodology to address the first of these problems: a preliminary design that is capable of transporting the largest amount of liquid hydrogen fuel to allow the planes to be capable of flying the required range for short to mid-haul travel, is feasible for retrofitting, and that the tanks are capable of surviving the crash, without causing significant leakage.

1.5. Thesis Outline

The thesis consists of three chapters. The first chapter includes literature reviews that discuss the challenges associated with hydrogen and hydrogen tanks, the crashworthiness certification requirements for aircraft carrying hydrogen tanks, and aircraft crashworthiness. The second chapter details the design and analysis methodologies and the computational analyses conducted for the aircraft's crashworthiness certification. This chapter also presents the results of the analyses, along with a discussion of the post-retrofit performance, retrofit cost, and crashworthiness of the retrofitted aircraft to facilitate tradeoffs of the designs. Lastly, the conclusion summarizes the thesis and lists recommendations for future studies.

[2]HAPSS (Hydrogen Aircraft Powertrain And Storage Systems) project is a project focusing on translating proven technologies from the automotive and maritime industries into solutions for aviation[20] and is launched as a part of the Luchtvaart in Transitie project to retrofit existing regional aircraft to hydrogen-powered aircraft.

[3]The Luchtvaart in Transitie (Aviation in Transition) is a Dutch project aimed at accelerating the transition towards climate-neutral aviation by 2050[21].

Part I

Literature Review

2

Challenges of Using Hydrogen Fuel

Hydrogen fuel is increasingly used in various industries, particularly in the automotive industry[22] to reduce emissions. There are also proposals for the aerospace industry to adopt this technology. However, some challenges need to be addressed in terms of on-airport and on-board storage.

The primary challenge of adapting current aircraft technology with hydrogen lies in the inherent properties of hydrogen and methods to enable the storage of sufficient mass within reasonable volumes. section 2.1 covers the topic of hydrogen storage technology and the associated challenges posed by these storage methods. section 2.2 will provide an explanation of the safety risks associated with storing hydrogen on board.

2.1. Storage

Table 2.1 shows the readiest technology for on-airport and on-board hydrogen storage. The difference between on-airport and on-board storage is that on-board emphasizes gravimetric and volumetric density. The major difference between these five technologies is the amount of energy required to process the hydrogen to its storage state and the storage conditions.

Table 2.1: Hydrogen storage technologies with high TRL [23].

Technology	Description	Gravimetric Density	TRL
Compression (50–150 bar)	A mechanical device increases hydrogen pressure in its cylinder. Hydrogen can be stored in steel cylinders at pressures of up to 200 bar	3.95–10.9	9
High pressure (350–700 bar, 25°C)	A mechanical device increases hydrogen pressure in its cylinder. Hydrogen can be stored in composite cylinders at pressures up to 700 bar	23–50	9
Liquefaction (1 bar, -253°C)	Hydrogen is liquefied and stored at -253°C at moderate ambient pressures in cryogenic tanks. The process occurs through a multi-stage process of compression and cooling.	70.8	9
Ammonia (10 bar, 25°C)	Hydrogen are converted to ammonia via the Haber-Bosch process and are liquid at ambient temperatures and mild pressure. It will need to be converted back to hydrogen at the point of use by hydrogen cracking technology.	107	9
Toluene/ methylcyclohexane (ambient conditions)	A type of liquid organic carrier. Hydrogen is reacted with toluene to form methylcyclohexane (MCH) which can be transported at ambient temperature and pressure. The hydrogen is then released through exposure to heat or catalysts.	47	9

Hydrogen can be stored in ammonia through the Haber-Bosch process, which combines hydrogen gas

with nitrogen gas to make ammonia. Ammonia can then be stored on-board in a tank in a liquid state at 10 bar pressure at room temperature. Hydrogen can be extracted when and where needed by heating ammonia to high temperatures. Although ammonia storage has the highest gravimetric density among the technologies, it is limited by the energy conversion rate. Hydrogen will first need to be converted to ammonia using the Haber-Bosch process and then be converted back to hydrogen using ammonia cracking. Although the Haber-Bosch process requires a low amount of energy, the ammonia cracking process requires the ammonia to be heated to 700°C; the energy conversion rate is significantly lowered, while hydrogen production is already energy-intensive. The potential scalability and sustainability of ammonia storage, therefore, are greatly limited. For the above reason, although ammonia storage may have the highest gravimetric density among the mentioned technologies, this method is not widely implemented[24].

Compared to chemically stored hydrogen, physically stored hydrogen does not require the extra conversion step from the storage medium to hydrogen, thus having less total energy loss. However, storing hydrogen in its state at room temperature and atmospheric pressure is infeasible due to the low-density nature of hydrogen. To achieve feasible storage volume, hydrogen must be either highly compressed or cooled to a cryogenic liquid form at 20 K, As shown in Figure 2.1. Unlike kerosene, which could be stored at ambient pressure and temperature in aircraft structures that could serve as both primary and secondary structures, hydrogen requires robust high-pressure vessels to keep the hydrogen in its gaseous state with a reasonably high density (700 bar, 40g/L) or in well-insulated cryogenic tanks to keep the hydrogen in a low-temperature liquid state (20K, 70g/L). This makes it less capable of functioning as a structural member.

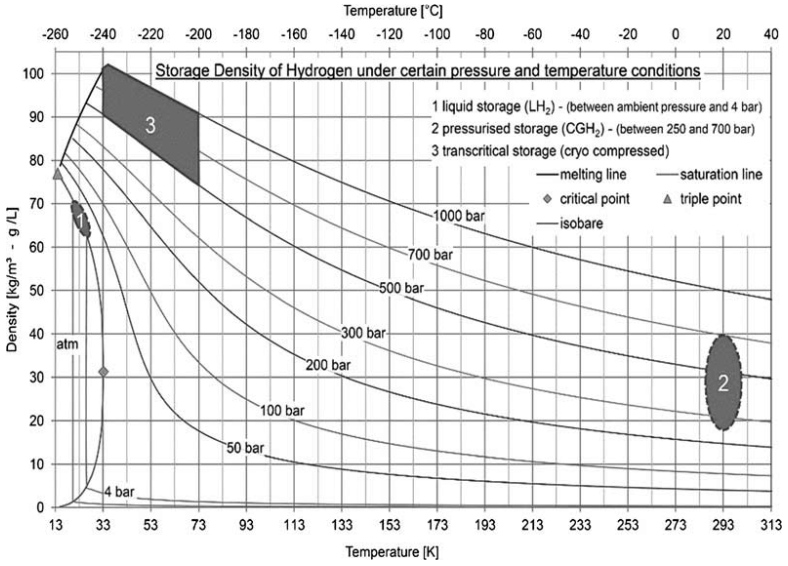

Figure 2.1: Hydrogen storage density under different pressure and temperature conditions.

A comparison could be made between the highly pressurized and liquefied hydrogen. Pressurized hydrogen costs less energy and is simpler to store. As seen in Figure 2.2, pressurized or compressed hydrogen could be stored longer. In contrast, liquefied hydrogen loses most of its input energy days after the initial energy input[1]. This is due to liquid hydrogen boil-off, where external heat leaks into the fuel tank and vaporizes the liquid hydrogen due to its low boiling point.

[1] initial energy input is derived from the maximum energy that one ton of hydrogen could provide subtracted by the energy inputs required for storage (liquefaction, compression, cracking)

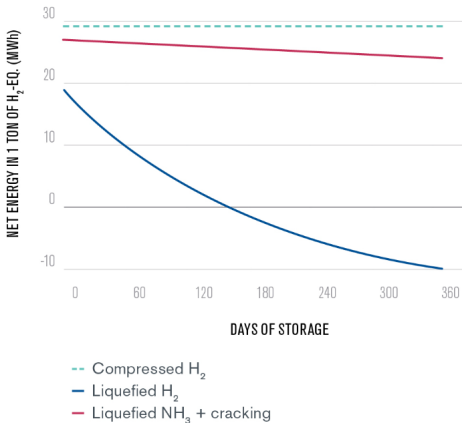

Figure 2.2: Net remaining energy of hydrogen storage over time[24].

Despite the initial energy input and boil-off, liquid hydrogen is still preferred by the aviation industry due to its higher gravimetric index[3][2] and its volumetric density. As mentioned in the above paragraph, on-board storage places a higher emphasis on gravimetric and volumetric density. Another reason liquid hydrogen is considered safer than highly compressed hydrogen gas is because it has a lower risk of leakage and explosion.

However, liquid hydrogen also poses unique challenges, such as the need for cryogenic cooling and insulation, the availability and cost of green hydrogen production, and compatibility with existing aircraft designs and infrastructure. Making a lightweight design for the tank is also difficult due to mandated safety factors ranging from 1.4 to 2.0. This safety factor is often augmented by conservative material strength estimates. Due to the embrittlement of the tank material from cryogenic temperature, repeated thermal and mechanical loading from filling and draining the hydrogen would cause severe fatigue damage to the tank structure. Creating a design that can be manufactured, inspected, and used with confidence also proved to be difficult [25].

2.1.1. Boil-off

One of the major challenges that on-board liquid hydrogen storage faces is the boil-off of liquid hydrogen. As much as 40% of the energy stored on-board could be lost to this phenomenon[26]. Boil-off is when the tank's temperature rises due to heat transfer, causing liquefied hydrogen to gasify. As the hydrogen expands and evaporates, the pressure inside the tank rises. Although cryogenic tanks that can take high pressure exist, liquefied hydrogen tanks are generally not designed to withstand high pressures. Thus, hydrogen boil-off must be released through a relief valve, which results in energy loss [27]. It is possible to prolong the dormancy time, which is the time between refuelling and relief valve opening, by strengthening the tanks or decreasing the boil-off rate by adding insulation. The method using the tanks that could sustain high pressure is cryo-compressed, or transcritical storage, as shown in Figure 2.1.

Boil-off is less of a problem for previous liquid hydrogen applications since they require a relatively short duration for operation. For instance, the Saturn V heavy launch vehicle, the space shuttle external tank, and the X–33 technology flight demonstrator all fly for a short duration and are only fuelled a short time before takeoff, which could allow a larger boil-off rate[25].

There exist a few mechanisms for hydrogen boil-off and ways to negate it[26]:

- Ortho-para conversion: The ortho-para conversion of hydrogen is the transition of ortho-protium hydrogen, in which nuclear spins of atoms in the same direction in the molecule point, to the para-protium, in which nuclear spins point to the opposite directions. The conversion is spontaneous, and when converting normal hydrogen to liquid para-hydrogen, the released energy is powerful enough to vaporize 64% of the initial liquid[28].
- Heat leak:

[2] the weight fraction of the hydrogen in a full tank

  - Shape and size effect: The shape and size of the storage tank influence how much heat the tank takes. It is proportional to the surface-to-volume ratio of the hydrogen tank. Therefore, the best way to counteract this phenomenon would be to manufacture a spherical tank or build a larger tank[27].
  - Thermal stratification and overfill: The phenomenon that the energy is distributed non-uniformly throughout the tank, leading to the liquid in a tank having different temperatures. The higher temperature, especially at the surface of the liquid, would lead to hydrogen boil-off. By installing highly conductive plates (conductors) vertically in the vessel, the thermal gradient within the tank is reduced, and these plates would also act as sloshing barriers.
  - Insulation, conduction and radiation: Heat conduction from the environment through the tank structure to heat the liquid hydrogen. The solution to this problem is an efficient insulating and re-cooling system that insulates the tank while adding minimum mass and cools down the hydrogen constantly [29]. Various investigations have been conducted to determine the most suitable materials for insulation in cryogenic liquid hydrogen tanks for aerospace applications. Foams, aerogels, and vacuum-based insulation combined with Multi-Layer Insulation (MLI) have been identified as the most desirable options.

- Sloshing: motion of liquid within a tank gathering on one side and hitting the tank wall, causing a hydraulic jump. This jump would then convert impact energy into thermal energy. By installing anti-slosh baffles, the sloshing could be decreased.
- Flashing: Flashing is when liquid hydrogen suddenly gasifies from higher pressure to a low-pressure environment. This problem is negated by transporting liquid hydrogen at atmospheric pressures or recapturing the gasified hydrogen into a secondary tank to be consumed later or liquefied to be put back into the cryogenic tank.

2.2. Safety risks

2.2.1. Leakage

Liquid hydrogen presents additional safety hazards during accidental leakage events since hydrogen is a colourless, odourless, tasteless, flammable gas that human senses cannot notice. Breathing in too much hydrogen may cause asphyxiation[23]. On top of that, hydrogen also has a high permeability through many materials due to the size of its molecule. Direct contact with cryogenically stored hydrogen would also cause severe cold burns, making handling hazardous[30].

2.2.2. Flammability

Hydrogen has a relatively low auto-ignition temperature at 585°C. Additionally, hydrogen can undergo detonation within a wide volumetric concentration range, spanning from as low as 4% to as high as 75% in an air mixture. Additionally, the ignition energy for hydrogen is relatively low, measuring at 0.017 MJ/kg with high burning velocity. Consequently, the potential for fire in the fuselage with a relatively low hydrogen concentration is one of the main concerns of adopting hydrogen fuel[31].

Hydrogen is also a clean burning gas[3], meaning that during normal daylight, hydrogen fire is nearly invisible[32]. The hydrogen fire poses additional challenges during the evacuation process as passengers may struggle to perceive the fire, thus compromising the safety of the evacuation. Additionally, ground crews may face difficulties in extinguishing hydrogen fires due to the lack of specialized equipment for detection.

Special design considerations will have to be made to detect hydrogen in the fuselage and venting leaked and boiled-off hydrogen to prevent on-board fires. Airports would also have to adapt to the adoption of hydrogen with new infrastructure and fire emergency measures.

[3] Burning without producing smoke

3

Certification of hydrogen-powered aircraft Fuselage

The main focus of this thesis is on crashworthiness certification of the new layout of the fuselage post retrofitting for regional transport aircraft for the installation of hydrogen tanks inside the fuselage. Certification of new fuselage designs involves rigorous evaluation and testing to ensure structural integrity, crashworthiness, and fire safety. Retrofitting existing fuselage structures requires adherence to guidelines and thorough analysis to maintain safety and airworthiness. EASA (European Union Aviation Safety Agency) and FAA (Federal Aviation Administration) are the aviation regulatory agencies of the European Union and the United States, respectively. The standards set by these two regulatory bodies are often used as benchmarks for global aviation regulatory bodies.

This chapter aims to provide a comprehensive overview on the certification of crashworthiness on retrofitting aircraft fuselage and fuel systems, crashworthiness, and hazardous material.

The related regulations are EASA's "Certification Specifications and Acceptable Means of Compliance for Large Aeroplanes (CS-25)" and FAA's "Federal Aviation Regulation Part 25—Airworthiness Standards: Transport Category Airplanes (FAR-25)". By examining EASA and FAA regulations and the certification processes for new fuselage designs and retrofitting, this thesis hopes to build a knowledge base for the design of future hydrogen-powered aircraft, speed up the transition of aviation through retrofitting, and set a knowledge base for certification of hydrogen-powered aircraft fuselages.

All text in italics is quoted from regulations.

3.1. Emergency Landing Conditions

The crashworthiness of an aircraft fuselage is regulated by the emergency landing conditions, which are regulated in chapters 25.561 25.563 of CS-25 and chapter 25.561 25.563 of FAR-25 and mainly considers the occupants.

This thesis focuses on the safety regulations of hydrogen-carrying fuselages, which do not involve passengers. Fatalities due to occupants' body parts being impacted by a flying object are therefore omitted from general emergency landing provisions and would only consider damage to fuel systems, structures, and rapid deceleration. Fuel tank damages due to flying objects will be considered in fuel tank provisions detailed in section 3.3.

3.1.1. General

1. *The aeroplane, although it may be damaged in emergency landing conditions on land or water, must be designed as prescribed in this paragraph to protect each occupant under those conditions.*
2. *The occupant experiences the following ultimate inertia forces acting separately relative to the surrounding structure:*

(a) *Upward, 3.0g*
(b) *Forward, 9·0g*
(c) *Sideward, 3.0g on the airframe and 4.0g on the seats and their attachments*
(d) *Downward, 6·0g*
(e) *Rearward, 1·5g*

3. *For equipment, cargo in the passenger compartments and any other large masses, the following apply:*

   (a) *These items must be positioned so that if they break loose, they will be unlikely to:*

      i. *Penetrate fuel tanks or lines or cause fire or explosion hazard by damage to adjacent systems; or*

   (b) *When such positioning is not practical (e.g. fuselage-mounted engines or auxiliary power units) each such item of mass shall be restrained under all loads up to those specified in paragraph 2 of this section. The local attachments for these items should be designed to withstand 1.33 times the specified loads if these items are subject to severe wear and tear through frequent removal (e.g. quick change interior items).*

To conclude, the general provisions of emergency landing conditions specified the inertia force limit experienced by occupants, the positioning and restraint requirements for equipment, cargo, and large masses to prevent occupants' injuries and damage to fuel systems[33].

3.1.2. Emergency landing dynamic conditions

1. *Each seat type design approved for occupancy must successfully complete dynamic tests or be demonstrated by rational analysis based on dynamic tests of a similar seat type, in accordance with each of the following emergency landing conditions. The tests must be conducted with an occupant simulated by a 77kg (170 lb) anthropomorphic test dummy sitting in the normal upright position:*

   (a) *A change in downward vertical velocity, (Δv) of not less than 10.7 m/s, (35 ft/s) with the aeroplane's longitudinal axis canted downward 30 degrees with respect to the horizontal plane and with the wings level. Peak floor deceleration must occur in not more than 0·08 seconds after impact and must reach a minimum of 14 g.*
   (b) *A change in forward longitudinal velocity (Δv) of not less than 13.4 m/s, (44 ft/s) with the aeroplane's longitudinal axis horizontal and yawed 10 degrees either right or left, whichever would cause the greatest likelihood of the upper torso restraint system (where installed) moving off the occupant's shoulder, and with the wings level. Peak floor deceleration must occur in not more than 0·09 seconds after impact and must reach a minimum of 16 g. With the exception of flight deck crew seats that are mounted in the forward conical area of the fuselage, where floor rails or floor fittings are used to attach the seating devices to the test fixture, the rails or fittings must be misaligned with respect to the adjacent set of rails or fittings by at least 10 degrees vertically (i.e. out of parallel) with one rolled 10 degrees.*

2. *The following performance measures must not be exceeded during the dynamic tests conducted in accordance with sub-paragraph 1 of this paragraph:*

   (a) *The maximum compressive load measured between the pelvis and the lumbar column of the anthropomorphic dummy must not exceed 680 kg. (1500lb)*
   (b) *Each occupant must be protected from serious head injury under the conditions prescribed in sub-paragraph 1 of this paragraph. Where head contact with seats or other structures can occur, protection must be provided so that the head impact does not exceed a Head Injury Criterion (HIC) of 1000 units.*

For emergency landing dynamic conditions, the provisions under CS 25.562 and FAR 25.562 prevent head and lumbar injury by limiting the experienced accelerations. These provisions are different from general provisions since loading on head and lumbar requires the impact to be damped (or amplified) throughout the entire structure, the seating system, the restraint system, and the lower bodies.

3.1.3. Structural ditching provisions

Structural strength considerations are also regulated with ditching regulations:

1. *Unless the effects of the collapse of external doors and windows are accounted for in the investigation of the probable behaviour of the aeroplane in a water landing, the external doors and windows must be designed to withstand the probable maximum local pressures.*
2. *It must be shown that, under reasonably probable water conditions, the flotation time and trim of the airplane will allow the occupants to leave the airplane and enter the life rafts required by ditching equipment regulations. If compliance with this provision is shown by buoyancy and trim computations, appropriate allowances must be made for probable structural damage and leakage. If the airplane has fuel tanks (with fuel jettisoning provisions) that can reasonably be expected to withstand ditching without leakage, the jettisonable volume of fuel may be considered as buoyancy volume.*
3. *The probable behaviour of the aeroplane in a water landing must be investigated by model tests or by comparison with aeroplanes of similar configuration for which the ditching characteristics are known. Scoops, wing-flaps, projections, and any other factor likely to affect the hydrodynamic characteristics of the aeroplane must be considered.*

3.2. Carbon fiber reinforced plastic aircraft special conditions

Since carbon fiber reinforced plastic (CFRP) semi-monocoque construction aircraft are a relatively new design concept, there is a need for new regulations to accommodate and regulate them. Notable examples of this type of aircraft include the Boeing Model 787-8 and the Airbus A350–900. CFRP structures demonstrate distinct behaviour when compared to metallic structures, resulting in differences in material ductility, stiffness, failure mechanisms, and energy absorption properties. To ensure the same level of safety as existing standards, the FAA requires special conditions that establish additional safety standards. The FAA dictates that, with 30 ft/s (9.144 m/s) vertical descent velocities, the aircraft must:

1. *Retention of items of mass. The occupants, i.e., passengers, flight attendants, and flight crew, must be protected during the impact event from the release of seats, overhead bins, and other items of mass due to the impact loads and resultant structural deformation of the supporting airframe and floor structures. The applicant must show that loads due to the impact event and resultant structural deformation of the supporting airframe and floor structure at the interface of the airplane structure to seats, overhead bins, and other items of mass are comparable to those of previously certificated widebody transports of similar size for the range of descent velocities stated above. The attachments of these items need not be designed for static emergency landing loads in excess of those defined in § 25.561 if impact response characteristics of the Boeing Model 7878 yield load factors at the attach points that are comparable to those for a previously certificated wide-body transport category airplane.*
2. *Maintenance of acceptable acceleration and loads experienced by the occupants. The applicant must show that the impact response characteristics of the Boeing Model 787–8, specifically the vertical acceleration levels experienced at the seat/floor interface and loads experienced by the occupants during the impact events, are consistent with those found in § 25.562(b) or with levels expected for a previously certificated wide-body transport category airplane for the conditions stated above.*
3. *Maintenance of a survivable volume. For the conditions stated above, the applicant must show that all areas of the airplane occupied for takeoff and landing provide a survivable volume comparable to that of previously certificated wide-body transports of similar size during and after the impact event. This means that structural deformation will not result in infringement of the occupants' normal living space so that passenger survivability will not be significantly affected.*
4. *Maintenance of occupant emergency egress paths. The evacuation of occupants must be comparable to that from a previously certified widebody transport of similar size. To show this, the applicant must show that the suitability of the egress paths, as determined following the vertical impact events, is comparable to the suitability of the egress paths of a comparable, certificated wide-body transport, as determined following the same vertical impact events.*

The special conditions, in conclusion, are very similar to that of the conventional aircraft. The conditions also specifically detailed the conditions of the vertical acceleration that the aircraft fuselage needs to withstand at 30 ft/s[34, 35].

3.3. Fuel Tanks

3.3.1. General

CS 25.963 Fuel tanks: general

1. *Each fuel tank must be able to withstand, without failure, the vibration, inertia, fluid and structural loads that it may be subjected to in operation.*
2. *Fuel tanks must, so far as it is practicable, be designed, located and installed so that no fuel is released in or near the fuselage or near the engines in quantities sufficient to start a serious fire in otherwise survivable emergency landing conditions, and:*

   (a) *Fuel tanks must be able to resist rupture and to retain fuel under ultimate hydrostatic design conditions in which the pressure P within the tank varies in accordance with the formula:*

   $$P = K\rho gL$$

   where:

   - *P = fuel pressure in Pa at each point within the tank*
   - *L = a reference distance in m between the point of pressure and the tank's farthest boundary in the direction of loading.*
   - *ρ= typical fuel density in kg/m^3*
   - *g = acceleration due to gravity in m/s^2*
   - *K = 4.5 for the forward loading condition for fuel tanks outside the fuselage contour*
   - *K = 9 for the forward loading condition for fuel tanks within the fuselage contour*
   - *K = 1.5 for the aft loading condition*
   - *K = 3.0 for the inboard and outboard loading conditions for fuel tanks within the fuselage contour*
   - *K = 1.5 for the inboard and outboard loading conditions for fuel tanks outside of the fuselage contour*
   - *K = 6 for the downward loading condition*
   - *K = 3 for the upward loading condition*

   (b) *For each fuel tank and surrounding airframe structure, the effects of crushing and scraping actions with the ground should not cause the spillage of enough fuel, or generate temperatures that would constitute a fire hazard under the conditions specified in CS 25.721(b).*

3. *Fuel tanks must comply with the following criteria in order to avoid hazardous fuel leak:*

   (a) *Fuel tanks located in an area where experience or analysis indicates a strike is likely, must be shown by analysis supported by test or by test to address penetration and deformation by tyre and wheel fragments, small debris from uncontained engine failure or APU failure, or other likely debris (such as runway debris).*

4. *For pressurised fuel tanks, a means with failsafe features must be provided to prevent the buildup of an excessive pressure difference between the inside and the outside of the tank.*

In conclusion, ensuring the structural integrity and safety of fuel tanks in aircraft is of utmost importance. Measures should be implemented to prevent fuel leakage in emergency landing conditions, particularly in areas that could lead to serious fires. Compliance with safety criteria is essential to avoid hazardous fuel leaks, including analysing the likelihood of strikes and conducting tests to address penetration and deformation by debris or fragments. Additionally, for pressurised fuel tanks such as hydrogen tanks, fail-safe mechanisms must be in place to prevent excessive pressure differentials between the inside and outside of the tank.

Overall, the general provisions of fuel tanks aim to mitigate the risks associated with fuel release and potential fires in emergency landings.

3.3.2. Fuel tank strength in emergency landing conditions

AMC 25.963(d)

1. *PURPOSE. This AMC sets forth an acceptable means, but not the only means, of demonstrating compliance with the provisions of CS-25 related to the strength of fuel tanks in emergency landing conditions.*

2. *BACKGROUND. For many years the JAA/EASA has required fuel tanks within the fuselage contour to be designed to withstand the inertial load factors prescribed for the emergency landing conditions as specified in JAR/CS 25.561. These load factors have been developed through many years of experience and are generally considered conservative design criteria applicable to objects of mass that could injure occupants if they came loose in a minor crash landing.*

   (a) *A minor crash landing is a complex dynamic condition with combined loading. However, in order to have simple and conservative design criteria, the emergency landing forces were established as conservative static ultimate load factors acting in each direction independently.*
   (b) *CS 25.963 has required that fuel tanks, both in and near the fuselage, resist rupture under survivable crash conditions. The advisory material previously associated with CS 25.963 specifies design requirements for all fuel tanks that, if ruptured, could release fuel in or near the fuselage or near the engines in quantities sufficient to start a serious fire.*
   (c) *Recognising that the emergency landing load factors were applicable to objects of mass that could cause injury to occupants and that the rupture of fuel tanks in the fuselage could also be a serious hazard to the occupants, § 4b.420 of the Civil Air Regulations (CAR) part 4b (the predecessor of FAR 25) extended the emergency landing load conditions to fuel tanks that are located within the fuselage contour. Even though the emergency landing load factors were originally intended for solid items of mass, they were applied to the liquid fuel mass in order to develop hydrostatic pressure loads on the fuel tank structure. The application of the inertia forces as a static load criterion (using the full static head pressure) has been considered a conservative criterion for the typical fuel tank configuration within the fuselage contour. This conservatism has been warranted considering the hazard associated with fuel spillage.*

3. *GENERAL. item 2 requires that fuel tanks must be designed, located, and installed so that no fuel is released in quantities sufficient to start a serious fire in otherwise survivable emergency landing conditions. The prescribed set of design conditions to be considered is as follows:*

   (a) *Fuel tank pressure loads. item 2a provides a conservative method for establishing the fuel tank ultimate emergency landing pressures. The phrase "fuel tanks outside the fuselage contour" is intended to include all fuel tanks where fuel spillage through any tank boundary would remain physically and environmentally isolated from occupied compartments by a barrier that is at least fire resistant as defined in CS-Definitions. In this regard, cargo compartments that share the same environment with occupied compartments would be treated the same as if they were occupied. The ultimate pressure criteria are different depending on whether the fuel tank under consideration is inside, or outside the fuselage contour. For the purposes of this paragraph a fuel tank should be considered inside the fuselage contour if it is inside the fuselage pressure shell. If part of the fuel tank pressure boundary also forms part of the fuselage pressure boundary then that part of the boundary should be considered as being within the fuselage contour. Figures 1 and 2 show examples of an underslung wing fuel tank and a fuel tank within a moveable tailplane, respectively, both of which would be considered as being entirely outside of the fuselage contour.*

The fuel tank should be able to sustain the inertia force of the emergency landing condition and apply a static ultimate load. If the fuselage includes a cargo compartment, it should be treated the same as if they were occupied. Precautions should be taken so that the fuel tank, both in and near the fuselage, should not rupture under a survivable crash. Or at least should not be able to gather a sufficient amount to cause a serious fire.

Fuel system regulation

Fuel system components in an engine nacelle or in the fuselage must be protected from damage, which could result in spillage of enough fuel to constitute a fire hazard as a result of a wheels-up landing on a paved runway under each of the conditions prescribed in CS 25.721(b)

3.3.3. Sloshing and fire hazards

Sloshing is the motion of fuel in a tank caused by acceleration or deceleration. Acceleration causes the liquid to gather and reflect on one side of the tank, causing a hydraulic jump. Deceleration then causes it to travel and gather on the other end, transforming the impact energy into thermal energy. The thermal energy dissipated eventually leads to an increase in hydrogen fuel boil-off.[26] This can pose a

potential hazard as it gradually raises the tank pressure and go against the provisions in item 2. These movements of fuel also create lateral forces, which the aircraft and surrounding structure need to be compensated for[36]. Though sloshing can concern both liquid hydrogen and conventional aircraft fuel tanks, sloshing is more critical for liquid hydrogen tanks because it increases the free surface area and accelerates boil-off. Additionally, liquid hydrogen must be kept at an extremely low temperature and stored in dedicated pressure vessels inside the fuselage, making sloshing management more challenging, as mentioned in AMC 25.963d.

CS 25.981 states that, to the extent practicable, design precautions must be taken to prevent the likelihood of flammable vapours within the fuel tanks by limiting heat and energy transfer. No unnecessary spraying, sloshing or creation of fuel mist is allowed under the provisions of AMC 25.981.

Sloshing could be prevented by vertically installing high conductivity plates in the tank to serve as anti-slosh baffles and reduce boil-off due to sloshing. With high thermal conductivity, these plates have the added benefit of providing a low-resistance heat path and eliminating temperature gradients in the tank, thus reducing boil-off[12].

3.4. Hydrogen tanks specific regulations

Due to its cryogenic temperature, hydrogen has specific hazardous qualities that require additional regulations beyond the typical fuel system regulations. It can weaken the material properties of surrounding structures and affect operating personnel, which calls for requirements of handling hazardous material under 29 CFR Part 1910 Subpart H Hazardous Materials. The requirement specifies that hydrogen containers shall comply with the following: *Storage containers shall be designed, constructed, and tested in accordance with appropriate requirements of the ASME (American Society of Mechanical Engineers) Boiler and Pressure Vessel Code, Section VIII—Unfired Pressure Vessels (1968) or applicable provisions of API (American Petroleum Institute) Standard 620, Recommended Rules for Design and Construction of Large, Welded, Low-Pressure Storage Tanks, Second Edition (June 1963) and appendix R (April 1965), which is incorporated by reference as specified in § 1910.6, and API Standard 620, "Design and Construction of Large, Welded Low-Pressure Storage Tanks".* Hydrogen's flammability also risks the supporting structure, which demands special requirements from the National Fire Protection Association (NFPA), specifically NFPA 55.

3.4.1. Inspection of tanks

According to CS 25.611 Accessibility provisions, means must be available to inspect, replace, adjust, and lubricate the principal structural elements and control systems for continued airworthiness. The inspection means must be practical for the inspection interval, and non-destructive inspection aids may be used for structural elements where direct visual inspection is not possible. It should be noted that the effectiveness of the inspection aids and procedures must be specified in the maintenance manual required by CS 25.1529.

Under API Standard 620, Recommended Rules for Design and Construction of Large, Welded, Low-Pressure Storage Tanks.[37]:

- *ACCESS FOR INSPECTOR. The inspector shall be permitted free access to all parts of the plant concerned with the manufacture of the tank during fabrication and to all parts of the plants of material suppliers who are concerned with the manufacture of materials to be used in the tank.*
- *Inspection Openings. Each tank shall be provided with at least two manhole openings to afford access to its interior for inspection and repair. Manholes shall in no event be smaller than 20 in. along any inside dimension. All manholes shall be made readily accessible by platforms and ladders, stairways, or other suitable facilities.*

3.4.2. Fire Protection of Structural Supports

National Fire Protection Association (NFPA) 55, Standard for the Storage, Use, and Handling of Compressed Gases and Cryogenic Fluids in Portable and Stationary Containers, Cylinders, and Tanks [38].

- *Steel supports in excess of 18 in. (46 cm) in height shall have a minimum 2 hour fire resistance rating in*

accordance with ASTM E 1529, Determining the Effects of Large Hydrocarbon Pool Fires on Structural Members and Assemblies.

- *Storage containers, piping, valves, regulating equipment, and other accessories shall be accessible and shall be protected against physical damage and tampering.*
- *Uninsulated piping and equipment that operates at liquefied hydrogen temperatures shall not be installed above asphalt or other combustible materials or surfaces in order to prevent the contact of liquid air with such materials.*

3.5. Injury Criteria

As stated in subsection 3.3.1, the strength of fuel tanks should be subjected to the provisions of emergency landing conditions and should survive the conditions of a survivable crash for humans. This subjects the fuel tanks to the same regulations as those concerned with the safety of humans. Olivares (2018) [39] compiled a list of injury criteria for the entire human body. A more general criteria to assess human injury is the BASE(overhead Bin falling objects, Accelerations, Space preservation, Escape route preservation) criteria to elucidate the provisions listed in the injury list and enable the comparison of the different designs[40].

However, since the focus of this study is on a fuel tank bay fuselage without passenger compartments, the preservation of escape routes and the risk of injury from falling objects are not applicable in this context. Instead, the primary concern lies in ensuring sufficient space for the liquid hydrogen tank post-crash to avoid damaging the fuel tank and the accelerative force.

3.5.1. Accelerative Force Tolerances

Out of the BASE criteria, the acceleration criterion is the most crucial to the survival of occupants and this study. This criterion encompasses all instances where occupant safety is affected by accelerations, such as the risk of spinal injury or seat failure. For the criteria of our concern, the most important is the dynamic vertical acceleration, or 'headward' acceleration.

In 1959, A. Martin Eiband of the National Aeronautics and Space Administration (NASA) developed the duration and magnitude of uniform acceleration to the degree of injury diagrams, better known today as the Eiband diagrams. It is one of the earliest examples of an accelerative force tolerance criterion. These diagrams are commonly used to determine the injury that the passengers sustained during a crash and determine the human tolerance of accelerative forces[41].

When acceleration pulses fall below the lower curve, minor to no injuries are expected, while pulses between the lower and higher curves indicate moderate injuries. Acceleration pulses exceeding the upper Eiband curve suggest severe injuries. In order to obtain information about the probability of injury for the simulated configurations, it was necessary to evaluate the pulses with regard to the duration of each acceleration level[40].

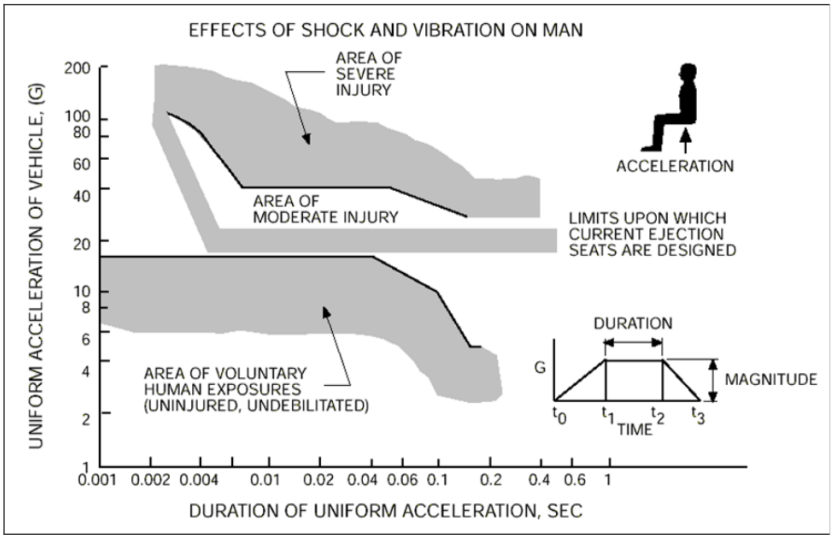

Figure 3.1: EIBAND diagram for vertical accelerations[40].

Eiband diagram, however, has its limitations. It is focused on full-body acceleration, and the specifics of the injury suffered are not detailed. Since it was developed in 1959, new injury mitigation methods are also not considered[42]. One of the key injuries that, though the acceleration and duration falls within the moderate injury section, still causes severe injury. That injury is a spinal fracture. A spinal fracture happens to occur at around 20g force, and under the Eiband diagram, a 20g acceleration, even at a long duration, should only induce moderate injury, but spinal injury might lead to permanent spinal cord injury, nerve damage and paralysis. A new type of injury criteria is then devised to mend this shortcoming of the Eiband diagram, and it is the Dynamic Response Index (DRI).

Spinal Injury

DRI derived the spinal column of the human occupant as a one-degree-of-freedom vertical lumped mass-spring-damper model[43]. The system has a massless spring with a spring constant k, upper body mass is lumped together into mass m, and a damping coefficient of the spine$c$. Note that the spring constant and damping ratio only account for the human body's damping and spring stiffness and are not representative of the human body on a seat. The seats will have to be represented separately.

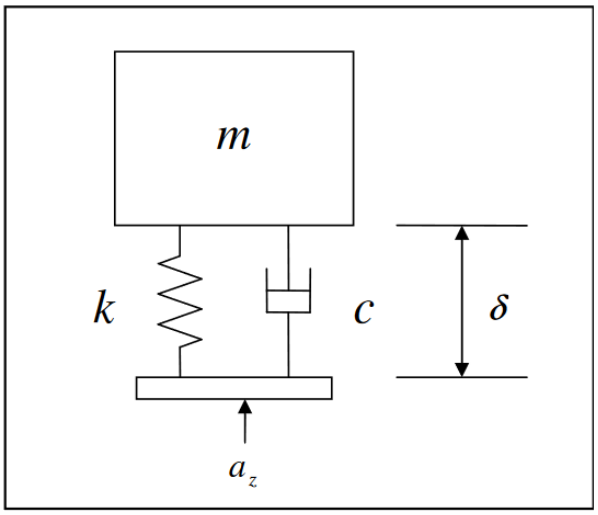

Figure 3.2: Single degree of freedom mass-spring-damper model of the human spine[43].

The model measures the maximum compression of the model and evaluates the degree of compression to judge the degree of injury. The equations of DRI are as follows:

$$\ddot{\delta} + 2\zeta\omega_n\dot{\delta} + \omega_n^2\delta = a_z \tag{3.1}$$

where:

- a_z is the acceleration-time input to the model.
- δ is the relative displacement of the model - compression of the lumbar spine.
- ω_n is the natural frequency of the system with $\omega_n = \sqrt{k/m}$.
- ζ is the damping ratio with $\zeta = \frac{c}{2\sqrt{mk}}$.

Calculate the second-order differential equation for a given acceleration to gain the deflection δ of the system. It functions like a digital filter for the input signal, which, in this case, is the system's acceleration.

$$DRI = \frac{\omega_n^2\delta_{max}}{g} \tag{3.2}$$

with:

- δ_{max} is the maximum compression of the spine for a given acceleration
- ω_n is the system's undamped natural frequency
- and g is gravitational acceleration

Stech and Payne conducted research on United States Air Force (USAF) Pilots and concluded the damping ratio ζ=0.224 and undamped natural frequency of ω_n=52.9 radians/s. These parameters are still used to evaluate the DRI of all seating systems with vertical accelerations. By conducting research on several age groups of USAF pilots, Stech and Payne derived a 50% probability of injury with the DRI of 21.3 [44]. Brinkley and Shaffer [45] later develop upon the work of Stech and Payne to relate DRI to the probability of injury. As shown in Figure 3.3, at 5% injury risk, is the DRI of 18, commonly used in literature and also adopted by the USAF. The North Atlantic Treaty Organization (NATO) conservatively set the design DRI threshold at 17.7, which corresponds to a 10% chance of suffering an AIS 2+ injury[1].

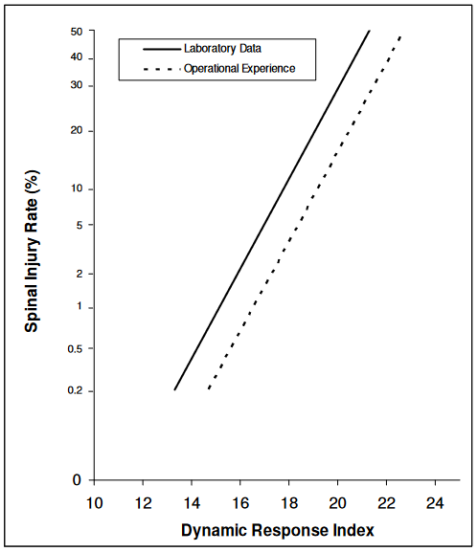

Figure 3.3: Probability of spinal injury estimated from laboratory data compared to operational experience[45].

The main downside of the DRI model is that it was developed on the test data of ejection seat tests in the 70s, which neglects the technological advancements of the past 50 years. Advanced seating cushions, safety restraint systems, or new anthropomorphic test dummies (ATD), though have little to no effect on DRI, would greatly improve the safety of occupants, especially around the lumbar area [42] [2].

[1] Abbreviated Injury Scale (AIS) is an anatomical-based coding system created by the Association for the Advancement of Automotive Medicine to classify and describe the severity of injuries

[2] ATDs measures the forces and accelerations experienced by the crash test dummy during crash events, and are capable of measuring the impact force exerted on the spine.

3.5.2. Loadings on Body Parts

Lumbar load

To mend the underperformance of DRI for lumbar injury on different body types, tests and simulations were done using seating systems with various-sized ATDs. The test results helped Joint Service Specification Guides (JSSG) devise lumbar criteria for maximum lumbar load on different body types. A lumbar load of 1500 pounds, measured by hybrid II ATDs, correlated with a DRI of 19, which means a spinal injury risk of 9%, is considered acceptable. Lumbar loading of 1500 pounds (453.592 kg) is also regulated under CS 25.562(c) provisions.

Femur load

Another loading that needs to be considered is the femur[3] load. Femur load regulations are common in the car industry, and the FAA determines that the axial loading on each femur should not exceed 2250 pounds (1020.583 kg)[46].

3.5.3. Head Injury

Under the provisions of CS 25.562, aircraft occupants need to be protected against head injury to prevent fatal accidents. The main criterion regulating head injuries is HIC, which is limited to 1000 units under regulations. HIC measures the injury risk of occupants based on the occupants' exposure to prolonged linear acceleration, which should be considered under the assumptions of this study.

$$HIC = \left\{ (t_2 - t_1) \left[\frac{1}{(t_2 - t_1)} \int_{t_1}^{t_2} a(t)dt \right]^{2.5} \right\}_{max} \tag{3.3}$$

Where

- t_2 and t_1 are any two arbitrary times during the acceleration pulse
- a(t) is the total acceleration which is measured in multiples of the acceleration of gravity (g), and time is measured in seconds

The HIC was developed from the New Car Assessment Programme (NCAP) tests conducted by the USA's National Highway Traffic Safety Administration (NHTSA). NHTSA proposed to limit this HIC time interval to 36 milliseconds in 1999 since the decrease in time interval also decreased the HIC unit. As shown in Figure 3.4, 700 unit of HIC_{15} correlates with 1000 unit of HIC_{36} at 1000[47]. Therefore, though the provisions in CS 25 and FAR 25 only limit the HIC to 1000 units without the limitations on time interval, it is assumed that it is HIC_{36}.

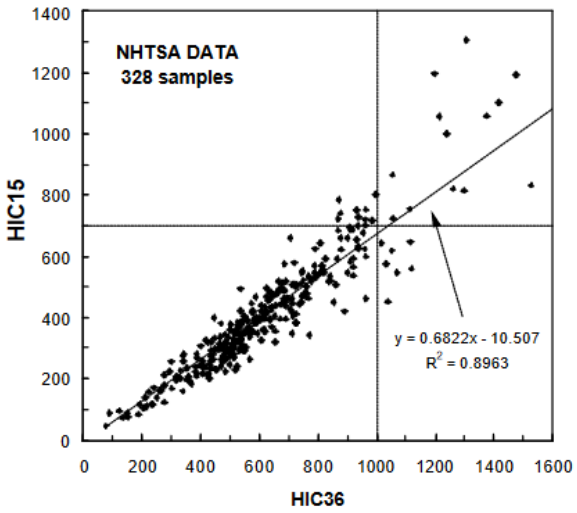

Figure 3.4: Comparison of HIC_{15} and HIC_{36} for NCAP data[47].

[3]Thigh bone

3.5.4. Neck Injury

Another critical injury risk is the neck area. Under the regulations of the FAA, aircraft with irregular design and seats not parallel to the centerline of the aircraft are subjected to the Side-Facing Seats Special Conditions [48]. The special condition of the side-facing seats indicates that the seating system must protect the occupant from experiencing serious neck injury.

Neck injury assessment will be conducted with deployed airbags unless the injury the occupants suffer is more severe before the airbag is allowed to deploy. There are two different types of regulated loading: peak loadings F_z and combined loading N_{ij}.

- $N_{ij} = \frac{F_z}{F_{zc}} + \frac{M_{ocy}}{M_{yc}} \leq 1$

    1. *The shear force (F_x), axial force (F_z), and bending moment (M_y) shall be measured by the dummy upper neck load cell for the duration of the crash event. Shear force, axial force, and bending moment shall be filtered for N_{ij} purposes at SAE Recommended Practice J211/1 MAR95 Channel Frequency Class 600.*
    2. *During the event, the axial force (F_z) can be either in tension or compression while the occipital condyle bending moment (M_{ocy}) can be in either flexion or extension. This results in four possible loading conditions for Nij: tension-extension (N_{te}), tension-flexion (N_{tf}), compression-extension (N_{ce}), or compression-flexion (N_{cf}).*
    3. $F_{zc} = 6806N$ *when* F_z *is in tension.*
    4. $F_{zc} = 6160N$ *when* F_z *is in compression.*
    5. $M_{yc} = 310N \cdot m$ **when a flexion moment exists at the occipital condyle.**
    6. $M_{yc} = 105N \cdot m$ *when an extension moment exists at the occipital condyle.*

- *Tension force (F_z), measured at the upper neck load cell, shall not exceed 4170 N (937 lbf) at any time.*
- *Compression force (F_z), measured at the upper neck load cell, shall not exceed 4000 N (899 lbf) at any time.*

4

Review of Crashworthiness of a Typical Section

Crashworthiness is the aircraft's ability to protect its occupants against serious harm in the event of a survivable crash. With the increase in the popularity of flying and the emphasis on passenger safety, rigorous experimental and numerical testing must be conducted at every level of the fuselage to ensure the safety of the occupants. To guarantee their protection, certifying and characterising the material, geometries, mechanisms, structure system, and, ultimately, the fuselage section is crucial. Due to the scarcity of literature on drop tests, especially for full-scale composite fuselage section drop tests, numerical simulation has become an important and effective tool for analyzing the crashworthiness of airframes and novel design solutions.

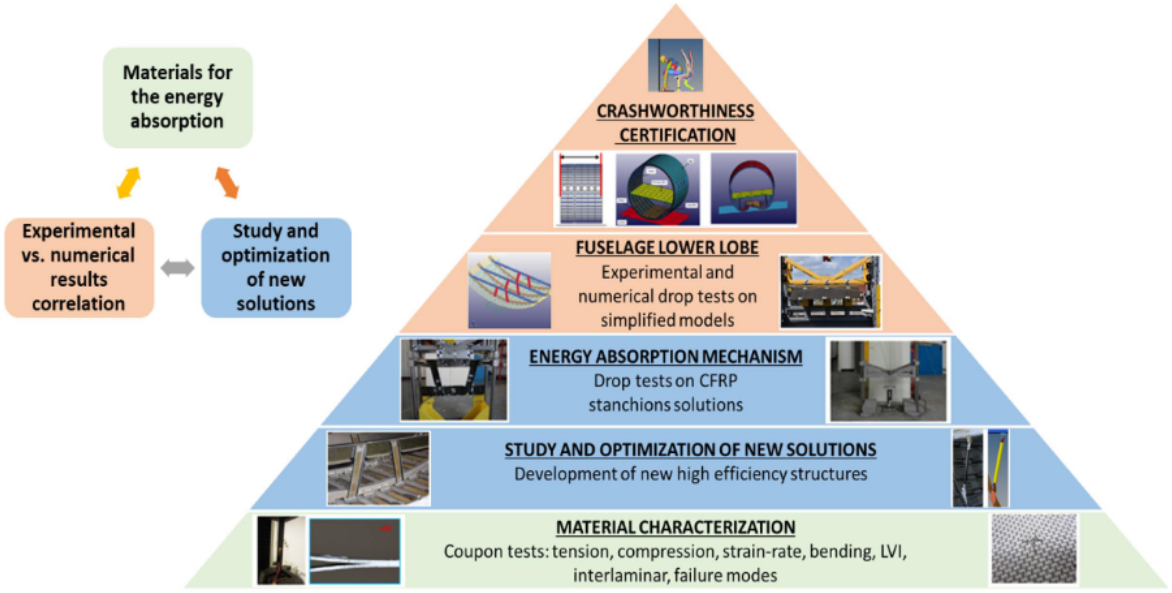

Figure 4.1: Building block approach[49].

This study focuses on reviewing the certification of a novel fuselage. As a result, the certification of the full fuselage section, the highest level, will be the primary area of focus in this chapter. However, a fuselage section is built from the structural components and the structural system, which would greatly affect the crashworthiness of the fuselage.

4.1. Introduction to fuselage crashworthiness

Crashworthiness is a complex attribute to be quantified, involving large deformations, material nonlinearity, and contact problems. The basic dynamic equation is as follows:

$$\sigma_{ij,j} + \rho f_i = \rho \ddot{x}_i + \mu \dot{x}_i$$

where σ_{ij} is the Cauchy stress, ρ is the density, f is the body force, $\ddot{x}_i$ is the acceleration, and $\dot{x}_i$ the velocity. Looking at the energy equation, E_{KE} is the kinetic energy, and E_g is the gravity force, which, added together, should equal the impact force E_F and the total energy loss E_{TL}.

$$E_{KE} + E_g = \frac{1}{2}mv^2 + mgh = \int Fds + E_{TL} \tag{4.1}$$

where m, v, g, h, F, and s are respectively the mass, impact velocity, gravitational acceleration, height change of the centre of gravity, impact force and impact displacement[50].

A typical aircraft fuselage section mainly comprises five structural components: frames, stringers, skin, stiff floors (cabin floor and cargo floor), and struts or stanchions, as shown in Figure 4.2. During an emergency landing, each component contributes to absorbing the impact energy through controlled structural deformation, crushing, and other failure modes, allowing for a gradual deceleration of the aircraft. It is also paramount that structural failures occur mostly beneath the cabin floor so that evacuation routes can be preserved and survivable conditions for the occupants are ensured. This analysis concept could be summarized into a stiff floor structure and the principal mass inertia directly above the crush zone. The safety cell above the stiff floor contains the principal mass inertia, representing the aircraft's occupants. The crush zone below the stiff floor can absorb impact kinetic energy by crushing[51].

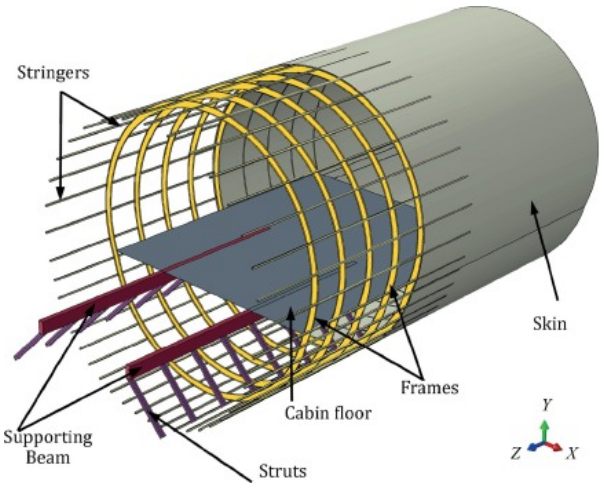

Figure 4.2: Typical fuselage section for transport aircraft[52].

Typically, there are two crash kinematic modes depending on the crash conditions and the fuselage configuration as displayed in Figure 4.3. These two kinematic modes are the unrolling mode and the flattening mode. These two dictate the crash sequence and post-crash forms. For the purpose of this study, the fuselage should be preserved, and thus, flattening crash behaviour is preferred.

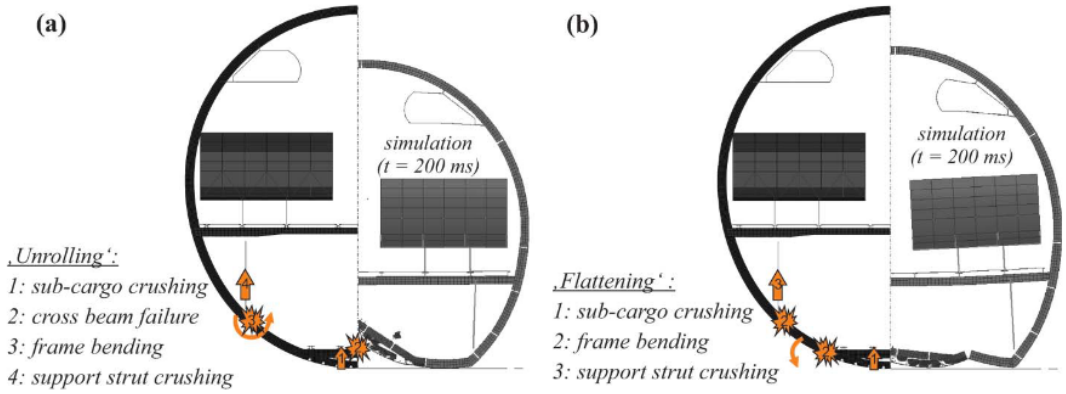

Figure 4.3: Cascading concepts based on typical fuselage section crash behaviour. (a) 'Unrolling' crash kinematics. (b) 'Flattening' crash kinematics.[18, 51].

The total energy of a system remains constant when we consider it as a whole. The components that contribute to this total energy are internal energy (E_I), energy dissipated by viscosity dissipation (E_V), energy dissipated by friction (E_{FD}), kinetic energy (E_{KE}), and work done by external loads (E_W). Viscous energy is the energy dissipated by damping mechanisms, such as bulk viscosity damping and material damping. It is a fundamental variable in the global energy balance, but it is not part of the energy dissipated through viscoelasticity or inelastic processes. In the context of a drop test, gravity loadings would represent the external loads. The sum of all these energy components is known as total energy (E_{total}), and it should always remain constant. However, in a numerical model, E_{total} is only approximately constant.

$$E_I + E_V + E_{FD} + E_{KE} - E_W = E_{\text{total}} = \text{constant} \tag{4.2}$$

The total internal energy of a system is the sum of the recoverable elastic strain energy (E_{SE}), the energy dissipated through inelastic processes such as plasticity (E_P), and the energy dissipated through viscoelasticity or creep (E_{CD}). Computationally, it's essential to take into account the artificial strain energy (E_A). This type of energy includes the energy stored in the hourglass resistances and the transverse shear in shell and beam elements. A high value of artificial strain energy indicates that the mesh needs refinement or other changes [53].

$$E_{IE} = E_{SE} + E_P + E_{CD} + E_A \tag{4.3}$$

4.2. Simulation methodology

Numerical analysis is becoming more common in certification procedures as the price and complexity of aircraft increases. With the advancements in commercial finite element methods (FEM) programs, design practices are becoming faster and more cost-effective than conducting physical experiments. By virtually testing different structural designs, numerical models can reduce prototyping and experimental testing costs. However, the complexity of composite properties and the nonlinearity of crash phenomena make analysis of aircraft fuselage complex. This section will provide a comprehensive overview of the modelling techniques used for the fuselage. Additionally, simulation methods for both metal and composite materials will be discussed, covering aspects such as plasticity and failure modelling.

4.2.1. Fuselage section modelling approach

Many computer simulation modelling approaches are currently being studied. However, none of these models is free from scrutiny and still requires testing and validation with drop-test data and/or validated data from previous studies. Analyzing structural deformation during crashes is complex due to factors like transient dynamic behaviour, complicated framework and shell assemblies, large deflections and rotations, extensive plastic deformation, damages, and component failures. None of the proposed modelling approaches can efficiently analyze detailed crash sequences with low uncertainty.

Finite element analysis
When analyzing structural deformation, FEM are one of the most detailed simulation methods, allowing for detailed simulation of structure and material behaviour. However, creating a model that accurately represents the fuselage structure requires a large amount of input data, which may not be fully available during the preliminary design phase of the aircraft. Additionally, the material formulations for CFRP used in the detailed FEM are not fully predictable. This means that the results of full FE analyses would have a significant level of uncertainty, especially in cases with no test cases to verify the numerical results of complex crash scenarios[54]. On top of that, conducting a detailed FEM analysis often demand a significant amount of computational capacity, making it a poor choice for preliminary design.

4.3. Crashworthiness of metal fuselage

Metal transport aircraft structures traditionally can provide sufficient crashworthiness even without a specific crashworthiness design; as a result, certification authorities did not typically require evidence of structural crashworthiness for metallic aircraft[55]. However, with the introduction of non-typical aircraft designs, like the one this study investigates, crashworthiness aspects have become relevant again for large fixed-wing aircraft. This section will cover a typical metal fuselage in subsection 4.3.1, followed by a closer examination of the F28 Fellowship aircraft, which is a full metal aircraft, in subsection 4.3.2, as drop test data for this model is widely made available by NASA.

4.3.1. Typical metallic fuselage

Xue et al.[56] present a general metallic aircraft crashworthiness study. The model is a three-frame, two windows section with vertical struts, cabin floor, and cargo floor support in the crush zone. The fuselage section was applied a vertical velocity of 9 m/s, with the ground modelled as a fixed, rigid plate. The model uses 2024 and 7075 aluminium as a material model. The model is shown in Figure 4.4. Generally, the cabin floor is where the passengers are located, and the cargo is placed beneath the cabin floor on top of the cargo floor. This is assumed to be an error by the author.

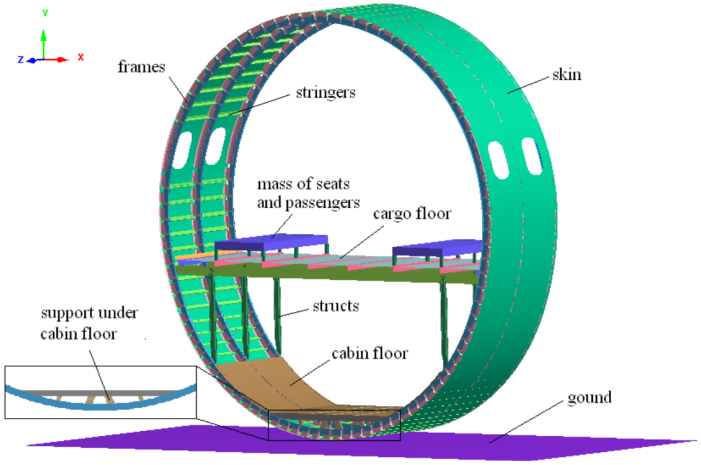

Figure 4.4: Geometry and numerical model of a fuselage section.

The acceleration is recorded at the seat positions, the data is filtered through the SAE CFC 60 filter, and the data is shown in Figure 4.5. The model at the peak of the acceleration data is shown in Figure 4.6. Significant events can be observed during the crash simulation at various time intervals. At approximately 17ms, the model initially makes contact with the ground, causing the first acceleration peak. Subsequently, at around 30ms, the fuselage experiences flexural failure below the cargo floor. The cargo floor support also fails, transferring stress to the cargo floor. As the crash progresses, the fuselage begins to ovalize, and the cabin floor starts to sag. Throughout this phase, the acceleration remains consistently low. Finally, around 110ms, stress concentration occurs at the base of the vertical struts, leading to another increase in acceleration, and at around 130ms, the struts come in contact with the ground, leading to the final stress peak. Unlike the previously mentioned crash scenario with a foam-like energy absorber under the cabin floor, the bottom fuselage deforms significantly. Leading to a

clearer crash sequence that pinpoints the key failure.

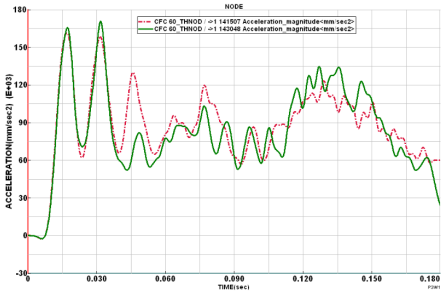

Figure 4.5: Geometry and numerical model of a fuselage section.

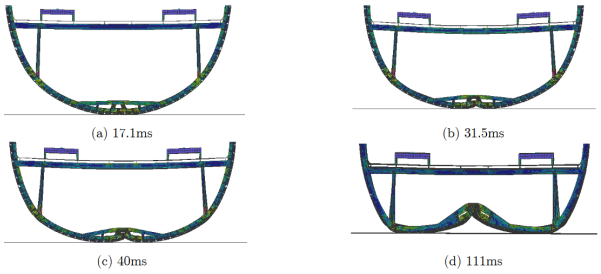

Figure 4.6: Model deformation sequence

Figure 4.7: Crashworthiness simulation[56].

Xue et al. also presented the energy-absorbing capabilities of each structural component. The frames play a crucial role in absorbing kinetic energy throughout the crash sequence. The frames ovalize and deform substantially until the struts contact the ground, absorbing significant energy. The skin and stringers are also constantly contributing to the energy-absorbing process. However, they are less effective due to their lower bending stiffness in the vertical direction. The cargo floor and support suffered a catastrophic failure, meaning it utilized all of its energy absorption capacity. However, this is only during the initial impact stage of the crash sequence, resulting in limited energy absorption. The energy-absorbing contribution of each component is shown in Table 4.1.

Table 4.1: Energy absorbing contribution of each component[56].

Part	Internal energy (kJ)	Percentage (%)
Frames	15.667	59.08
Skin and Stringers	3.607	13.59
Cabin floor	0.614	2.31
Struts	2.112	7.96
Cargo floor and its supports	4.332	16.33

4.3.2. F28 Fellowship Drop Test and Simulation

Drop test

Large-scale drop testing has decreased significantly since the early days of crashworthiness study due to the recent development in numerical simulation and the huge costs associated with a full fuselage drop test. One of the recent major drop tests is conducted by NASA and FAA in support of the Aviation Rulemaking Advisory Committee (ARAC) [1]. The test was conducted in 2017 on two fuselage sections of the Fokker F28 Fellowship, which is a single-aisle aircraft first launched in 1969, making it an all-metal aircraft. The test is done on the forward section and the wingbox section, with the forward section being a much more typical fuselage section, as shown in Figure 4.8a. This drop test is conducted to observe the structural response of the aircraft and occupant injury under severe but survivable conditions. This study will focus on the forward section because it represents better a typical fuselage section, being far enough from the wing stub structures, having a constant cross-sectional radius, and without large cutouts due to doors or emergency exits.

The forward section of the aircraft is situated between Fuselage Station (FS) 5803 and FS 7805 and comprises six frames and five windows, which is one of the most commonly used sections for drop tests. During this test, two rows of ATDs and seats are installed along with cargo, hat racks, floor panels, and the necessary sensors to measure accelerative data. The ATDs are installed to measure the accelerative data, while the cargo, hat racks, and floor panels are installed to simulate a real crash. This fuselage

[1]Created in 2015 by the FAA, which set its goal on generating recommendations on whole airframe crashworthiness and ditching requirements for transport aircraft [57].

configuration demonstrates the crashworthiness characteristics of a fuselage containing cargo in the cargo hold.

The section was elevated by 14 feet in the air and released to impact a 2-foot-high soil bed, with an impact velocity of 346.8 inches per second (8.81 m/s). In Figure 4.8, the photo of the section pre- and post-test are shown, with cargo, hat racks, floor panels, and ATDs removed.

(a) Pre-test. **(b)** Post-test.

Figure 4.8: F-28 forward section without hat racks, seats, ATDs, and floor panels[58].

As shown in Figure 4.8b, the structure exhibits bottom centerline failure at the lower frame, with the frame showcasing bending failure and flattening crash behaviour. The stiff floor also showcased multiple flexural and tensile failures on floor cross beams and seat tracks. These failures are caused by the ovalization of the fuselage, which forces the cabin floor to sag in the middle and causes the seats to roll towards the middle. Numerous plastic deformations could also be observed in the fuselage's crush zone, especially in the lower fuselage structure between the two vertical struts.

The F28's cabin cross beams sustained significant damage at the centre during this drop test setup, which could pose a safety hazard. This is particularly concerning for a single-aisle aircraft such as F28 as it may obstruct evacuation routes and fail to meet regulatory standards.

Simulation

Numerical analysis is also done with the same exact test setup. The luggage is represented with a large solid block, and the ATDs are replaced with a digital model, Livermore Software Technology Corporation (LSTC) Detailed FEM model, which is developed to simulate a Hybrid III ATD. As an initial simulation, the inertial properties of the seats, ATDs, and restraints were simplified and represented by concentrated masses. These masses were positioned on the floor to approximate the locations of the seat attachment points. An initial velocity of 346.8 inches per second (8.81 m/s) is also applied to all nodes. The model is placed directly above the simulated ground, fixed on all sides and bottom. Contact is also applied to prevent penetration of nodes to the element surface.

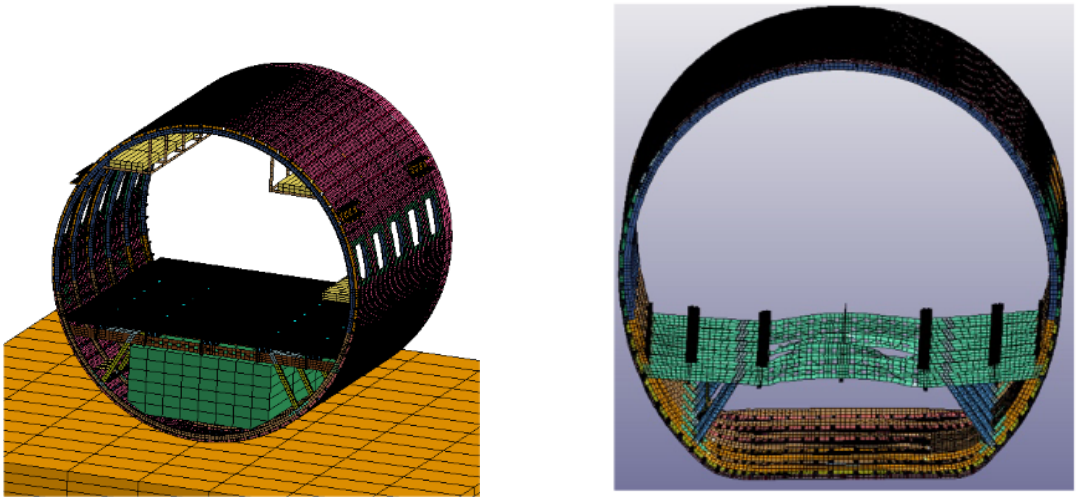

(a) Model of the F-28.

(b) Model photo at 0.038-s.

Figure 4.9: F-28 forward section numerical simulation[57].

As shown in Figure 4.11, the floor support structure shows multiple failures at 0.038-s. The failure is again most common in the central region of the cabin floor, though it is only plastic deformation without ultimate failure. What is interesting about the post-test model is the cabin floor arcs downwards in the middle. This is due to the drastic deformation of the luggage cargo model. On top of that, though the struts should not limit the cargo's deformation, it didn't deform past the struts.

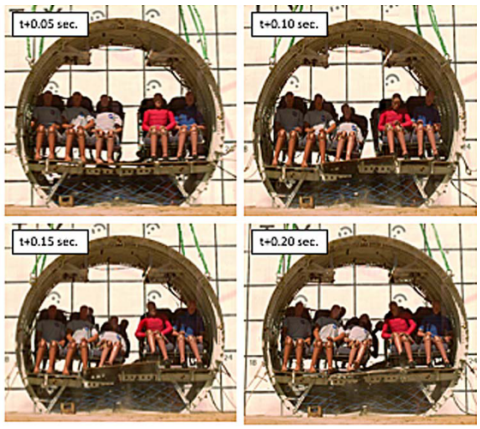

Figure 4.10: Impact sequence of the drop test.

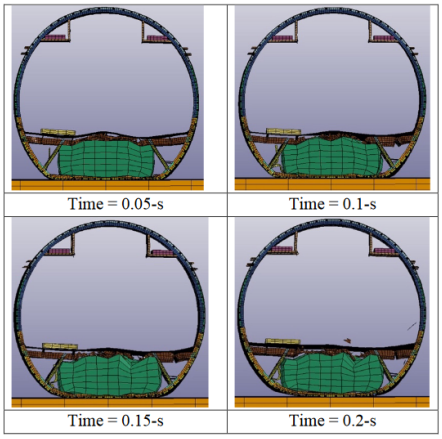

Figure 4.11: Model deformation sequence.

Figure 4.12: Deformation sequence[57].

Comparison and conclusion

Comparing the post-test fuselage, it is apparent that the cabin floors both suffer damage in the centerline. Unlike the real-life drop test, the floor of the numerical model is squeezed upwards due to the drastic deformation of the luggage. This suggests that the material property of the luggage is insufficient to simulate the luggage[2]. This leads to the cargo floor of the numerical model arcing downwards, which is different from the result of the typical fuselage of Xue et al. Both test articles suffer from flattening.

Acceleration data is recorded and compared from both ATD and simulation. The data is first filtered through SAE CFC 60 low-pass filter[3] to simplify the data. The acceleration data of the simulation

[2]The material model of the luggage is from quasi-static crush test of stacked luggage from Karen and Fasanella[59]

[3]SAE, formerly known as Society of Automotive Engineers, developed a series of channel frequency filter, CFC stands for Channel Frequency Class, CFC filter has a 3-dB limit frequency of 100 Hz, a stop damping of –30 dB, and Sampling frequency of at least 600 Hz[60]

generally agrees with the acceleration data of the drop test, both in frequency and general trend, especially before 0.075-s. The peak acceleration, in this case, is quite similar as well.

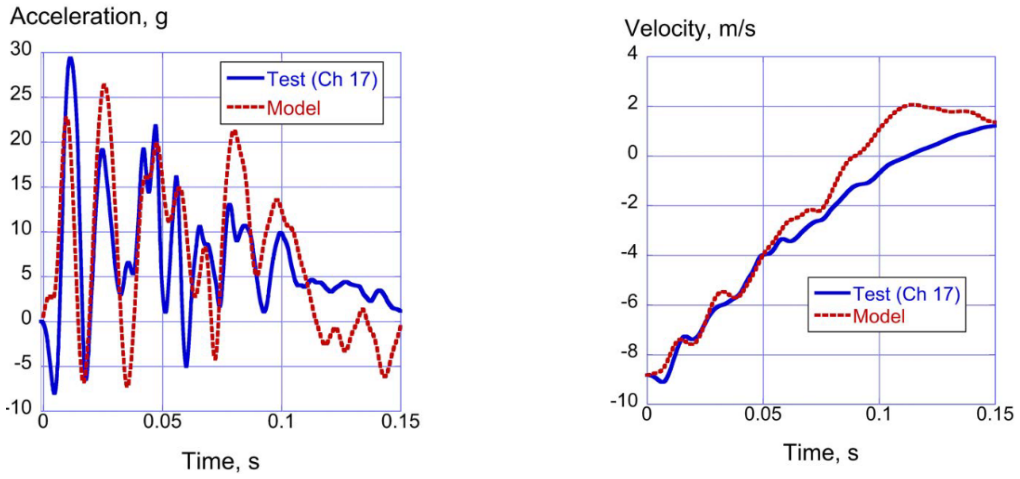

(a) Acceleration responses.

(b) Velocity responses.

Figure 4.13: Vertical acceleration and velocity comparisons at the starboard window at FS 5805[57].

The average acceleration was used to simplify the acquired data at each ATD position and each simulation mass point. The average acceleration stems from integrating the area under the acceleration curve divided by the time duration. The time duration is determined at the maximum vertical velocity. The result is shown in Table 4.2. It could be seen that all of the percentage differences in average acceleration are lower than 15%, which means that the test and the analysis could be correlated.

Table 4.2: Test-analysis comparisons[57].

Location	Average Acceleration, g		Percent Difference
	Test	Model	%
Port Window at FS 5805	7.4	8.1	9.5
Port Aisle at FS 5805	8.05	8.24	2.4
Starboard Window at FS 5805	7.5	8.5	13.3
Port Window at FS 6805	7.6	8.2	7.9
Port Aisle at FS 6805	9.2	8.1	11.9
Starboard Aisle at FS 6805	7.84	7.65	2.4
Starboard Window at FS 6805	7.7	8.47	10.0

Another detail of note is the effect of the cargo door, which is located on only one side of the fuselage. This induced an asymmetric deformation for the test section. But this phenomenon is not present within the numerical model, likely due to the deformed luggage[57].

Part II

Design Methodology

5

Aircraft retrofit conceptual design

This chapter proposes a design methodology for the retrofit based on packing solutions, where cylindrical tanks are packed within a designated volume (DV) under the constraints of the fuselage. The tanks are then filled inside a designed volume whose shape is based on their orientation to maximize the packing density.

Efficiently using the space inside the aircraft's fuselage to install hydrogen tanks is crucial for increasing the aircraft's operational capacity and ensuring the feasibility of the retrofit. Considering the low density of hydrogen and the complex conditions experienced by aircraft during crashes, the design methodology for retrofitting the aircraft with hydrogen tanks must account for multiple factors to determine the retrofit configuration. Firstly, we need to consider design assumptions due to uncertainties within the designs, such as the shape and sizing of the tanks, retrofit assumptions and limitations, tank crashworthiness considerations, and the aircraft for which the design is intended. Secondly, we need to determine the design methods for maximizing the utilization of available volume with tanks while ensuring crashworthiness. These two often can not be achieved at the same time due to the limited space within the fuselage, which will have to be distributed between the tanks, tank supports, and the crush zone.

5.1. Aircraft Orientation

Establishing an aircraft's global orientation is essential for effectively describing the design and analysis methods of the retrofit. The loading applied to the aircraft also needs to be clearly established to conduct the analyses accordingly.

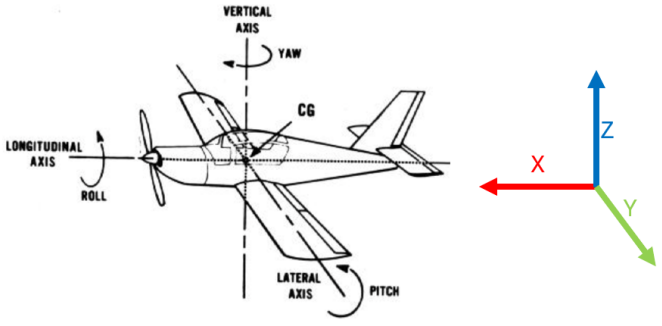

Figure 5.1: The flow chart of the design process.

With the longitudinal direction being assigned the x direction, the lateral direction assigned the Y direction, and the vertical, or vertical direction, assigned the Z direction.

5.2. Design baseline

Establishing a design baseline is crucial for minimizing the variables within a design and reducing the number of potential designs. This framework provides essential guidance for the design process, ensuring that feasible solutions are pursued while managing the complexity of the designs.

Among the assumptions that need to be set are the method and limitations of retrofitting and the allowed dimensions of the tanks. The method of retrofitting is set so that there could be a decreased consideration when it comes to possible designs and configuration. For instance, moving the cabin cross beams is determined to be crucial to allow for more space above the crush zone while strengthening the components and changing their size. However, this is deemed unfeasible due to the complexity of the retrofit operations that these changes will entail. Another possibility considered is the retrofit of the struts; this is deemed much more feasible. However, this is not considered to simplify the design.

5.2.1. Tank volume design assumptions

- Tanks are considered to be cylindrical with tank heads on both ends. This assumption is made so that the shape of the tanks can be predetermined.
- All tanks will be in the same orientations, lengths, and diameters. These assumptions are made to facilitate ease of retrofit and retrofitting. With the tanks being the same, the manufacturing of tanks can become much easier. With the tanks being in the same orientation, the retrofitting process should be simplified since the tank's support system and fuel systems can also be simplified.
- Tanks are required to have a smaller diameter than the door width to allow retrofitting to be done. By limiting the diameter, tanks could be easily transported through the preexisting openings of the fuselage and not require the retrofitting process to create a new opening, which would demand more certification process, which is not preferred.
- Tank fuel weight fraction (FWF) $\frac{W_T}{W_{LH_2}}$ is 0.4[61]. This number can range from 0.2[62] to 0.7 based on the volume of the tank and the S/V ratio of the tank. However, there is no clear explanation for the origin of these differences [63].
- The outer skin of the tanks will be used to represent the entire tank, and the hydrogen tanks are made of Al-2219-T87, with the skin thickness being 2mm [13].

5.2.2. Tank modelling

The chosen model for the tanks consists of an empty cylinder with heads on both ends. Cylindrical and spherical-shaped tanks have the lowest surface area to volume ratio (S/V), which gives them the lowest boil-off rate. Spherical tanks have the best S/V and are often used for large-volume storage because of their excellent mechanical strength. However, manufacturing and transporting spherical tanks can be challenging. Due to limitations on the maximum allowable diameter of the vessel, cylindrical tanks are preferred for transporting liquid hydrogen by trailers or railway cars. Cylindrical vessels with dish, elliptical or hemispherical heads also exhibit excellent S/V ratios, only about 10% [26] greater than that of a sphere. Therefore, cylindrical tanks are preferred over spherical tanks and other possible tank shapes.

The two heads are included to add a weight penalty to the tanks. The goal of implementing these designs is to develop retrofitting methods, regardless of the length of the fuselage converted for fuel tank storage. Technically, the tank heads should not be in the model, but they are included to give the tank a penalty in terms of weight. This penalty is more apparent when the implemented length is short, which is typically true for any pressurized tanks [63].

5.2.3. Retrofit design assumption

- The hydrogen tanks will be simulated using an empty cylindrical container. The weight will be applied according to the tank FWF. The weight would be the combination of the tank weight and the weight of the liquid hydrogen contained within the tanks. The simulation will disregard the hydrodynamic force and consider only the static and dynamic forces of the tank structure and the static forces of the fuel.
- No tanks will be designed in the vertical orientation to avoid bottom openings; this is done to prevent uncontrollable leaks, as leakage or damaged openings on the lower end would cause an

uncontrollable leak [64].

- All designed retrofitting parts, including the tank supports or components, should be small enough to fit through the door of the retrofitting aircraft. Components above the cabin floor must pass through the cabin door[1] while retrofitting components below the cabin floor will be transported through the cargo door.
- Cargo planes are not eligible for retrofit, even if they have cargo doors on the main deck. This is due to the fact that most cargo planes do not come equipped with windows, and lack of windows means that the structure is weakened in order to reduce weight[65]. This would result in a significant increase in certification efforts. While standards and regulations do not require passenger planes to have windows, it is generally expected that they are equipped with windows.
- Passenger aircraft with a cargo door on the main deck will be considered viable for retrofit.
- The existing primary structure, which includes the floor cross beams, frames, skin, struts, and stringers, of the aircraft could not be altered or removed. However, reinforcement could be added to strengthen the loading-bearing capacity or energy-absorbing capability of the aircraft. This assumption is set to limit the amount of effort that would be required during certification due to the removal or alteration of structural members.
- The remaining DV not used for housing tank supports or tanks is designated for fuel systems, inspection tunnels, electrical wiring integrated systems (EWIS), or catwalks. Drop tests typically remove components other than the primary structural systems, seats, and anthropomorphic dummies, and since this is a preliminary design, the fuel systems and catwalks will not be modelled. However, the tank supports will be modelled so that the acceleration data will be more accurate.
- All designs require similar development costs. The retrofit cost analysis will be conducted mainly using recurring costs, as it gets the lion's share in terms of total cost if the fleet size is of a respected size.
- The tanks should be larger than 400 mm in diameter. This is to decrease the total complexity of the fuel systems and decrease development cost, conversion cost, and equipment cost. Another reason for this assumption is smaller tanks will lead to a larger fuel tank weight fraction, which increases the tank weight per unit volume of liquid hydrogen fuel. Though the weight fraction is assumed to be constant in subsection 5.2.1, it is assumed that to cut down on the operating cost of the retrofitted aircraft as well as the equipment cost of the retrofitting operation, as mentioned in Appendix A, weight could be used as a preliminary estimation for equipment cost, the tanks are to be as large as possible under the constraint of the retrofitting aircraft.
- The designs should be as symmetric as possible to help with the stability of the aircraft.

Figure 5.2: Left: Kawasaki heavy industry concept design for liquid hydrogen carriers and on the right: Cryogenic trailer [66].

5.3. Aircraft retrofit design baseline

A validated numerical model is necessary to analyze the crashworthiness characteristics of a retrofitted aircraft's typical fuselage section and make retrofitting modifications to accommodate the liquid

[1] if the retrofitting aircraft is equipped with cargo doors above the main deck, the components could also be transported through the above floor cargo door

hydrogen tanks. The most cost-effective and time-efficient way to achieve this is to conduct a drop test of the typical section, for which the test results are already available, followed by the validation of the model. Once validated, the same modelling techniques can be used to perform a virtual drop test on the retrofitted typical section. There is a vast amount of readily available test data from various physical tests that have been conducted in the past, which can be used as a reference, as discussed in chapter 4.

Obtaining detailed computer-aided design (CAD) models of specific aircraft can be a challenge due to restrictions on intellectual property. This lack of reliable data, including skin thicknesses and cross-sectional dimensions of the structural elements, makes it challenging to develop a validated model. M. Desiderio [67, 68] developed a Fokker F28 Fellowship model based on the dimensions of the real-life F28 section possessed by TU Delft Aerospace Engineering Faculty. The model is then validated with probability with methods developed by Lyle et al. [69][2]. The F28 is a jet-powered regional airliner with dimensions and uses that fit the current trend of retrofitting regional airliners with hydrogen tanks.

Figure 5.3: The Air France Fokker F28-4000.

Though there are some discrepancies in acceleration data and minor differences exist between the model and the actual fuselage section, the post-test deformed shape is similar enough to the drop test and the model developed by Deciderio. The models are proven to be validated. Deciderio commented that the discrepancies in the energy data might be due to the overestimation of the thickness of the skin. However, this should have a negligible effect on the energy-absorbing capability of the entire fuselage[67]. The skin is the main energy absorber when the total drop energy is low since it is the first component to make contact with the ground. The added weight due to the increased thickness also has a negligible effect on the drop test since the total weight of the test envelope is significantly higher than the weight of the skin, meaning that the added energy due to increased thickness should not affect the total energy that needed to be absorbed by a significant margin.

Now that the baseline aircraft is decided, the designs can be applied to it. This model will undergo several tests and simulations using FEA to ensure that it meets the necessary standards and regulations introduced in chapter 3. This process helped to ensure that the Fokker F28 Fellowship aircraft met all the necessary safety and performance standards to ensure that the designs were applicable and could be certified. However, using the F28 as a baseline model also introduces certain presumptions, which influence the DV that is designated to be retrofitted; they are listed below:

- The model is a cylindrical typical fuselage section which is located before the tail of an aircraft with structural systems such as floor cross beams, frames, skin, struts, and stringers. The dimensions of the model are shown in Figure 5.4 and Table 5.1.
- Window cutouts in the fuselage skin are not included. This should not affect the results, as the windows are not located near the crush zone where energy-absorbing or stress concentration occurs.

[2]The mean acceleration of the drop test done by NASA, the upper bounds and lower bounds gained by conducting Monte Carlo simulation, and models developed by Deciderio are compared. There is a general correlation between the NASA physical drop test and upper and lower bounds. For further information, the dataset is available on `https://doi.org/10.5281/zenodo.7724227`.

- The fuselage length will be that of a six-frame model, the most commonly utilised test envelope for drop tests[70]. The total length of the six-frame of the F28 is 2.6 meters.
- The dimensions of the cabin door are estimated from Figure 5.5 to be 196 cm in height and 75 cm in width. This estimation is also based on the size of the door of the Fokker F27 Friendship aircraft, which has a 75 cm door width.
- The fuselage is made of aluminium alloy AA 2024-T3.

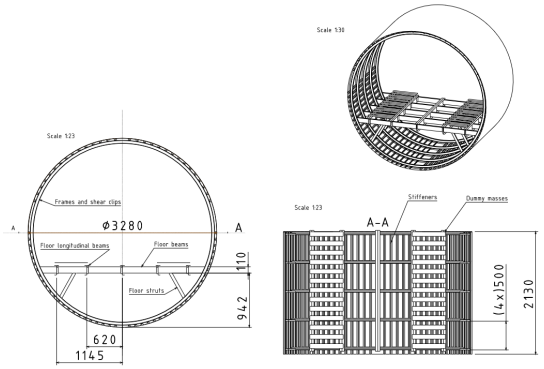

Figure 5.4: The fuselage dimensions of the validated model of the Fokker F28 Fellowship[67].

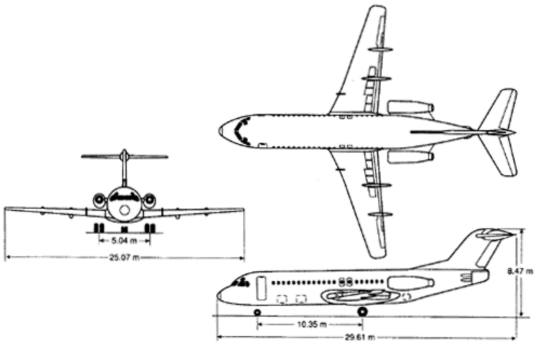

Figure 5.5: The dimensions of the Fokker F28 Fellowship [71].

Table 5.1: Thickness of different structural components, F-28 typical fuselage section[67].

Item	Shell thickness (mm)	Item	Shell thickness (mm)
Skin	1.5	Stiffeners	2
Frames	1.8	Shear clips	0.5
Floor struts	1.8	Floor trans. beams	1.8
Floor long. beams	1.8		

To ensure the drop test is conducted properly, the mass is compared since the input kinetic energy is dictated by the mass. It could be shown in Table 5.2 that the mass difference, though it exists, is only a 17 kg difference.

Table 5.2: Mass comparison between the two models.

	Desiderio's six frame model	Current six frame model
Mass	1475 kg	1458 kg

5.3.1. Verification of model

To guarantee the safety and efficacy of our designs, the designs will have to undergo analyses to ensure they adhere to safety regulations. As part of this process, a model of the F28 six-frame fuselage closely resembles Desiderio's validated model, which has already been tested against real-world drop tests and has proven to be a reliable benchmark. Therefore, any new designs implemented on this new model can be confidently applied to the actual F28 Fellowship.

However, to ensure the analysis results' accuracy and reliability, we must verify our new model against Marco's F28 model. This step will enable us to identify any inconsistencies between the two models and guarantee that our new model precisely represents the actual F28 Fellowship. By adhering to this rigorous testing and validation process, we can ensure that all designs implemented on the F28 six-frame fuselage are safe, effective, and dependable.

The new model is created with similar dimensions and is adapted from Lyle et al. [69], with only minor differences between the models, mostly stemming from rounding errors. The fuselage is modelled with

the same material model as the ones of Desiderio's model, with material later mentioned on Table 6.1 and Table 6.2. Steel is used for the dummy masses, applied using general steel material properties shown in Table 5.3. The purpose of these dummy masses is to simulate the weight and location of the weight of passengers; the weight would also added to the energy that needed to be dissipated by the components.

Table 5.3: Material model for steel [67].

ρ	E	v
7800 (kg/m3)	210 GPa	0.33

Drop test analyses are conducted to verify the F28 fuselage model against Desiderio's model. This is the most crucial test that needs to be conducted to ensure the safety of the passengers and tanks in case of a crash. The element size for each structural element of the verification analyses is shown in Table 5.4. The details of the analyses will be discussed in section 6.1. All drop tests will be conducted with an impact velocity of 9.14 m/s (30 ft/s).

Table 5.4: General element sizes for different structural components, baseline configuration [67].

Item	Element size [mm]	Item	Element size [mm]
Skin	40	Stiffeners	15
Frames	15	Shear Clips	12.5
Floor struts	10	Floor transv. beams	15
Floor long. beams	20	Dummy masses	40

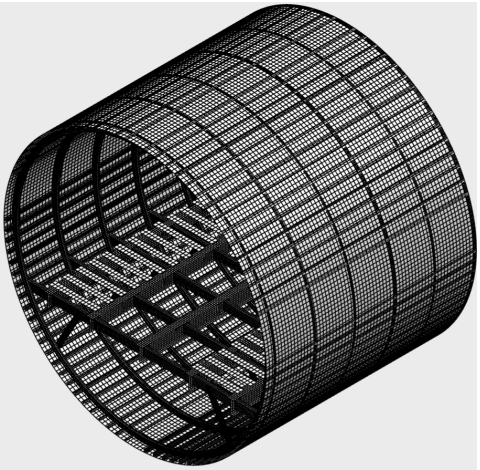

Figure 5.6: Desiderio's six frame model.

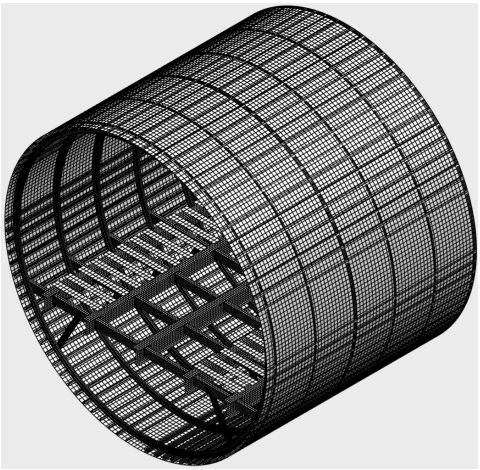

Figure 5.7: The newly created model.

To compare and verify the model, energy absorption of components and visual comparison will be utilized.

Comparison

Upon conducting a thorough visual comparison of the post-crash model, it was noted that the damage model is quite similar. Specifically, both models displayed initial flattening of the bottom fuselage, followed by the unrolling of the bottom fuselage approximately 0.02 seconds after impact. The frame began to bend upwards, resulting in hinges forming under the struts, eventually leading to the struts making contact with the ground.

Furthermore, the upper flange of the transverse beams showed multiple instances of crippling failures, particularly in the areas surrounding the inner longitudinal beams. These failures were due to localized compressive stress concentrations, which led to the distortion of the beams.

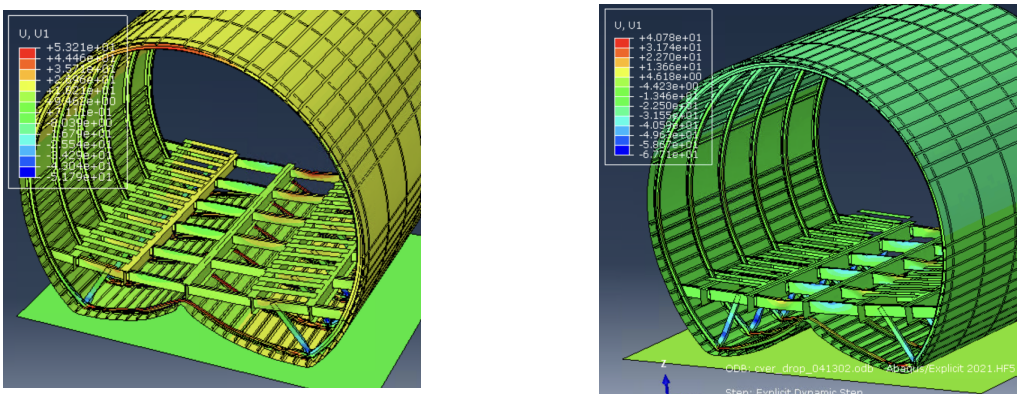

Figure 5.8: Crippling failure at the transverse cross beams, left being the model of Desiderio, M., and right is the newly created model.

Additionally, both frames displayed ovalization, and the transverse beams exhibited sagging. It should be noted, however, that the degree of ovalization and sagging of the transverse beam varied between the two models. This was attributed to the post-impact bounce back of the fuselage, which released the stored elastic energy within the frames. As a result, the lower frame opened while the transverse crossbeams sagged less, thereby opening up the fuselage.

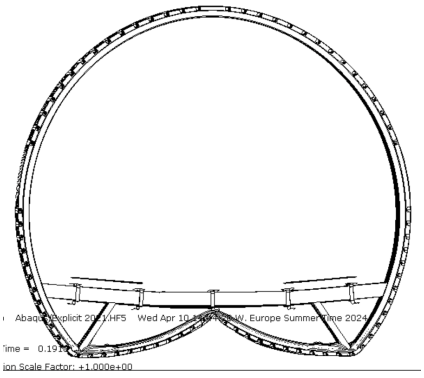

Figure 5.9: Post crash of Desiderio's six-frame model.

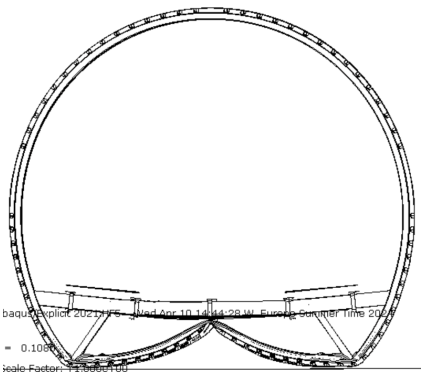

Figure 5.10: Post crash of created six-frame model.

In summary, both models displayed identical crash sequences, with similar damage sustained at the transverse beam flange, and exhibited similar crash behaviour. There were no observable issues with the tie constraints used to simulate the riveted locations, and the impact interaction property appeared to function as intended.

Plastic energy time history

Upon analysis of the plastic energy dissipation history of each component, it is apparent that the six-frame model we created is capable of absorbing energy through plastic failure, similar to the model created by Desiderio [68].

Both models exhibit similar behaviour in terms of plastic dissipation energy following an impact. In each model, the struts impact the ground due to the failure of the lower fuselage. The plastic dissipation energy of the struts peaks at approximately 0.06 seconds, and the initial impact energy is fully dissipated by around 0.08 seconds. This means that the two models experienced similar crash sequences and crash duration.

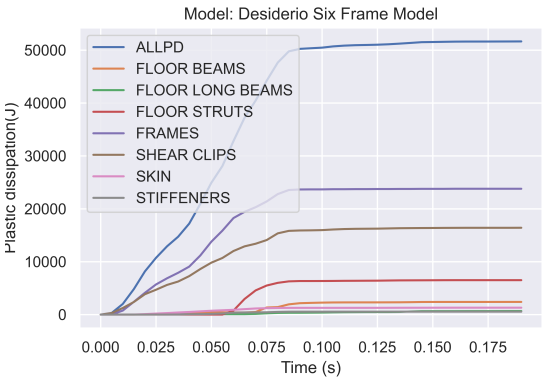

Figure 5.11: Plastic energy dissipation of Desiderio's six frame model

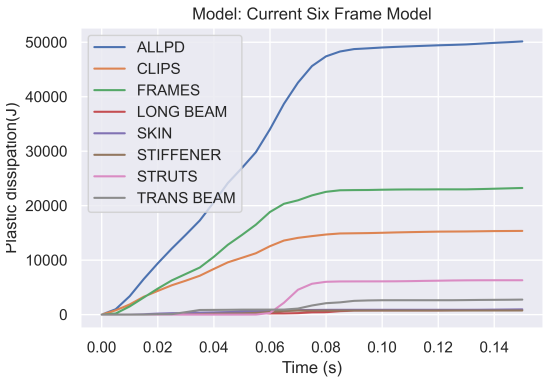

Figure 5.12: Plastic energy dissipation of created six frame model

It is worth noting that there is a slight discrepancy in the total plastic dissipation energy between the two models, which may be due to minor differences in total mass. Additionally, the total calculation time of the analyses varies as the components continue to plastically deform under the force of gravity acting on the fuselage after the impact, resulting in further plastic energy dissipation.

The plastic energy absorption of each component also showcased similar results in terms of the fraction of total energy absorbed. Each component experienced similar plastic deformation by percentage, as shown in Table 5.5. With the material model between the two being the same, this also means that each component is comparable to Desiderio's model, with the difference in terms of total energy absorbed by each component at less than 2%.

Table 5.5: Plastic dissipation of each component between the two models

	Desiderio's six-frame (J)	Percentage	Six frame (J)	Percentage	Difference
Frames	23790.1	46.06%	23264.4	46.39%	0.33%
Clips	16416.5	31.79%	15359.5	30.63%	1.16%
Skin	1305.5	2.53%	959.4	1.91%	0.62%
Stiffeners	556.3	1.08%	753.9	1.50%	0.32%
Struts	6509.6	12.60%	6304	12.57%	0.03%
Longitudinal beam	674.2	1.31%	771.2	1.54%	0.23%
Transverse beam	2394.9	4.64%	2751.5	5.49%	0.85%
Total Plastic Dissipation	51647.1	100.00%	50153.2	100.00%	

To sum up, it could be argued that both models showcased similar energy-absorbing capabilities in total energy and each component's capability. This includes the total energy absorbed by each component and the time when each component starts to absorb energy.

5.4. Design methods

The design process can commence once the design limitations and the baseline aircraft have been established. The designs are based on packing solutions. As mentioned in subsection 5.2.3, the design focuses on two main tank orientations: lateral and longitudinal direction, with vertical orientation, recommended not to be designed. The lateral orientation is along the width of the fuselage, while the longitudinal orientation is along the length. The proposed design must comply with the regulations and constraints listed in chapter 3 and assumptions listed in section 5.2.

The design method will involve two main designs: the tank configuration design and the support design. The tank configuration design will utilize packing problems, which are often used in real-life packaging, storage, and transportation problems. After the tanks are in place, the supports will need to be designed to support them within the fuselage.

The design would then be applied to the fuselage, as shown in Figure 5.13. Color coding is added so that the components can be easily identified. Without the heavy dummies within the fuselage, the empty weight of the fuselage totals 248kg.

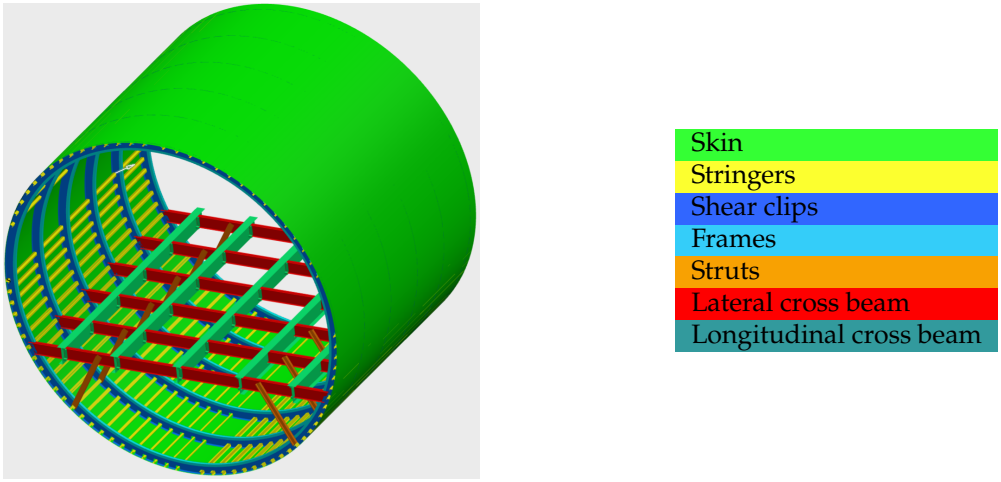

Figure 5.13: The newly created model with color coding.

Weight is especially important since it increases the total kinetic energy that is required to be dissipated by the structure.

5.4.1. Tank configuration design methods

Packing problems are optimization problems in mathematics that involve fitting objects into containers. The goal is to either pack a single container as densely as possible or pack all objects using as few containers as possible.

The thesis addresses the design challenge of fitting as many tanks as possible within an aircraft's fuselage and flying with these tanks on board—in other words, transporting tank objects of the same dimensions in a cylindrical fuselage container. Each design highlights a different packing problem, which will be later explained in each methodology.

The 3D packing problems can be simplified by treating the fuselage and the tanks as 2D shapes. The tanks can be represented as a circle along their length, and by following the orientation discussed in subsection 5.2.3, the fuselage can be viewed as a circle from the longitudinal direction and as a rectangle from the side. This tank configuration design, then, can be treated as a circle packing problem.

A circle packing is a layout of circles inside a given boundary such that they do not overlap and some or all of them are tangent to each other. These arrangements correspond to tessellations of regular polygons. There are two typical types of circle packing: hexagonal packing and square packing. The densest packing of circles in the plane is the hexagonal packing, which is commonly seen in the lattice of a honeycomb created by bees [72]. Meanwhile, the square packing allows the best solution for unloading and offloading the tanks with ease, potentially allowing the possibility of interchangeable fuel tanks. This allows the turnaround time to be reduced, meaning that the liquefied hydrogen does not need to be stored on-site near the airport.

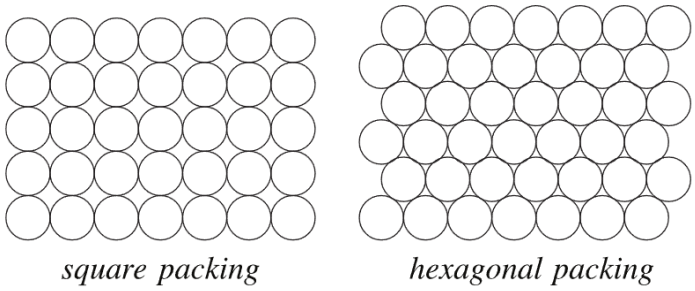

Figure 5.14: Circle packing in a plane [72] .

Each packing solution must take into account a DV determined by the orientation of the tanks. This is necessary because the typical fuselage is not a simple shape, and the 2D designs must conform to the actual fuselage. The DV is based on specific design parameters derived from the baseline aircraft. Tanks must be located within this DV, while any volume outside of the DV can be used for tank supports or other purposes.

Another thing to note is that it's clear that the tanks with infinitesimally small radius would provide the best packing density, approaching 1, the maxima. However, as mentioned in section 5.2, this solution is not feasible due to the excessively heavy aircraft it would lead to. The smaller tank diameter will lead to a much higher tank FWF due to higher S/V. The increased amount of tanks would also lead to much more complex fuel systems and retrofitting processes, leading to an increase in the total cost and weight of the system.

5.4.2. Supports designs

The supports are designed to be mounted within the fuselage to support the tanks during flight and to help them avoid damage and possible fires. They act as the principal shock absorbers for the tanks during crash tests, and their main purpose is to hold the tanks in place so that scrapping or penetration won't occur unless a catastrophic event happens.

The supports for the tanks will be designed to take into account the door's limitations. This means that the size of each component will be carefully considered so that it does not exceed the door's size. If any component is larger than the door, it will require more procedures and assemblies in the limited space within the fuselage, which will increase the total time of the retrofit and incur a penalty on the cost of the retrofit.

The primary objective of the support design is to hold the tanks in place to avoid scrapping with the fuselage and to simulate the effect actual support would have on the tanks during a crash event. As such, all the supports will be designed conservatively, at 4mm in thickness, without considering any detailed designs, such as hole cutouts for fuel systems, electrical wiring interconnect systems and catwalks, as these are beyond the scope of the support design and this thesis. This would also result in a much stiffer support, which would get higher peak acceleration. This would have an effect on the peak acceleration experienced by the tanks. This means that acceleration-related injury indexes such as DRI and Eiband injury criteria will be harder to account for. However, as stated in subsection 3.3.2, the tanks are required to survive the loading conditions under a crash and not the human injury criteria itself.

5.4.3. Design parameters

Several parameters constrain the total DV within the aircraft and are used as design constraints. Among these are the permissible length (P_L) [3], floor width (F_W), floor height (F_H) [4], door width (D_W), door height (D_H), and inner frame radius (r_{IF}), along with a safety spacing of 10mm to account for deformation during ground impact or large acceleratory loadings. These parameters limit the design space within the fuselage so that the tanks don't directly impact each other or decrease their impact during drop tests

[3]The total length of the fuselage allowed to be designed, as mentioned in section 5.2 will be the length of the six-frame fuselage

[4]the height of the floor above the mid-point of the frame

or in particular load cases.

Table 5.6: Design parameters

P_L	F_W	D_W	D_H	F_H	Spacing	r_{IF}
2600 mm	2880 mm	750 mm	1800 mm	980 mm	10 mm	1550 mm

5.5. Longitudinal retrofit design

Using a typical fuselage section has several advantages, including maintaining structural consistency throughout its length. This allows longitudinal packing solutions to simplify the retrofit design into a 2D process. Since the aircraft is usually longitudinally oriented, most of the available volume within the fuselage can be used to house hydrogen tanks and their supports.

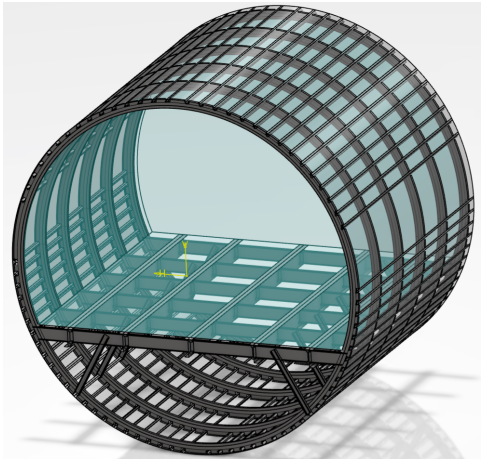

Figure 5.15: The DV for longitudinal orientation, in aqua.

However, the entire designed volume for the tanks and the door height restrictions make it more complex to retrofit with longitudinal packing. This is because it aims to use the entire height of the fuselage, requiring the associated supports to reach the same height. The restrictions introduced by the dimensions of the door can potentially increase the complexity of the retrofit. Additionally, using the entire volume as the DV would leave no space for other fuel systems, such as fuel systems and the catwalk, and increase the difficulty in the retrofit due to decreased space to manoeuvre the tanks around at the later stage of the retrofit.

Furthermore, longitudinal tanks also need to contend with turning the tanks after they are moved through the doors. This will involve heavier machinery required for the operation, which will heighten the cost of retrofitting.

5.5.1. Longitudinal circle packing concept

When looking at the fuselage longitudinally packing from the front, both the typical cylindrical fuselage and the cylindrical tanks can be considered circles. This equates to the classic packing problem of packing equal circles in a circle. Solving this problem is computationally challenging, with the solution for the larger inner circles (or the lowest amount of inner circles) being well studied and documented [73]. To utilize this already-solved problem, we need to determine the radius ratio between the inner and outer circles. Thankfully, the design parameters serve this purpose.

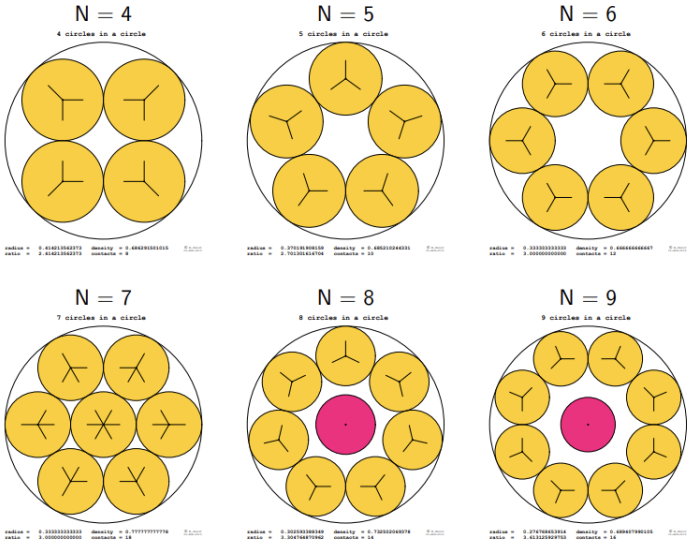

Figure 5.16: Circles packing in circle solutions for the number of inner circles from 4 to 9 [74].

The inner frame radius and the skin constrain the packing solution's outer diameter. As a result, we will opt for the smallest radius between these components, which is the inner frame radius r_{IF}. The size of the tanks is limited by the door, which determines the size of the inner circles. Assuming we want to maximize the tank size, the diameter of the tanks is determined by the smaller of the door's width or height. In this case, the width of the F28 fellowship aircraft is the smaller dimension. The ratio can then be calculated using Equation 5.1.

$$\begin{aligned} r_{IF}/r_{tanks} = ratio, \quad r_{tanks} < \frac{D_W}{2} \\ r_{IF}/ratio < \frac{D_W}{2} \end{aligned} \tag{5.1}$$

By selecting a design that has a slightly higher inner circle diameter and then decreasing the diameter down to the constraint of the doors, it is possible to maximize the diameter of the tanks while ensuring that the configuration will still be viable. In contrast to picking the design with a smaller diameter, it is impossible to increase the tank diameter since the tanks are already tightly packed, so therefore it is impossible to maximize the tank diameter. This method would maximize the tank diameter while keeping the number of tanks minimum, as assumed in subsection 5.2.1.

With the calculated outer-to-inner circle ratio being 4.133, the chosen solution for the baseline regional aircraft has a ratio of 4.029, with 12 inner circles. This would allow for the packing of 12 tanks, as shown in Figure 5.17.

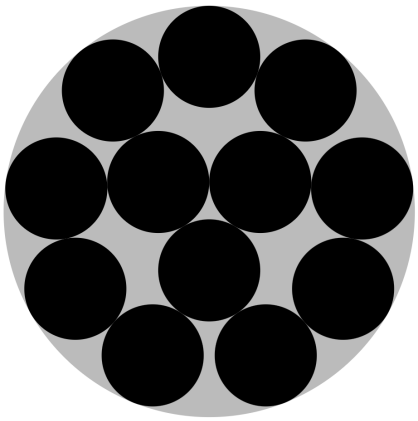

Figure 5.17: The Longitudinal packing solution for 12 tanks [75].

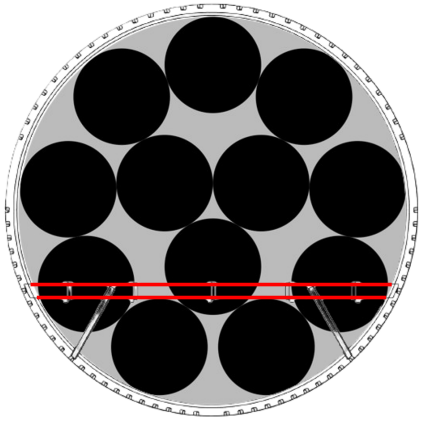

Figure 5.18: Longitudinal packing solution due to floor limitations.

This design allows maximum volume utilisation for liquid hydrogen storage since the packing solution utilizes both the shape of the fuselage and the shape of the tanks while fully utilizing the entire retrofittable fuselage volume, meaning above the cabin cross beam. This design is also the best to scale up or down the length of the fuselage to be designated for tank storage by the customer's demand since no matter the length of the retrofitted length, the supports and the packing solution stay the same.

However, As shown in Figure 5.18, the packing plane for this design case is a circle with a disc trimmed due to the limitations of the cabin cross beams. This means that this packing solution for 12 tanks can only fit in 7 of the tanks due to the limitations of the cross beams.

Due to the lack of packing methods outside of computational methods for packing circles in an arbitrary shape, the best solution for this method would still require careful estimation of the best packing solution chosen from the diameter ratio.

This packing solution would result in a total of 7 tanks, each with a radius of 375 mm and a tank length of 2600 mm. This would result in a packing density of 56.79% and a tank plus fuel weight of 786.6 kg.

Support

The longitudinal circle packing configuration is quite complex due to the shape of the DV. The tanks are positioned randomly, posing a difficulty in providing them with support through floor cross beams. Given the limitations of the available space and the height limitations imposed by the dimensions of the door, the top and bottom sections of the plate had to be trimmed. In addition, holes were cut into the plate to accommodate the tanks. Flanges were also included to extend from the holes and offer added stabilization to the tanks, preventing bending, twisting, or puncturing by sharp edges. The flanges could also facilitate the even distribution of the loading on the tanks. Since the tank configuration is wider than the tanks themselves, and due to the trimming of the plate, the plate could not be supported by the floor cross beams. Thus, the plates have to be secured to the fuselage by connecting to the frames. This led to a design that is showcased in Figure 5.19.

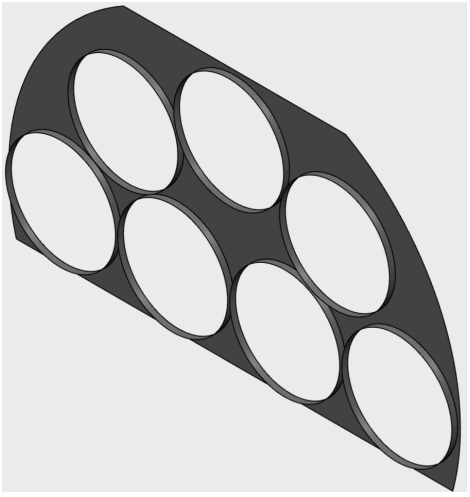

Figure 5.19: Lateral hexagonal packing as seen in the lateral direction, the outer bounds are the size of the DV.

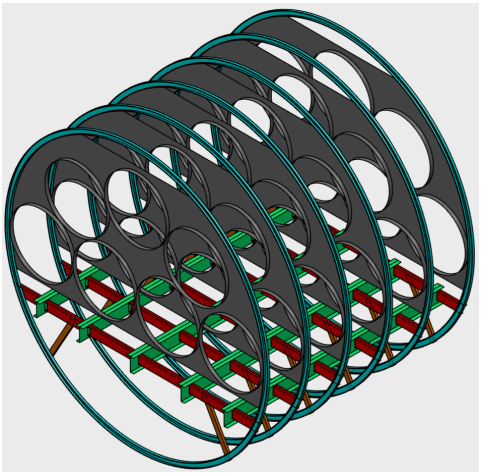

Figure 5.20: Lateral hexagonal packing as seen in the fuselage.

By applying this plate to every frame in the six-frame fuselage, the support applied is shown in Figure 5.20. This support should be able to accommodate different packing solutions designed for different diameter ratios. The main change would be the limiting door dimensions. If the total utilized height is taller than the diagonal length of the door, the installation of the plate would have to be considered.

This support design would result in a total support weight of 158 kg.

5.6. Lateral retrofit design

Lateral orientation is inherently worse than longitudinal orientation for tank designs since the fuselage itself is not in the lateral orientation. With the tanks being limited to the same dimensions and orientations, the fuselage's changing width with height increase will force the DV of the lateral-oriented tanks to be a rectangular cuboid volume. This would leave gaps between the frames and the DV, which would not be utilised for storing liquefied hydrogen.

However, laterally aligned designs have a few distinct advantages compared to longitudinal orientation designs. Due to the orientation of the doors being in the lateral direction and their primary use of being the main opening during retrofitting, the installation of tanks could be easily done. Since no manoeuvring of the tanks is required, lighter or less complex machinery could also be utilized. This will decrease the cost of equipment and the amount of time required to conduct the retrofitting.

It is also assumed that the tanks in lateral orientation could be installed on the cross beams, which requires the smallest amount of certification process since the floor cross beams serve the same purpose of being able to carry the vertical load. This would again decrease the development cost required.

To simplify the lateral orientation tank designs into 2D designs to conduct packing analysis, when viewed from the side of the fuselage, the fuselage resembles a rectangle. However, unlike the longitudinal orientation, the profile across the width of the fuselage is not consistent. As the height increases, the width decreases. With the design of the tanks being enforced to the same size and orientation, a tank of a certain length can only fit at a certain height of the fuselage. The DV can then be seen as a rectangular cuboid volume bounded by the curvature of the frames, cross beams, and skin of the aircraft. The DV could be shown with Equation 5.2 and Figure 5.21.

$$\begin{aligned} DV_{Wmax} &= F_W \\ DV_{Hmax} &= 2 \cdot r_{IF} - F_H \\ DV_L &= P_L \\ DV_W &= F_W \cdot \theta \\ DV_H &= r_{IF} \cdot (1 + sin\theta) - F_H \\ \theta_{min} &= cos^{-1}(\tfrac{F_H}{2 \cdot r_{IF}}) \end{aligned} \tag{5.2}$$

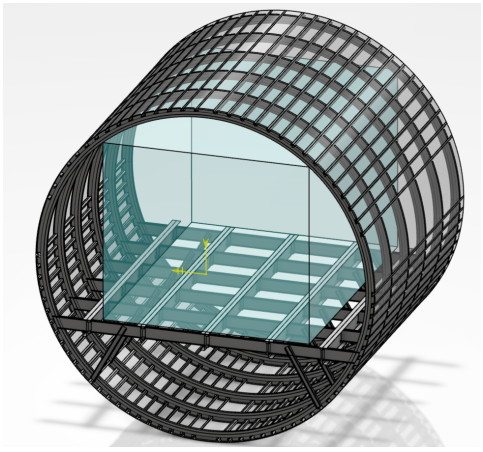

Figure 5.21: The DV for lateral orientation

5.6.1. Lateral hexagonal packing concept

This method tessellates the square DV by using hexagons. Hexagon packing is the densest packing solution for all circle packing solutions when packing in a plane [76], with a packing density of 90%. With the DV being in the shape of a rectangle, this solution should provide the best packing solution in the rectangle.

The design process begins with a minimum tank diameter of 400mm to ensure the tanks are not too small. Equation 5.2 is used to determine the size of the DV per degree, which then provides the height and width of the DV while keeping the length fixed. Each degree of DV is then optimized using hexagonal packing in the lateral direction, and the total volume of the tanks can be calculated using the DV's width, the diameter of the tanks, and the total number of tanks. The total number of tanks could be calculated with Equation 5.3. X represents the number of tanks along the length of the fuselage, while Y represents the number of tanks along the vertical direction of the fuselage. E can be either 0 or 1, depending on whether the odd-numbered row of tanks has the same number of tanks as the even-numbered row, and N represents the total number of tanks.

$$\begin{aligned} L &= X \cdot D + E\cdot \\ H &= D \cdot [1 + \tfrac{\sqrt{3}}{2}(Y-1)] \\ \theta &= cos^{-1}\tfrac{(H - r_{IF} + F_H)}{r_{IF}} \\ W &= 2(H - r_{IF} + F_H)\tfrac{cos\theta}{sin\theta} \\ N &= (X-1)\cdot Y + E \cdot Z(\tfrac{Y}{2}) \\ V_{tanks} &= 2\pi(\tfrac{D}{2})^2 \cdot W \cdot N \end{aligned} \tag{5.3}$$

By utilizing the L, H, and W values from the equation, we can match them with their respective DV. This will enable us to determine the optimal solution for the total volume of the hydrogen tanks. As a result, the diameter is calculated to be 518mm, factoring in spacing, which ultimately yields an actual tank diameter of 498mm and, in total, 14 tanks. The results are shown in Figure 5.22 and Figure 5.23.

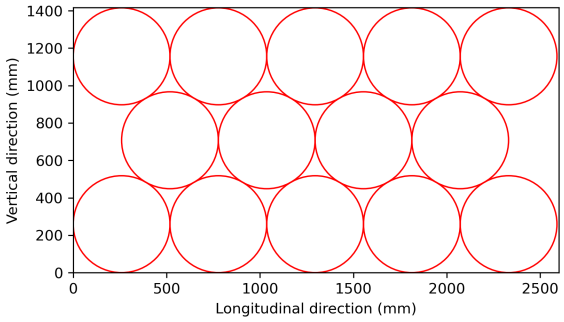

Figure 5.22: Lateral hexagonal packing as seen in the lateral direction, the outer bounds are the size of the DV.

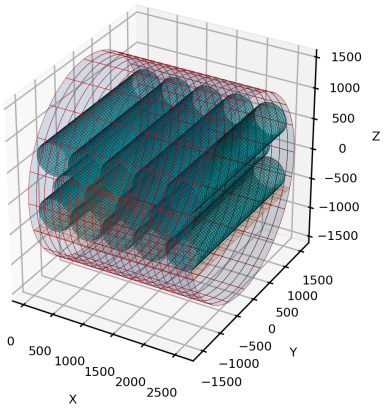

Figure 5.23: Lateral hexagonal packing as seen in the fuselage.

This packing solution would result in a total of 14 tanks, each with a radius of 249 mm and a tank length of 2570 mm. This would result in a packing density of 49.57% and a tank plus fuel weight of 686.8 kg.

Supports

The DV for lateral tanks is designed so that the supports can be installed on the floor cross beams. A plate is designed to have the height and length of the DV. This means the plate has the same height as the DV, and the plate of the plate is the length of the DV. Hole cutouts are applied for the hexagonally packed tanks, and flanges are designed. For added stability, a flange is attached to each cutout. Finally, a shell can cover the longitudinal beam shells on both sides, providing additional support. This results in a plate that is shown in Figure 5.24. This plate is then designed to be placed on each of the longitudinal beams.

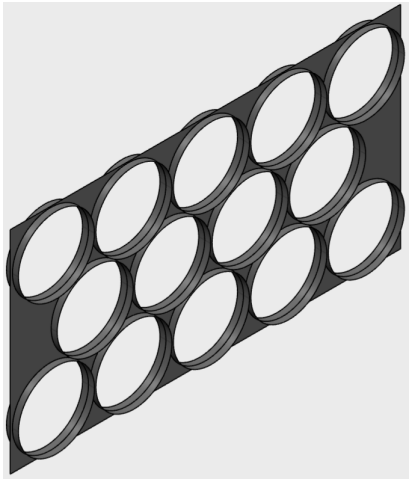

Figure 5.24: Lateral hexagonal packing as seen in the lateral direction, the outer bounds are the size of the DV.

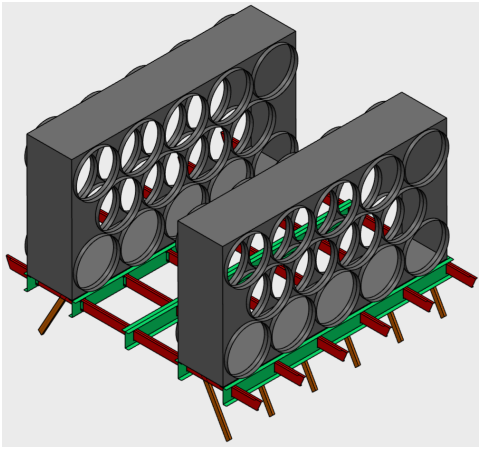

Figure 5.25: Lateral hexagonal packing as seen in the fuselage.

To provide lateral stability and resistance against rotation, an additional layer of support is necessary, as there is no support in the lateral direction. In this regard, a shell can be created to cover the two plates on either side, while removing the middle plate from the design. This design allows the inspection of the tanks to be more comfortable. By enclosing the two plates on either side, the tank can be accessed from the sides, and the tank heads will remain accessible. The ultimate goal of this design is to provide access to the tank in the middle section. When the plates and the shells are assembled into the fuselage, it results in the design shown in the Figure 5.25.

This support design would result in a total support weight of 169.2 kg.

Other packing method

Computational discrete conformal mapping could produce packing solutions with better packing density than hexagonal packing for a specific size rectangle when paired with a specific size circle [72]. However, it requires significant computational power, and the solution would require a change in the tesselation pattern. Specht, E. develops another method by first hexagonally tesselating the rectangle until it could no longer fit in more tanks, then the method tries to locate vacancies and then optimising the vacancies to pack more circles. The packing solution can be seen in Figure 5.26.

However, this method also disrupts the established patterns from tessellation, as shown in the right side of Figure 5.26, making it challenging to manufacture tank supports when the retrofitted length alters. This becomes especially problematic when considering changes in size due to the curvature of the frames.

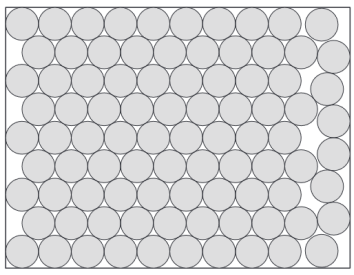

Figure 5.26: The Lateral computational packing [77].

5.6.2. Lateral square packing concept

Lateral square packing is a method of tessellating the rectangular DV with squares by treating the circles that the tanks represent as squares, where the square can not rotate [5]. It has the unique advantage of pre-aligning all the tanks, making them easily packable and transportable. All the squares are aligned both in columns and in rows, which makes it possible to swap the tanks without difficulties, assuming that the supports and tanks need to pass through the cabin door. This also means that the tanks don't need to be permanently installed in the fuselage. The retrofitting effort will focus on finding ways to strap down the tanks and their support.

To concisely pack the tanks and their support inside the fuselage, the matching dimensions must be adjusted using the same equations for DV. The equations for the square packing solutions are presented below in Equation 5.4. Here, X represents the number of tanks along the length of the fuselage, while Y represents the number of tanks along the vertical direction of the fuselage, and D represents the diameter of the tanks. N equates to the total number of tanks with square packing solutions.

$$\begin{aligned} L &= X \cdot D \\ H &= Y \cdot D \\ \theta &= cos^{-1}\frac{(H - r_{IF} + F_H)}{r_{IF}} \\ W &= 2(H - r_{IF} + F_H)\frac{cos\theta}{sin\theta} \\ N &= X \cdot Y \\ V_{tanks} &= 2\pi(\frac{D}{2})^2 \cdot W \cdot N \end{aligned} \tag{5.4}$$

This would net a packing solution as shown in Figure 5.27 and Figure 5.28 if seen in the fuselage.

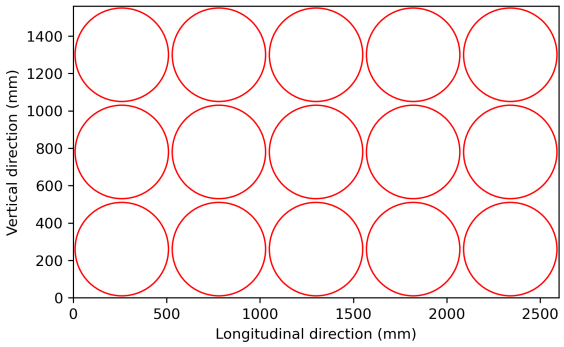

Figure 5.27: Lateral square packing as seen in the lateral direction, the outer bounds are the size of the DV.

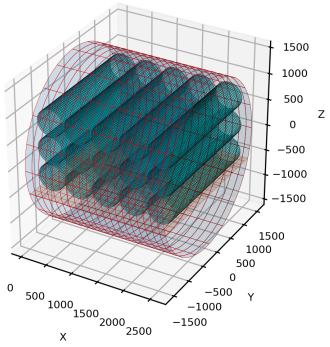

Figure 5.28: Lateral square packing as seen in the fuselage.

This packing solution would result in a total of 15 tanks, each with a radius of 248 mm and a tank length of 2339 mm. This would result in a packing density of 48.7% and a tank plus fuel weight of 675.1 kg.

Support

The support would be designed as a long rectangular box with openings on two ends to facilitate tank loading and unloading and to facilitate connections with the aircraft's fuel systems during fuel tank swapping. The support would be designed as before, with a plate on each side and the box structure to wrap it together. This will result in a design shown in Figure 5.29.

[5] The packing solutions that involve packing a rotated circle usually require complex computational methodology and mostly utilised when the side of the rectangle is fixed, which is not the case for this packing solution

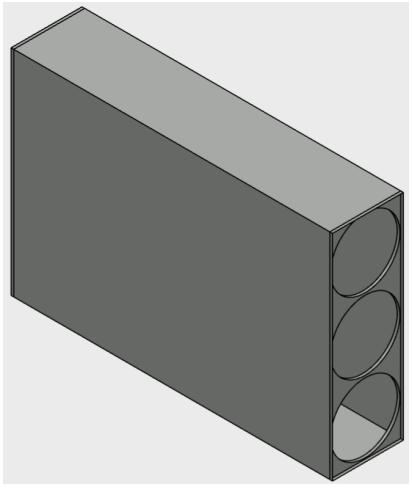

Figure 5.29: Lateral hexagonal packing as seen in the lateral direction, the outer bounds are the size of the DV.

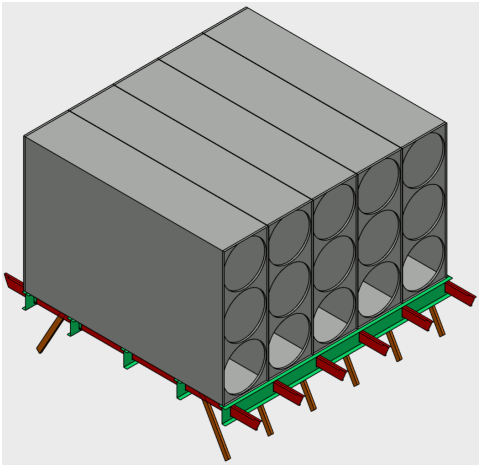

Figure 5.30: Lateral hexagonal packing as seen in the fuselage.

Putting all five box tank supports onto the cross beams, and the results are shown in Figure 5.30.

However, to enable the tanks to be swapped, each column of tanks would require a box of its own, making the total weight of the supports much higher than that of the other designs. This support design would result in a total support weight of 548.4 kg.

6 Analysis

6.1. Finite element analysis setup

6.1.1. Material model

In order to simulate drop tests of any degree in severity, materials will exhibit non-linear and plastic behaviour, as seen in a real-life drop test. For that, a material model capable of simulating plastic behaviours is required. The Johnson-Cook model is a phenomenological material model capable of simulating the elasticity, plasticity, and ultimate failure of metal material and accounts for strain hardening, strain rate hardening, and thermal softening during material deformation. The Johnson-Cook plasticity material model is often used for impact simulations modelling [78] and materials' flow behaviour [79]. The equation is as follows:

$$\sigma_{eq} = (A + B\varepsilon^n)(1 + C \ln \dot{\varepsilon}^*)(1 - T^{*m}) \tag{6.1}$$

where σ_{eq} is the equivalent stress, accounting for plastic and elastic properties. ε is the plastic strain. The material constants are *A, B, n, C, and m*. A is the yield stress of the material under reference conditions, B is the constant associated with strain hardening, and n is the strain hardening coefficient. With A, B, and n, the first parenthesis equates to the strain-hardening effect of the material. C is the strengthening coefficient related to strain rate, which makes the material's second parenthesis, strain rate strengthening effect. Finally, m is the thermal softening coefficient, making the last parenthesis the temperature effect of the material.

$$\dot{\varepsilon}^* = \frac{\dot{\varepsilon}}{\dot{\varepsilon}'_{ref}}, \qquad T^* = \frac{T - T_{ref}}{T_{melt} - T_{ref}} \tag{6.2}$$

where $\dot{\varepsilon}^*$ is the dimensionless strain rate, T^* is the homologous temperature, T_{melt} is the material's melting temperature, and T is the deformation temperature. $\dot{\varepsilon}'_{ref}$ and T_{ref} are the reference strain rate and the reference deformation temperature[79].

The Johnson-Cook dynamic failure model is based on the value of the equivalent plastic strain at element integration points; failure is assumed to occur when the damage parameter exceeds 1. The damage parameter, ω, is defined as:

$$\omega = \sum \left(\frac{\Delta \bar{\varepsilon}^{pl}}{\bar{\varepsilon}^{pl}_f} \right) \tag{6.3}$$

Where $\Delta \bar{\varepsilon}^{pl}$ denotes an increment in equivalent plastic strain, $\bar{\varepsilon}^{pl}_f$ represents the equivalent plastic strain at the initiation of damage, and the summation is performed over all increments in the analysis.

$$\bar{\varepsilon}^{pl}_f = \left[d_1 + d_2 \exp\left(d_3 \frac{p}{q} \right) \right] \left[1 + d_4 \ln \left(\frac{\dot{\bar{\varepsilon}}^{pl}}{\dot{\varepsilon}_0} \right) \right] (1 + d_5 T^*) \tag{6.4}$$

The failure parameters d_1 to d_5 are gained by testing on the material. The strain at failure, represented by $\bar{\varepsilon}_f^{pl}$, is influenced by a nondimensional plastic strain rate, $\frac{\dot{\bar{\varepsilon}}^{pl}}{\dot{\varepsilon}_0}$, a dimensionless pressure-deviatoric stress ratio p/q (where p is the pressure stress and q is the Mises stress), and the nondimensional temperature, denoted as T^* in the Johnson-Cook model.

6.1.2. Material assignment

The entire fuselage, including the supports, will be modelled using the AA 2024-T3 aluminium alloy, while the tank itself will be modelled with AA 2219-T87 aluminium alloy. The Johnson-Cook material parameters are shown in Table 6.1. The Johnson-Cook damage parameters of the aluminium alloy AA2024-T3 are shown in Table 6.2.

Table 6.1: AA2024-T3 aluminium alloy Johnson–Cook plasticity parameters.

ρ	E	ν	A	B	n	m	C
2690(kg/m^3)	74 GPa	0.29	369 MPa	684 MPa	0.73	0	0

It's worth noting that although the d_4 parameter is shown to be non-zero in the analysis, it will be considered as zero. Research conducted by Kay [78] concluded that the term $\left(\frac{\dot{\bar{\varepsilon}}^{pl}}{\dot{\varepsilon}_0}\right)$ in the Johnson-Cook damage initiation criteria is typically equal to zero for the AA 2024-T3. This means that any effect d_4 would have on damage would be negated, making the parameter unnecessary.

Table 6.2: AA2024-T3 aluminium alloy Johnson–Cook damage parameters[80].

d_1	d_2	d_3	d_4	d_5
0.13	0.13	-1.5	0	0

The Johnson-Cook material parameters of the aluminium alloy AA2219-T87 are shown in Table 6.3. However, during the analyses, the density will be replaced so that it can represent the weight of the tanks along with the hydrogen fuel.

Table 6.3: AA2219-T87 aluminium alloy Johnson–Cook plasticity parameters.

ρ	E	ν	A	B	n	m	C
var	73.1 GPa	0.33	390 MPa	300 MPa	0.11	0	0

6.1.3. Mesh parameters

Using the validated model from Desiderio, M., we can get the structural components' thicknesses and element sizes. They are listed in Table 6.4 and Table 6.5. The thickness of the tank supports is listed as a conservative design. During the X-direction inertia loading in one of the designs, a 2mm tank support started to develop cracks along the edge where the tanks made contact with the supports. To avoid any potential damage in the future, it is decided that the supports should have a thickness of 4mm, considering the conservative design. Although the same model was used for 3mm thickness, it is designated that the supports should be 4mm. This increased thickness is likely to enhance the manufacturability of the tanks.

According to API 620(2002) R.5.3.1, "Design and Construction of Large, Welded, Low-Pressure Storage Tanks", the outer tank bottom, shell, and roof shall be a minimum nominal thickness of 3/16 in., which would equate to 4.7625 mm. Hence, the tank's outer shell is designated at 5 mm.

Table 6.4: Thickness of different structural components, retrofitted F-28 fuselage section.

Component	Shell thickness (mm)	Component	Shell thickness (mm)
Skin	1.5	Stiffeners	2
Frames	1.8	Shear clips	0.5
Floor struts	1.8	Floor trans. beams	1.8
Floor long. beams	1.8	Tank supports	4
Tank outer shell	5		

Due to the likelihood of the tank supports making contact or tying with the transverse beams, the element size of the tank supports is then designated to use a similar element size. Some adjustments are needed to the tank support size to account for element distortion or analysis convergence, but overall, the tank support element size is around 20mm. Using the same logic, the tank element size is designated to be 20mm as well.

Table 6.5: Element size of different structural components, retrofitted F-28 fuselage section.

Component	Element size (mm)	Component	Element size (mm)
Skin	40	Stiffeners	15
Frames	15	Shear clips	12.5
Floor struts	10	Floor trans. beams	15
Floor long. beams	20	Tank supports	20
Tank outer shell	20		

6.2. Certification requirement

Certifying a fuselage retrofitted with hydrogen fuel tanks for crash scenarios involves two primary certification requirements: fuel system certifications and general crashworthiness certification. These certifications adhere to the guidelines laid out in CS 25.963, CS 25.56, and AMC 25.963. It's crucial that each fuel tank can withstand various types of loads during operation, such as vibration, inertia, fluid, and structural loads, without failing. This involves the crashworthiness criteria for both emergency landing conditions and emergency landing dynamic conditions.

6.2.1. Inertia loading conditions

To comply with AMC 25.963, the fuel tanks must be designed to endure the prescribed inertial load factors for emergency landing conditions within the fuselage contour, as specified in JAR/CS 25.561. These load factors are based on years of experience and are considered conservative design criteria.

A minor crash landing is a complex dynamic condition with combined loading. However, to have simple and conservative design criteria, the emergency landing forces were established as conservative static ultimate load factors acting independently in each direction. These series of inertia force loadings are listed in subsection 3.1.1. Applying the listed inertia loading conditions to the analysis model would translate to the quasi-static test listed below:

- Forward 9.0g inertia loading, rearward 1.5g is omitted since the retrofitted fuselage is mostly symmetric in the x-direction; rearward inertia loading would equate to forward loading.
- Upward 3.0g inertia loading.
- Sideward 3.0g inertia loading. Since the retrofitted fuselage is symmetrical in the lateral direction, only one analysis will be conducted in the sideward direction.
- Downward 6.0g inertia loading.

CS 25.963 mandates that fuel tanks located both inside and near the fuselage should be able to withstand rupture during a crash that can be survived. This means that the inner tank of the hydrogen fuel tank should not show any damage. The advisory material that was previously associated with CS 25.963 outlines the design requirements for all fuel tanks that could release fuel in or near the fuselage or near the engines, in quantities that are sufficient to cause a serious fire if ruptured.

6.2.2. Dynamic condition

CS 25.963 mandates that fuel tanks, located both inside and near the fuselage, must be able to withstand rupture during survivable crash conditions. The guidance previously associated with CS 25.963 outlines design criteria for all fuel tanks that, if ruptured, could release fuel within or near the fuselage or near the engines in quantities capable of igniting a serious fire. The key issue is determining what constitutes a survivable crash condition.

CS 25.562 specifies that a change in downward vertical velocity of at least 10.7 m/s and peak floor

deceleration must occur within 0.08 seconds after impact, reaching a minimum of 14 g. However, this requirement cannot be directly applied as a simple loading condition for the fuselage.

Recently, the Transport Aircraft Crashworthiness and Ditching Working Group (TACDWG) of the FAA collaborated with original equipment manufacturers (OEMs) to address legislative gaps by assessing the vertical impact capabilities of current aircraft. According to their report, most aircraft under the CS-25 legislation can protect passengers within a range of 20 to 30 ft/s vertical impact velocity. The report also notes a trend where wide-body aircraft from the same manufacturer can withstand higher speed impacts, likely due to a larger crushing zone that reduces the loads transmitted to passengers.

TACDWG proposed a vertical impact velocity requirement based on the aircraft's maximum takeoff weight (MTOW), self-assessment of OEMs, and accident studies. Using this method, the impact vertical velocity for an F28 Fellowship with an MTOW of 29,480 kg (65,000 lb) [81] is calculated to be 18 ft/s (5.5 m/s), as per the TACDWG report.

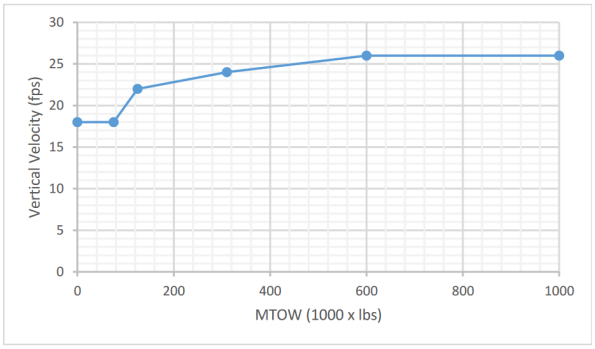

Figure 6.1: Vertical impact velocity requirement of different MTOW [82].

Additionally, the report provides another criterion for assessing vertical impact velocity based on underfloor structural depth, of which the F28 has around 942 mm (37.1 in). This translates to an estimated 26 ft/s (7.9 m/s) of vertical impact speed.

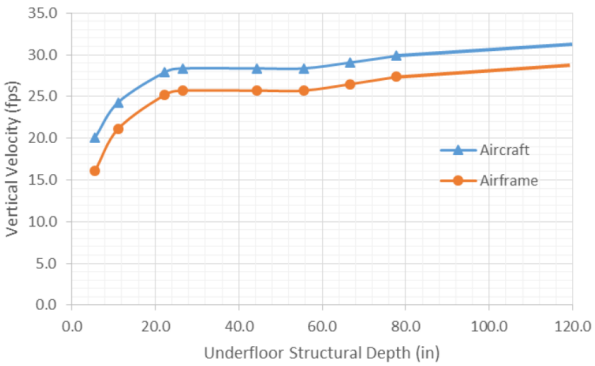

Figure 6.2: Vertical impact velocity requirement of different underfloor structural depth [82].

As per the TACDWG report, the ideal impact velocity for aircraft is 7.9 m/s. However, the FAA mandates that single-aisle aircraft should withstand an impact velocity of 9.14 m/s [34, 35] . It is noteworthy that most crashworthiness analyses [56, 83, 84, 59, 57, 85], including Lyle et al.'s [69] study on the F28 aircraft, use 9.14 m/s as the standard speed. Waimer, on the other hand, sets the maximum initial impact velocity at 9.1 m/s [18].

It is also worth noting that previous drop tests conducted by Caputo et al. and Di Palma et al. [49, 86] have used higher impact velocities of 9.14 m/s, as have studies by Littel, J.D. on the F28 aircraft [87]. Therefore, it is concluded that, as a conservative estimate, the impact speed should be

set at 9.14 m/s (30 ft/s) despite the recommendation by TACDWG. This impact speed will be utilised to certify fuel tank strength in emergency landing conditions, which dictates that for each fuel tank and surrounding airframe structure, the effects of crushing and scraping actions with the ground should not cause the spillage of enough fuel or generate temperatures that would constitute a fire hazard.

Fuel tanks are required to have the ability to withstand rupture during a crash, which can be survived. This means that in dynamic crash conditions, single-wall tanks should not be damaged and for double-wall tanks, no damage should occur to the inner wall. However, due to modelling limitations, only one wall of the tanks will be detailed, which is the outer wall, and it should be able to withstand any damage despite the crash.

6.3. Crashworthiness Evaluation Criteria

6.3.1. Inertia loading

The inertia loading test is a fundamental evaluation method for assessing crashworthiness in different scenarios. It is a conservative design criterion used for objects with mass that may cause harm to occupants in the case of a minor crash landing. The main objective of this test is to determine whether the tank support or the tank itself would come loose and collide with surrounding structures, resulting in damage to the tanks. The intention of this test is to ensure that no damage could be inflicted upon the tanks during any crash scenario, thereby ensuring their crashworthiness.

The plastic strain equivalent (PEEQ) serves as a scalar variable that indicates a material's inelastic deformation. It is a crucial parameter used to evaluate the extent of damage to fuel tanks. If PEEQ is greater than zero, it implies that the material used for the tanks (AA 2219-T87) has undergone yielding. Though this may not necessarily lead to rupturing, once the material has yielded and undergone plastic deformation, its susceptibility to rupture increases significantly.

6.3.2. Visual inspection of the crash sections

Performing a visual examination is crucial in assessing the effectiveness of a crash simulation. This examination involves checking the tie constraints, modelling errors, and verifying the interaction and contact properties. It is essential to ensure that the components are deforming realistically and that the crash simulation is functioning as intended, without any constraints or interaction setting errors.

Additionally, it is crucial to validate that the crash sequence is functioning correctly. The crash sequence is critical for the energy dissipation mechanisms that are designed into the fuselage to function as intended. When the payload is too light, the fuselage will absorb most of the impact energy through elastic deformation, which will then rebound and cause significant acceleration on the fuselage, leading to it bouncing back off the ground. This is caused by the energy dissipation mechanism being triggered too early, making the fuselage too stiff.

Examining the time history of the crash simulation and comparing it with the time history of the crash, specifically the kinetic energy history, plastic energy dissipation history, and friction energy history can provide invaluable insights into how the fuselage and its components dissipate the impact energy.

6.3.3. Energy dissipation by energy type

For the energy dissipation, three types of energies are highlighted based on their percentage of the total energy: the maximum strain energy E_{Emax} through the impact history, the stabilized plastic energy dissipation E_{PD}, and friction energy dissipation E_{FD}. Outside of being the main energy dissipation during the crash, it is also a great indicator of how the fuselage is deforming and how different designs affect the energy dissipation.

The strain energy is chosen at the maximum so that it is easier to understand how much strain energy is stored within the components before the elastic rebound happens. The elastic energy is then allowed back into the system for other components to dissipate. As discussed before, this is not desired.

Plastic energy dissipation is and should be the main energy dissipater of the entire crash simulation.

The lower the plastic energy dissipation in regards to total energy, the more the impact will be directly inflicted on the occupants and components or absorbed via friction.

Friction dissipation is a good indicator of how much the fuselage ovalizes. Desiderio, M.'s research showed that, through the ovalization of the fuselage, the friction energy dissipation became less in terms of total energy dissipated [67].

6.3.4. Acceleration-based criteria

As specified in chapter 3, the acceleration-based criteria include DRI, HIC, and Eiband injury criteria.

The DRI requires the acceleration pulse at the lumbar area, which can be derived using Equation 3.1. In the equation, the variable "m" represents the upper body mass, while "k" and "c" represent the spring and damping coefficients of the lower body and spine. However, to obtain an accurate acceleration pulse, we must consider the dampening or amplifying effect of the seats and restraining system. This requires us to model the entire seating system, including the body's mass.

Desiderio [67] proposed a simplified approach, where a point mass of 100kg is added to represent the body seated and restrained on a seat. This mass is located at the spine's height, connected to cross beams with springs. This deviates from the anthropological test as specified in CS 25.562, which is listed in subsection 3.1.2. Waimer M. [18] also developed a similar method but with anthropological data and a simplified but realistic seat model with shell elements.

Although it is possible to include these simplified models by directly adding them to the model without contact so that it won't cause interference with the other components in the fuselage. The mass added to the fuselage would significantly increase the amount of energy that needs to be dissipated and thus would invalidate the test, making it impractical. This is because doing so would increase the amount of mass and, thus, the energy required to dissipate the force during impact.

Measuring the acceleration on the tanks and then using that as an input for the DRI could also be done. However, due to the stiff nature of the tank supports compared to the seating systems, the peak acceleration pulse is higher than that measured from an ATD's spine location. This would then be translated in Equation 3.2 to show a much higher DRI number due to the equation taking the maximum number. This is also detailed in the work of Desiderio [67].

The same could be said for HIC. According to CS 25.562 regulations, aircraft occupants should not experience a HIC value exceeding 1000 units, as listed in subsection 3.1.2. The HIC is a measure of acceleration calculated over a specific time interval. This acceleration is measured using an accelerometer that is placed on the dummy's head at the center of gravity, as mentioned in [88]. Although the acceleration pulse is taken through a time interval, the HIC value can be affected by the peak acceleration pulse, which makes it unsuitable as a criterion for comparing different designs despite its inclusion in the CS 25.562 regulations.

Despite the shortcomings of the DRI due to the lack of applicability of the anthropological model, DRI still considers the whole time history of the acceleration pulse and concludes neatly to a single index. Thus, DRI will be utilised as an index to discern the crashworthiness of the designs.

6.3.5. Plastic energy dissipation distribution by component

The distribution of energy dissipation by each component is an important criterion for judging the crashworthiness capabilities. The energy dissipated through plastic deformation would be absorbed through plastic deformation, which could not then be released and applied to the occupants and cargo that the fuselage contains. If the fuselage absorbs the impact energy through elastic deformation, that elastic potential energy would then be released through elastic rebound to become kinetic energy, sound (vibration) energy, and heat, which would then be inflicted on the occupants and cargo. Therefore, it is important to judge that most energy is dissipated through plastic energy and friction energy.

Comparing the absolute energy dissipation values of components with visual observations can help

validate or invalidate theories about the energy-absorbing mechanisms involved in a crash. However, relying solely on visual observations may not provide a complete understanding of the crash event, and the same applies vice versa.

The normalized energy dissipation distribution is a straightforward metric for identifying the most critical components in dissipating crash energy. Analyzing this distribution can provide insights into how the relative importance of each component varies for different geometric parameters and configurations. Identifying these crucial components is necessary to dissipate energy effectively.

6.3.6. Kinetic and plastic energy time history

The time history plots of kinetic energy are the most holistic metric to gain insight into the speed and behaviour of the entire model. The slope of the curve that shows the relationship between the kinetic energy and the force of gravity over time is known as $\dot{K}_{eg}$. It represents the rate at which the kinetic energy of the fuselage section and the passengers is transformed into friction, elastic, and plastic energy. A higher rate of energy dissipation means that the plane experienced a harder impact on the ground. This results in larger acceleration pulses that will then be reflected on the passengers and the retrofitted fuel tanks. Therefore, it is better to have a higher rate of plastic energy conversion to minimize the impact on the passengers.

After the initial impact, the structure experiences a point of maximum deformation. This is the moment when most of the kinetic energy has been dissipated through plastic deformation. However, the kinetic energy does not become zero at this point despite the velocity of the components tending towards zero. This is because different nodes reach zero velocity at different times, resulting in residual kinetic energy.

The rebound phase follows, during which all the elastic energy stored in the structure is released and converted back into kinetic energy. However, if there is a material failure, the energy will be dissipated through vibrations. Rebounds are generally not desired as they prolong the duration of the acceleration pulse experienced by the occupants. Humans can tolerate high-magnitude, low-duration acceleration pulses better than long-duration ones. The longer the pulse, the lower the acceleration magnitude, which can be tolerated without increasing the risk of injuries.

The same could be said for plastic energy. The faster the kinetic energy, which is the input energy of the system, could be transferred to plastic energy, the better. The main difference between these two energies is, as shown in Equation 4.2 and Equation 4.3, the kinetic energy is not just converted to plastic energy. This energy data could show if the energy is dissipated not with plastic and friction energy but through strain energy, which is undesired, as discussed before.

6.4. Model and analyses

The model is built using the 3DEXPERIENCE platform and mesher and solved using Abaqus/Explicit. Using the design methods in the chapter 5, the F28 model is modified with the tanks and their related supports. This section will provide designs into the final model for all the designs.

6.4.1. Loading condition

The loading condition will be as discussed in section 6.2. This includes four quasi-static loading and one dynamic loading. The tests are listed below:

- Forward 9.0g inertia loading, rearward 1.5g is omitted since the retrofitted fuselage is mostly symmetric in the x-direction; rearward inertia loading would equate to forward loading.
- Upward 3.0g inertia loading.
- Sideward 3.0g inertia loading. Since the retrofitted fuselage is symmetrical in the lateral direction, only one analysis will be conducted in the sideward direction.
- Downward 6.0g inertia loading.
- Drop test with an impact speed of 9.14 m/s (30 ft/s) with a gravity acceleration of $9.81 m/s^2$.

To start the analysis and understand the total energy involved in the dynamic loading condition, the mass of each design needs to first be understood. These masses would then be converted to kinetic energy by means of the 9.14 m/s^2 impact speed, which is the main energy input of the system, as shown in Equation 4.1.

Table 6.6: Mass comparison of the three designs

	LCP	LHP	LSP
Mass	1192.6 kg	1104 kg	1471.5 kg
Initial kinetic energy	49.815 kJ	46.114 kJ	61.464 kJ

The kinetic energy will then be dissipated through means shown in Equation 4.2 and Equation 4.3. During the analysis, it is shown that the prominent energy is the internal energy

6.4.2. Boundary condition

In terms of the quasi-static test, AMC 25.963 states that the fuel tanks experience the ultimate inertia forces listed in subsection 6.2.1 acting separately relative to the surrounding structure. To simulate these conditions, the entire permissible length of the fuselage is deemed as a fuel tank compartment, and the boundary condition is set accordingly. For sidewards, upward, and downward loading, a layer of elements at the first and last frame, shear clips, and longitudinal beam[1] are encastred to simulate connections to surrounding structures.

During the forward loading test, it is considered that one of the layers of elements does not need to be constrained. This is because the loading conditions are set to simulate the ultimate loading condition during a minor crash landing. A 9g forward loading is likely to simulate the effect of rapid deceleration and cause the section to collide with the section in front of it. If the other side is constrained, it would interfere with the testing procedure.

The boundary condition for the dynamic test is only applied to the ground, where it is encastred. This will allow the drop test to be performed accordingly.

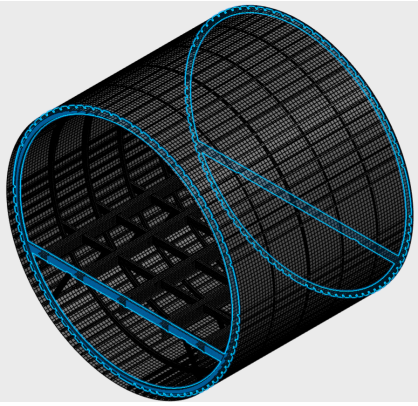

Figure 6.3: Boundary condition for quasi-static loading.

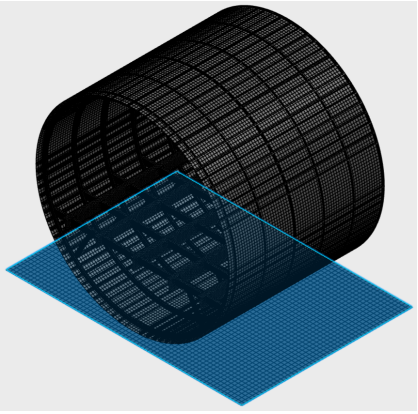

Figure 6.4: Boundary condition for dynamic loading.

6.4.3. Interaction and contact properties

All the riveted connections of the baseline aircraft have been modelled through tie constraints to prevent joint failure. The fasteners from the support to the tanks will also be modelled with tie constraints. Joint failure is not desired and is unlikely to occur in a crash scenario, as experimentally demonstrated. This will prevent scraping between the flange of the supports and the tanks. However, it will still allow the tanks to scrape with the tank support itself, which is necessary for certification.

[1] at x = 0 and x = permissible length location

A general contact interaction property has been defined to allow drop tests to be conducted and avoid element penetration, which would result in results that do not make physical sense. Along with general contact, normal behaviour interaction is also specified. To allow scraping damage, friction will have to be applied to the interaction. The contact formulation is hard to contact, while the tangential behaviour is defined using a penalty friction formulation by specifying the friction coefficient. The chosen coefficient is 0.5 (slip-rate independent), which is a good estimate for both aluminium/aluminium and aluminium/asphalt contact interfaces [67].

6.4.4. Longitudinal circle packing

Finite element model

The following pictures show the analysis model of the longitudinal circle packing (LCP) concept.

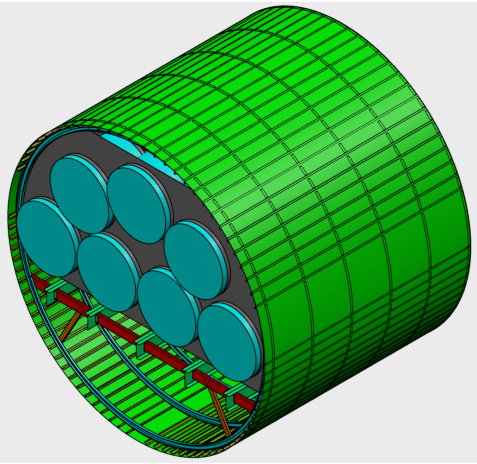

Figure 6.5: LCP solution ISO view

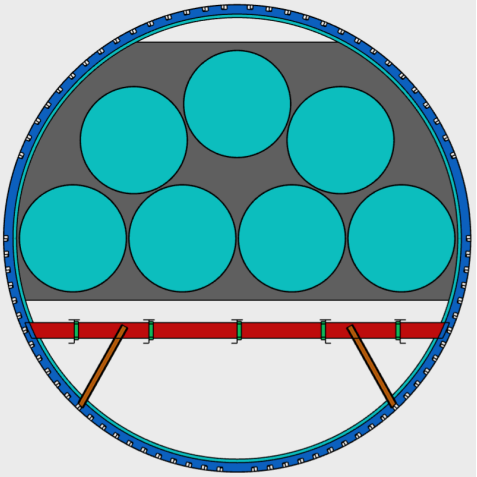

Figure 6.6: LCP solution X-direction view.

Inertia loading

The test results for the four inertia loading tests are shown in the figures below. All showcased no plastic deformation or damage on the tanks. The loading is applied to the entire fuselage using the boundary condition discussed earlier in the chapter. Only the tanks are shown since this is the only component that needs to be judged based on PEEQ.

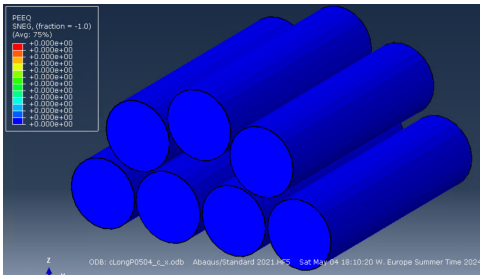

Figure 6.7: LCP X-direction quasi-static loading PEEQ.

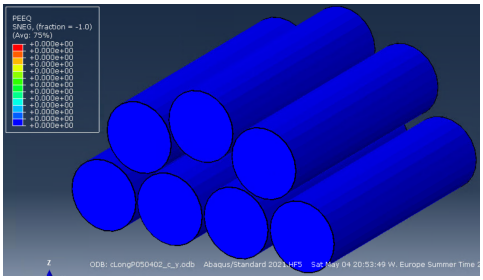

Figure 6.8: LCP Y-direction quasi-static loading PEEQ.

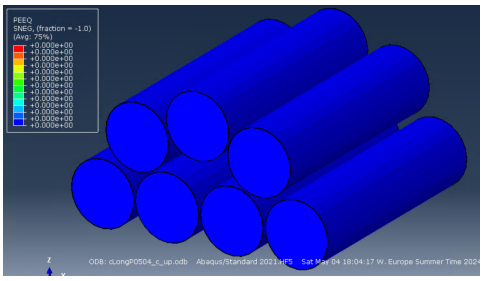

Figure 6.9: LCP +Z-direction quasi-static loading PEEQ.

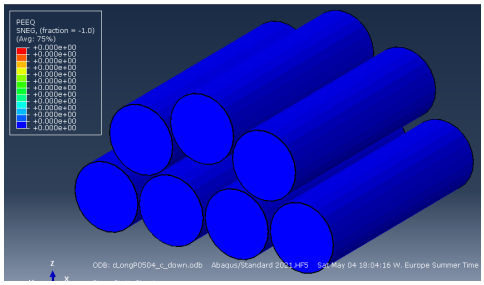

Figure 6.10: LCP -Z-direction quasi-static loading PEEQ.

Dynamic loading

Looking at the total energy time history, it can be observed that the total energy, plastic energy, kinetic energy, and strain energy stabilized at the end of 150 ms, so the analysis can be considered stable, and the crash simulation can be concluded.

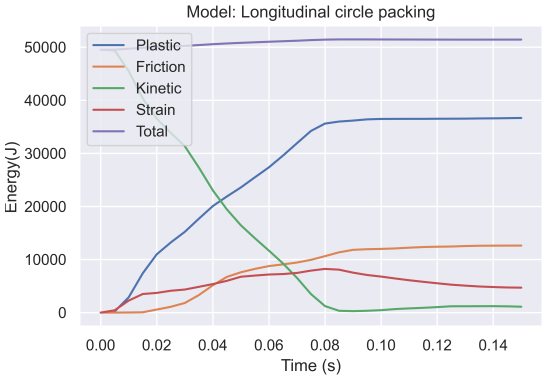

Figure 6.11: LCP total energy history.

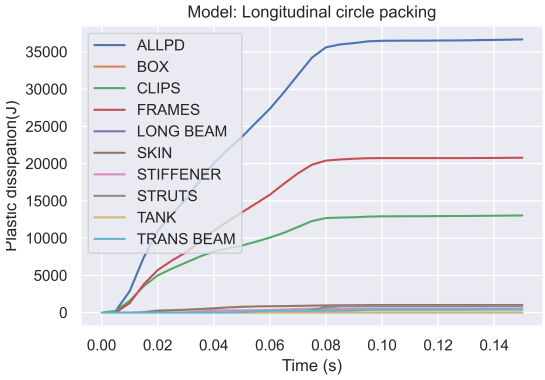

Figure 6.12: Plastic energy dissipation of LCP.

Table 6.7: Energy fraction of each main energy dissipation.

E_{Emax}/E_{TOTAL}	E_{PD}/E_{TOTAL}	E_{FD}/E_{TOTAL}
15.99%	71.245%	24.531%

It has been observed that during the crash simulation, a significant amount of energy is dissipated through friction energy. Almost a quarter of all energy is dissipated through friction. Interestingly, the fuselage did not deform as much as expected based on the verification model. Furthermore, the release of strain energy coincides with an increase in friction energy rather than a return to kinetic energy. Additionally, there was no significant increase in kinetic energy after the impact, which occurred approximately 80 ms after the impact. This suggests that plastic hinges did not form under the struts, and there was no significant rebound where the fuselage jumped back up after impact. Instead, the elastic strain contributes to the opening of the bottom fuselage while it remains grounded. This is also shown in Figure 6.13. This also decreases the plastic energy dissipation and only 71% of total energy dissipation.

In regards to plastic energy, it is shown in Figure 6.12 that the plastic energy dissipation mainly occurs only through the frames and the shear clips instead of frames, shear clips, and struts. Although struts' plastic energy dissipation is non-zero, it's low enough to ignore. This also suggests that no plastic energy is formed under the struts.

It has been noticed that in this particular design, there is a significant increase in stress at the roots of the transverse cross beams where they connect to the frames. This stress concentration is high enough to cause plastic deformation at the frames and the shear clips, resulting in a PEEQ of 0.05. This is likely due to the tanks being supported by the frames instead of the cross beams, which causes significant stress concentration at the cutoff point of the tank support.

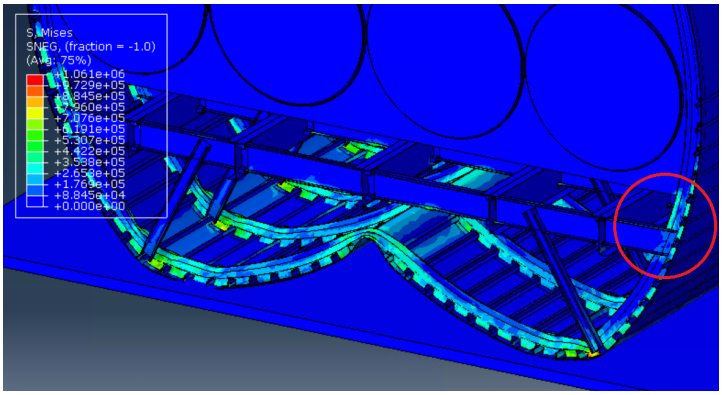

Figure 6.13: Stress at the roots of the transverse cross beam.

Compiling the information about the energy dissipation and plastic deformation at the cross beams, it is concluded that this design showcased less ovalization than the verification case. This is due to the tank support plates connecting to the frames, limiting the degree of ovalization allowed for the frames.

Looking at the acceleration-based criteria, acceleration is taken from the tanks' heads in and near the center point of the flat heads, as this is the crucial point where the tanks have to connect to the fuel systems. These accelerations will be useful when the connections to the tanks need to be designed.

After processing these data, the DRI is calculated accordingly; as mentioned, directly applying the acceleration measured from the tank heads to the DRI calculation will lead to a severely higher DRI, well outside of the range for humans. For LCP, the acceleration pulse is measured at 4 tanks in 8 locations, all in the center or near the center of the tank heads[2]. Due to the symmetricity of the fuselage, the tanks on the -Y side are selected to place the accelerometers. This includes the three tanks on the -Y side and the center tank. The accelerometer is placed at both ends of the tanks.

The acceleration is then calculated into DRI, and the results are shown below in Figure 6.14. The tanks are numbered according to their position along the -Y direction. Tank 1 is located furthest to the -Y side, while tank 4 is in the center.

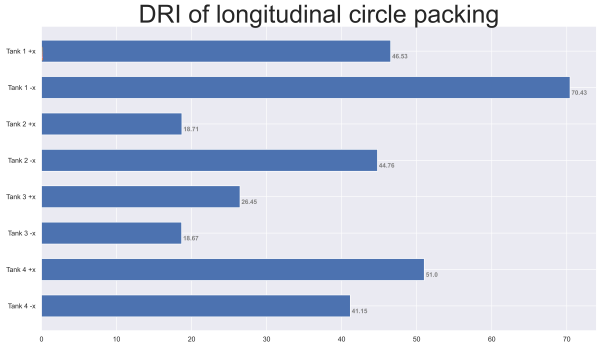

Figure 6.14: DRI of LCP.

6.4.5. Lateral hexagonal packing

Finite element model

The following pictures show the lateral hexagonal packing (LHP) design analysis model.

[2]Due to meshing limitations, some tanks will not have a node exactly at the center

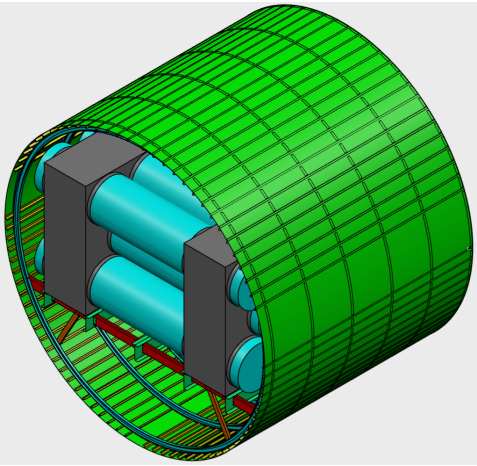

Figure 6.15: LHP solution ISO view.

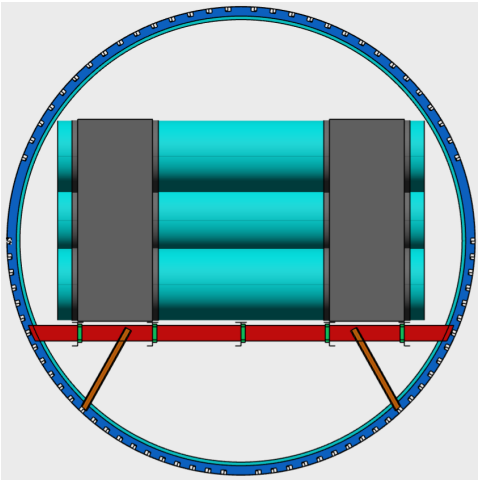

Figure 6.16: LHP solution x-directional view.

Inertia loading

The test results for the four inertia loading tests are shown in the figures below. All showcased no plastic deformation or damage on the tanks.

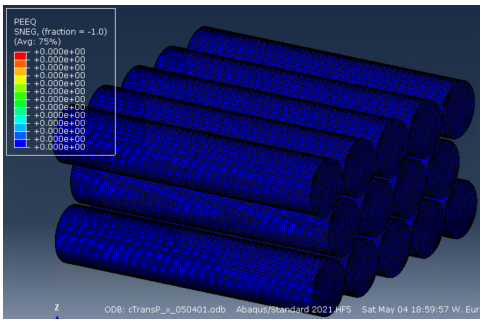

Figure 6.17: LHP X-direction quasi-static loading PEEQ.

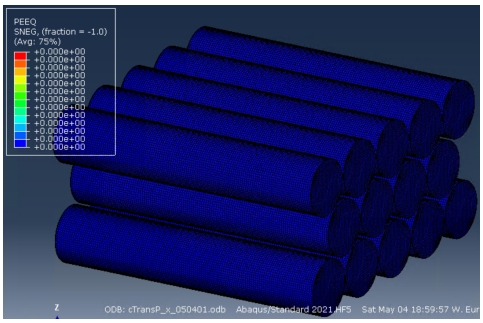

Figure 6.18: LHP Y-direction quasi-static loading PEEQ.

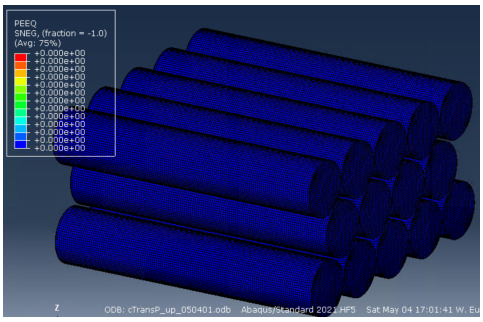

Figure 6.19: LHP +Z-direction quasi-static loading PEEQ.

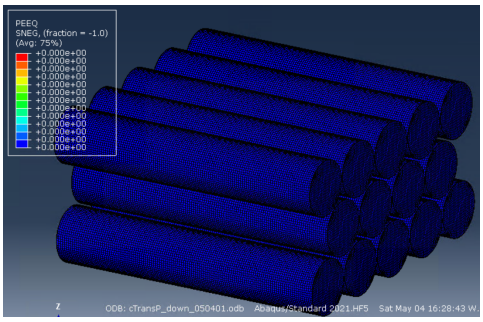

Figure 6.20: LHP -Z-direction quasi-static loading PEEQ.

Dynamic loading

Looking at the total energy time history, it can be observed that the total energy, plastic energy, kinetic energy, and strain energy stabilized at the end of 150 ms, so the analysis can be considered stable, and the crash simulation can be concluded.

Though the LHP and LCP have similar weights and thus total kinetic energy that needs to be dissipated, the energy dissipation is quite different. The strain energy is released through kinetic energy, meaning there is a rebound where the fuselage bounces back up. The increase in kinetic energy happens during

10 ms after the lowest point of the kinematic energy. This high rate of strain energy release would lead to a high positive vertical acceleration.

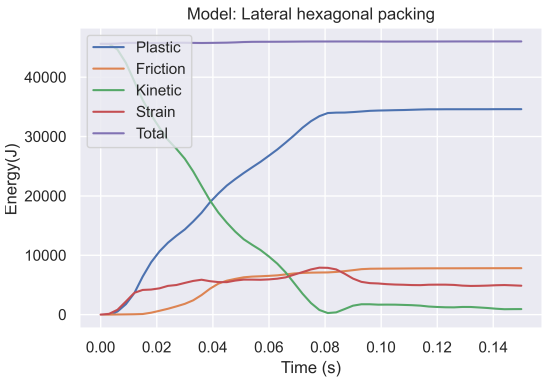

Figure 6.21: LHP total energy history.

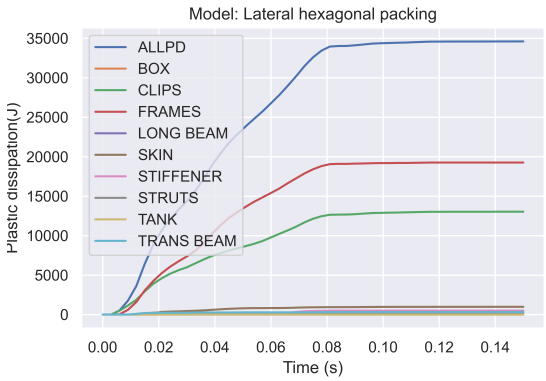

Figure 6.22: Plastic energy dissipation of LHP.

Table 6.8: Energy fraction of each main energy dissipation.

E_{Emax}/E_{TOTAL}	E_{PD}/E_{TOTAL}	E_{FD}/E_{TOTAL}
17.176%	75.201%	19.992%

In regards to plastic energy, it is shown in Figure 6.22 that the plastic energy dissipation mainly occurs only through the frames and the shear clips instead of frames, shear clips, and struts. Like LCP, the impact did not reach the struts, meaning that the plastic hinge that is supposed to form under the struts under a normal crash sequence didn't form. However, unlike LCP, the fuselage can ovalize due to the fact that there are no tank supports stiffening the frames and shear clips. The fuselage rebounded off the ground due to the strain energy release of the frames and shear clips. This is due to the fact that at the moment of maximum stress concentration, the stress is not high enough to plastically deform the lower end of the struts and the surrounding frames and shear clips. Instead, this part of the structure acts as a spring, and the elastic strain energy quickly transfers to kinetic energy. The lack of a plastic hinge could be shown by comparing Figure 6.23 to Figure 6.24. There is significant plastic deformation and, therefore, stress concentration just at the bottom of the strut compared to the frames closer to the centerline.

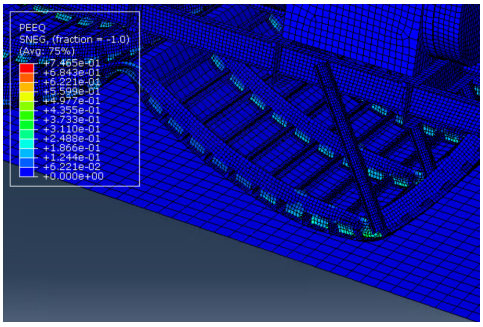

Figure 6.23: LHP bottom of the strut.

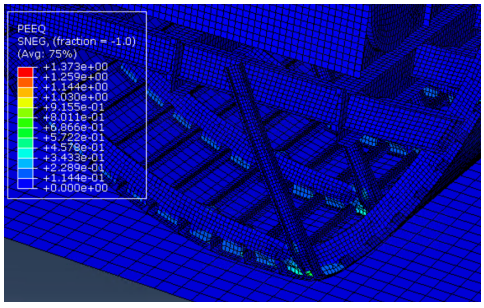

Figure 6.24: LSP bottom of the strut.

Acceleration pulses will be measured at 12 locations across six tanks for LHP. These accelerometers are located in the center or near the center of the tank heads. The selection of these six tanks is intended to replicate the accelerometer placement used by Lyle et al. [69], who placed sensors in the front, middle, and back of the fuselage. To ensure accurate measurement, the acceleration will be measured at both the bottom and top tanks. This is because placing the tank higher up may cause the acceleration pulse to be amplified. In conclusion, the acceleration will be measured at X = 1, 3, 5 and Y = 1, 3 tanks [3].

[3]For the annotation of the tanks, check chapter 5

Upon examining the DRI, it was observed that the lower tanks located near the cross beams have an exceptionally high DRI. This is caused by the disruption of the crash sequence. Furthermore, the bottom tanks generally exhibit a higher DRI than the top tanks. In fact, some of the DRI values in this design exceed 200. This means that the maximum acceleration on these tanks is significant and thus needs to be closely examined.

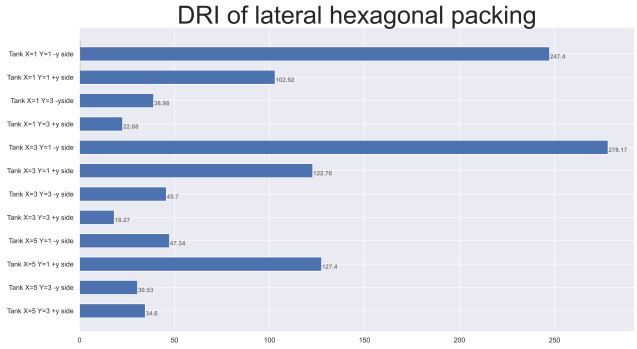

Figure 6.25: DRI of LHP.

High peak acceleration

The figure shown below shows the acceleration pulse of all measured locations. It can be observed that the acceleration pulse in the positive vertical direction experiences an abrupt surge after 60 ms. This sudden increase in acceleration corresponds to the flattening of the bottom frames and shear clips, which accumulate stress around the bottom of the struts. The accumulation of stress ends around 80 ms after impact, which coincides with the rebound of the struts and cross beams. Together, the rebound of the struts and cross beams leads to a quick increase in kinetic energy, which is caused by the release of strain energy. The high strain energy release rate contributes to the high rate of vertical acceleration.

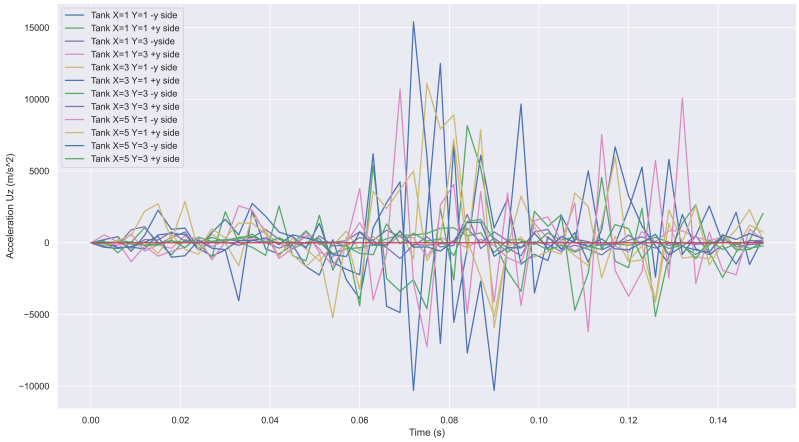

Figure 6.26: Acceleration pulse measured from all accelerometer locations for LHP.

In the course of the drop test, it was noted that the spaces between the tanks on the tank supports are consistently under stress when the fuselage is in descent. This stress buildup is a result of the hexagonal packing design, which maximizes packing density within its DV, clustering the tanks together and limiting their movement. Consequently, when the lower tanks impact the bottom tank, their movement is restricted by the upper tanks, leading to a brief period of stress concentration around the lower tanks

and their related supports. This leads to acceleration and significant vibration along the lower tank supports, as depicted in the graph.

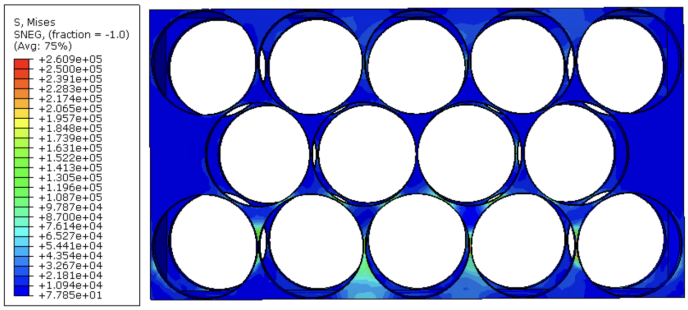

Figure 6.27: Stress accumulation around the tank supports for LHP at 72 ms.

6.4.6. Lateral square packing

Finite element model

The following pictures show the analysis model of the lateral square packing (LSP) design.

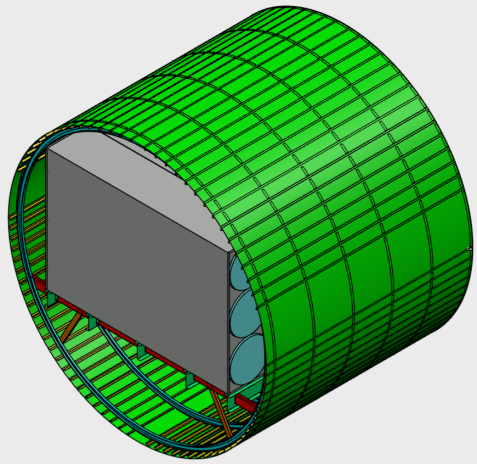

Figure 6.28: LSP solution ISO view.

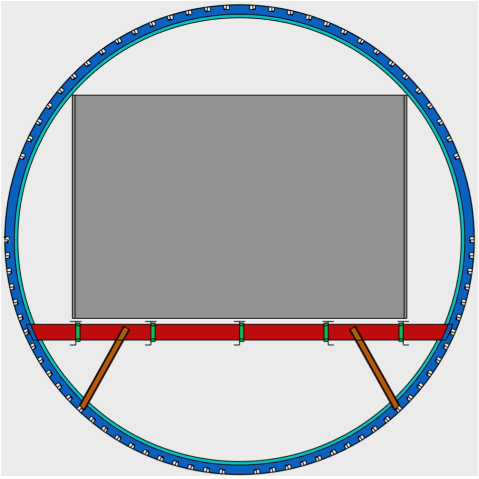

Figure 6.29: LSP solution x-directional view.

Inertia loading

The test results for the four inertia loading tests are shown in the figures below. All showcased no plastic deformation or damage on the tanks. Note that, due to the allowing of tank swapping, the inertia loadings have to be modified by a factor of 1.33 to allow for extra wear and tear,

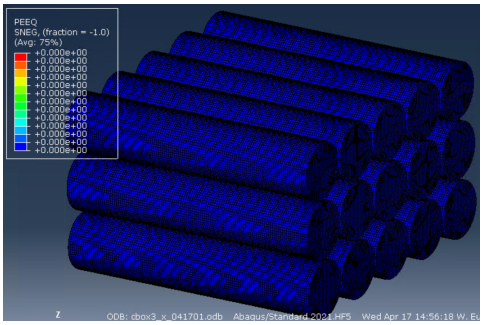

Figure 6.30: LSP X-direction quasi-static loading PEEQ.

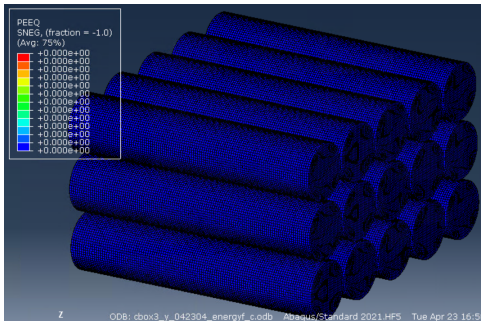

Figure 6.31: LSP Y-direction quasi-static loading PEEQ.

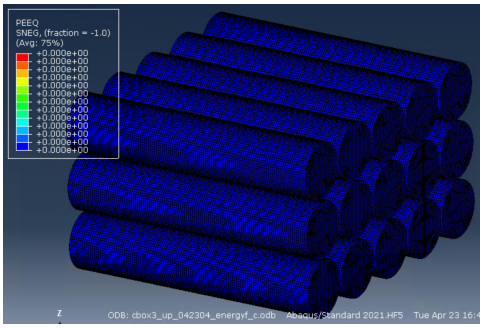

Figure 6.32: LSP +Z-direction quasi-static loading PEEQ.

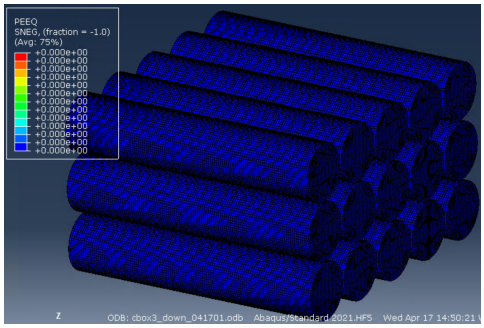

Figure 6.33: LSP -Z-direction quasi-static loading PEEQ.

Dynamic loading

Looking at the total energy time history, it can be observed that the total energy, plastic energy, kinetic energy, and strain energy stabilized at the end of 150 ms, so the analysis can be considered stable, and the crash simulation can be concluded.

The heaviest design concept is LSP, and the highest amount of energy is required to be dissipated. Similar to LHP, the strain energy is also released through kinematic energy. However, this period of elastic strain rebound occurs during a span of 20 ms, from 60 to 80 ms.

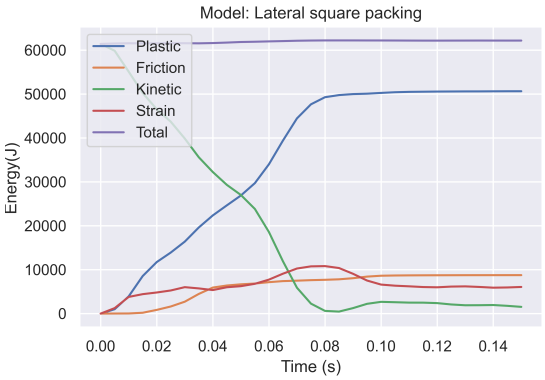

Figure 6.34: LSP total energy history.

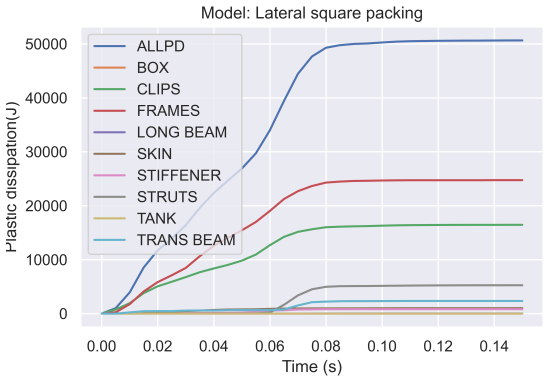

Figure 6.35: Plastic energy dissipation of LSP.

Table 6.9: Energy fraction of each main energy dissipation.

E_{Emax}/E_{TOTAL}	E_{PD}/E_{TOTAL}	E_{FD}/E_{TOTAL}
17.385%	81.399%	14.079%

This extra mass also increases the total energy absorbed by plastic deformation, which absorbs 81.4% of the energy. Due to the activation and inclusion of the struts in the crash sequence, the struts and the transverse beams start to deform plastic. This is most likely the reason why plastic dissipation is higher than total energy.

For LSP, acceleration pulses will be measured at 12 locations across six tanks. These tanks will be located in the centre or near the centre of the tank heads. The selection of these six tanks is intended to replicate the accelerometer placement used by Lyle et al. [69] , who placed sensors in the front, middle, and back of the fuselage. To ensure accurate measurement, the acceleration will be measured at both the bottom and top tanks. This is because placing the tank higher may cause the acceleration pulse to be amplified. Specifically, the acceleration will be measured at X = 1, 3, 5 and Y = 1, 3 tanks [4]. The DRI of LSP is generally low, except for one. The median is 31.73, and the maximum is 91.

[4]For the annotation of the tanks, check chapter 5

The reason for this heightened acceleration and, therefore, DRI is because of the unbalanced impact of the fuselage. Due to the fuselage being slightly leaning to the front during the impact, since the tanks are installed from 0 to 2570mm in length, the fuselage is slightly front-heavy. This causes the fuselage to rotate, which causes the fuselage to rotate to be slightly front-leaning. Though this doesn't cause any problem with the acceleration peak around the time of the impact, the back end actually slams to the ground later than the typical impact timing and causes a 673g acceleration at 105 ms, which is around 30 ms after impact.

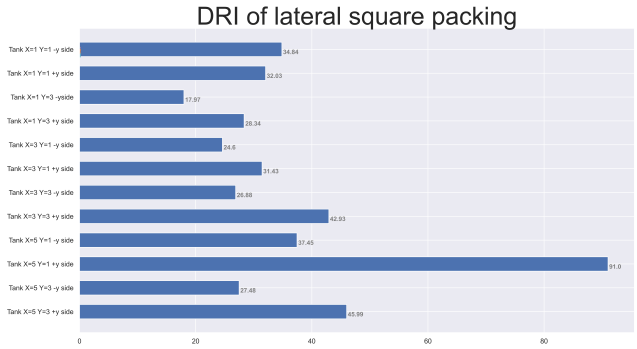

Figure 6.36: DRI of LSP.

6.5. Drop test comparison

6.5.1. Visual and stress comparison

The three designs are shown in the bottom figures, depicting their highest von Mises stresses throughout the analyses. It's important to note that the maximum stresses between the designs are not consistent, both in degree and timing. For LCP, it is at 84 ms, LHP at 78 ms, and LSP 72 ms after impact. This means that at this point, most of the initial kinetic energy has been depleted, which also concludes the initial impact.

In the LCP, there's a significant stress concentration around the connection point of the transverse beams and frames due to the tank support. As mentioned before, this design causes significant friction dissipation, thus decreasing the acceleration applied to the tanks and fuselage post-impact. Though this may be a cause for concern for scrapping damage, in terms of a pure drop test without designating a specific impact to the ground surface outside of the friction coefficient, this is acceptable since skin scrapping on the ground itself should be a cause of concern for fuel leak. The stress concentration around the transverse beams is a cause for concern since the accumulation of elastic strain energy usually causes elastic rebound and inflicts significant acceleration. It is hypothesized that the elastic rebound around this area causes the disparity in acceleration among the four tanks, as shown in Figure 6.14.

It is likely that the increase in friction energy dissipation is caused by a change in the load path and constraints. In typical designs, the load is introduced on the floor cross beams and then transferred to the lower fuselage through the struts. However, with the main loading on the frames, the load is introduced to the lower fuselage by the frames themselves. As a result, there is more sliding on the lower fuselage, leading to a significant increase in friction dissipation. This heightened degree of sliding and friction energy dissipation is because the cross-beams are no longer being constrained. The cross beams are allowed to deform and bend upwards as the frames at the lower fuselage unroll. This bending of cross beams also allows the lower fuselage to scrape the floor considerably more as the struts rotate. This phenomenon also occurs when the beams rebounded. This explains the strain energy and friction energy dissipation showed in Figure 6.11, as the strain energy stored in the cross beams converted to fiction energy.

The LHP exhibits the lowest peak stress among the structures that didn't suffer plastic deformation.

Though around the same weight as the LCP, without a mechanism to force scrapping of the fuselage with the ground, it jumps off the ground while causing significant vibration among the higher fuselage frames. On top of that, the stressed area is much larger than other designs, meaning that instead of accumulating around the strut and, therefore, forming the plastic hinge required for the crash sequence, the stress is instead spread throughout the lower frames and shear clips, which is later released as kinetic energy.

The LSP has much higher stresses because it carries extra weight due to the ability to swap tanks. The center of the lower fuselage has more unrolling, and the struts have buckled due to the extra energy that needs to be dissipated, leading to more plastic deformation. This phenomenon is also present in the verification model, which is around the same weight.

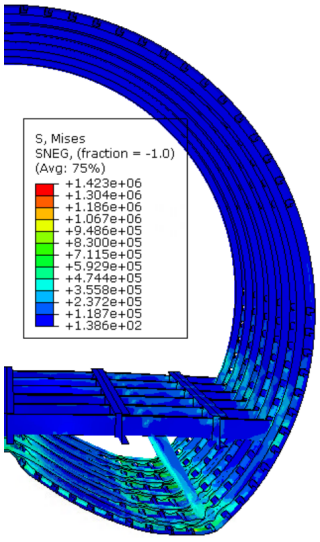

Figure 6.37: LCP von Mises stress.

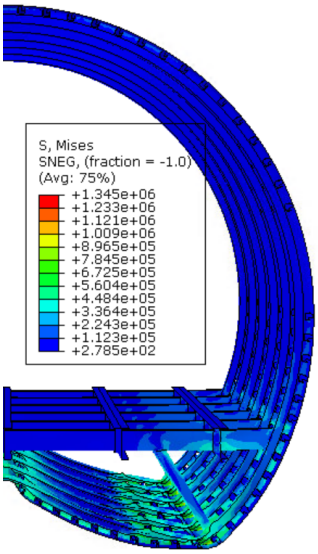

Figure 6.38: LHP von Mises stress.

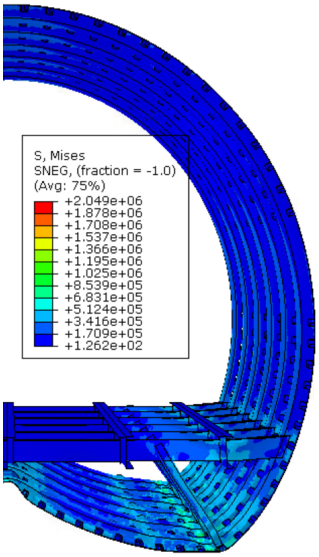

Figure 6.39: LSP von Mises stress.

Looking solely at plastic deformation, it can be seen that LCP and LHP showcased the same degree of plastic damage in the lower fuselage. Though both showcased plastic deformation at the roots of the struts, it was mostly on the surrounding frames and shear clips and not on the struts themselves; this means that the plastic hinge didn't form as planned in the designed crash sequence.

Compared to LSP, the lower end of LHP's struts has suffered significant plastic damage, and the flanges of the struts have suffered crippling. This means that the plastic hinge did form correctly, and the impact was then transferred to the transverse beam. This could be proven through the crippling damage on the transverse beam that is shown in Figure 6.42 and the stress concentration shown in the same location in Figure 6.39.

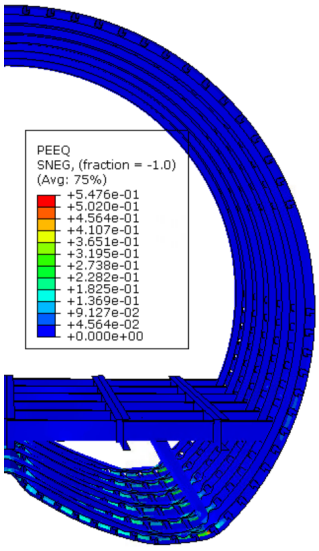

Figure 6.40: LCP PEEQ.

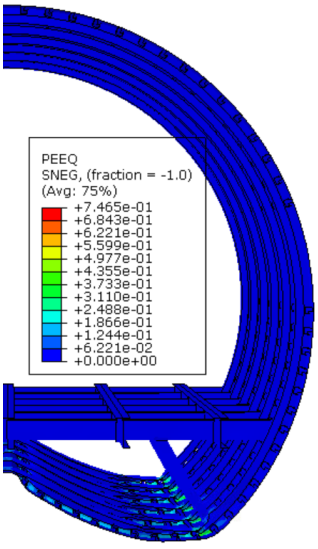

Figure 6.41: LHP PEEQ.

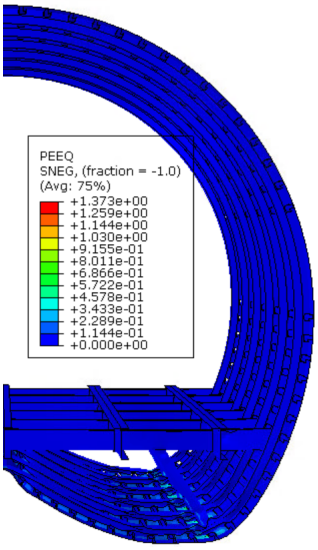

Figure 6.42: LSP PEEQ.

6.5.2. Energy time history and visual comparison

Below is a time history of kinetic, friction energy dissipation, and plastic energy dissipation. Mass normalization is necessary for comparison since the designs differ in mass and thus differ in total energy.

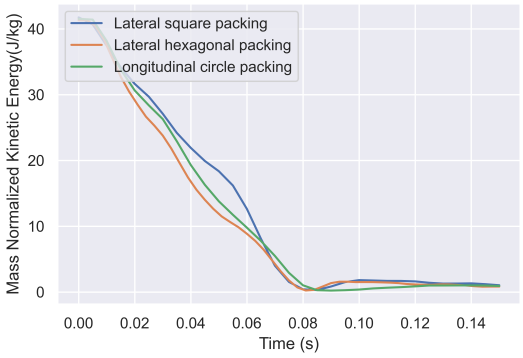

Figure 6.43: Mass normalized kinetic energy history.

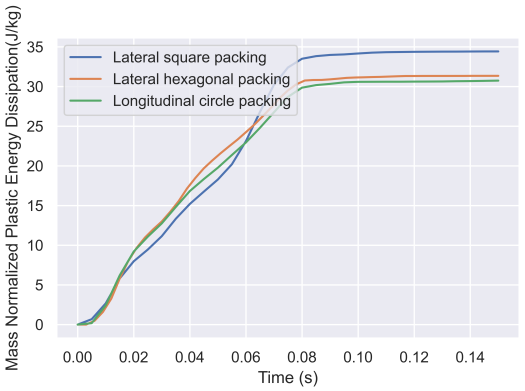

Figure 6.44: Mass normalized plastic energy dissipation history.

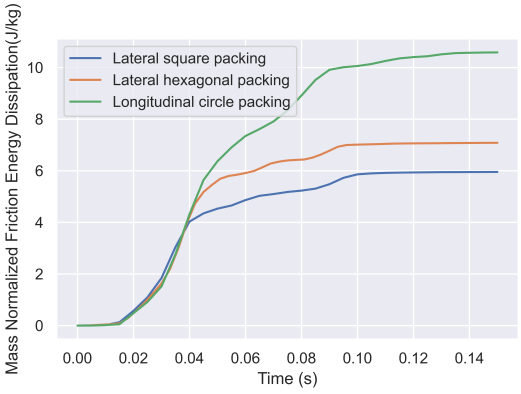

Figure 6.45: Mass normalized friction energy dissipation history.

The LCP showcased the smoothest and longest kinetic energy dissipation, with the lowest kinetic energy

occurring around 90 ms after impact rather than 80 ms, which is present in the other two designs. This means that the velocity of LCP reaches its inflection point at the latest, and this mechanism starts to be triggered around the 40ms mark. This could be explained by the friction energy dissipation, where LCP is significantly higher in magnitude. The friction energy differs for the three designs after the 40ms mark, while the shape and the trend are all similar.

The kinetic also didn't show a rapid bounce back, which peaks at 140 ms. This means that the fuselage took 50 ms to rebound fully, and the acceleration post-crash is quite low. Looking at the friction energy of LCP, this is because the friction energy still increases after 40 ms, which is not present in both LHP and LSP. In terms of plastic energy dissipation, LCP and LHP have very similar plastic energy dissipation capabilities. LSP, while exhibiting the lowest

The LHP initially showed the quickest kinetic energy dissipation, but as Figure 6.21 shown, the highest initial dissipating energy is the strain energy. This observation supports the hypothesis stated in the previous section that the stress is distributed throughout the lower fuselage during the initial impact. However, after 50 ms of the impact, the dissipation of the kinetic energy slows down, and the kinetic energy of LHP rebounds back in 10 ms. In comparison, LSP bounces back after 20 ms. This difference is probably due to the increased plastic deformation in the lower fuselage, making it weaker at pushing against the ground.

Although LSP initially has the lowest kinetic energy dissipation, its dissipation rate increases rapidly after the 50 ms time mark, when the plastic hinge starts to migrate towards the struts. This increase in dissipation rate is reflected in the higher rate of plastic energy dissipation at the 50 ms mark. When mass-normalized plastic dissipation is considered, LSP shows the highest dissipation level, which is also reflected in the acceleration of the fuselage.

6.5.3. DRI and acceleration comparison

DRI index

The acceleration differences between the three designs could be shown using their DRI index. The average, standard deviation and maximum of the DRI data are shown below. While the average DRI of LCP and LSP are similar, the DRI of LHP is comparatively higher. As discussed before, this is likely due to the lack of plastic hinges and deformation at the struts.

	LCP	LHP	LSP
DRI average	39.713	93.063	36.745
DRI std. dev	17.747	88.1	18.771
DRI max	70.43	278.17	91

Peak acceleration

Though all designs experienced a degree of bouncing off the ground post-impact, and this is also true for the verification case, the degree of positive acceleration that each design shows is different. As kinetic energies in Figure 6.43 show, LHP shows both a rapid decrease and increase of kinetic energy after impact. With kinetic energy being directly related to speed, this showcased that the entire model showcased the most amount of rapid vertical positive acceleration. This results in a ten-time peak acceleration compared to other designs.

The LHP showcases a significant gap between the peak acceleration of the lower tanks and the upper tanks, but this phenomenon is not present in LCP and LSP. The peak acceleration of the upper tanks is much closer to that of the other two designs.

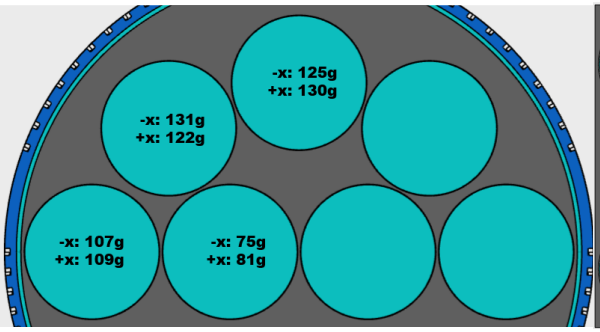

Figure 6.46: LCP peak acceleration.

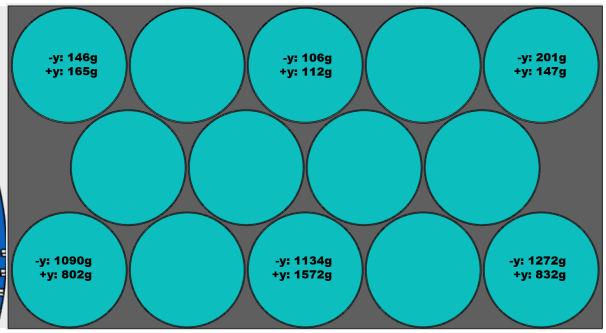

Figure 6.47: LHP peak acceleration.

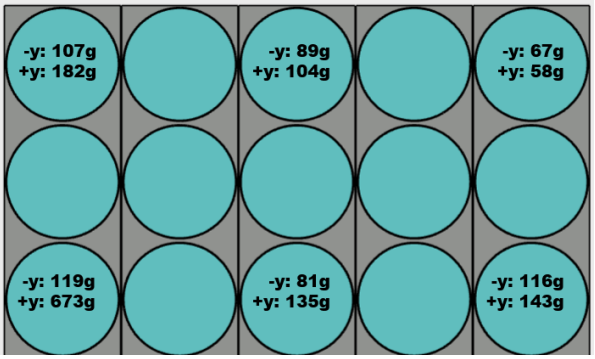

Figure 6.48: LSP peak acceleration.

It is also observed that LHP has its peak acceleration for all 12 measured locations between 69 96ms, while for LSP, it ranges from 12 138 ms and LCP 30 75ms. The larger the peak acceleration range, the more equally distributed are the loadings throughout the time of the drop test, which lowers the average acceleration.

6.5.4. Comparison result

The three designs showcased the fuselage's capability of absorbing kinetic energy via three different types of energy dissipation.

LCP had the least stored strain energy in the system and plastic deformation. Instead, due to its design, which supports the tanks through the upper frame through tank supports and unconstrained the cross beams, a significant amount of energy was dissipated via friction energy. LHP, on the other hand, did not dissipate enough energy to undergo significant plastic damage to the lower fuselage due to its lower total mass compared to the design load capacity. Since there were no other damage dissipation mechanisms in place, the energy was stored throughout the system as elastic strain energy. This energy was quickly dissipated through kinetic energy, resulting in a high degree of positive acceleration post-crash on the tanks. However, this could not fully explain the high peak acceleration. It could also be shown that, for LHP, the higher tanks are shown to have significantly reduced peak accelerations, much closer to that of the other two designs. This phenomenon is not as significant in the other two designs. There also isn't any obvious impact or penetration on the tank heads; thus, it is concluded that this is due to the tank supports.

LSP, being similar in weight to the desired load capacity for the retrofitted fuselage, dissipated the energy through plastic deformation and the correct crash sequence. This resulted in the lowest average acceleration of the three designs.

Despite the energy being too low to form plastic deformation, LCP doesn't showcase the strain energy release problem of LHP. This is because the friction actually slowed down or prevented the lower fuselage from rolling itself out to release the strain energy. As shown in Figure 6.11, as the strain energy releases, it is mainly converted to friction energy. This differs from the other two designs, which convert

the strain energy primarily through kinetic energy. This difference in strain energy dissipation, in turn, decreases the acceleration incurred on the fuel tanks.

6.6. Sensitivity study

For designs that are underloaded, such as LHP, the peak acceleration will be heightened due to the lack of plastic deformation and the formation of plastic hinges. In these kinds of situations, two methods are possible. One is to add mass to the fuselage, such as with EWIS or other related systems, or by decreasing the stiffness of the structure to encourage plastic deformation.

6.6.1. Total mass

Mass is the main parameter that generates the energy required to be dissipated for the fuselage during a drop test. In this thesis, the primary loading structure itself is assumed to stay the same, while the mass of the retrofitting components is varied by design. It is concluded from the comparison that due to a lack of total input energy, the peak acceleration becomes much higher.

Mass changes are made by adjusting the density of the tanks to add in the required mass while not changing the mechanical behaviour, such as the stiffness. This is done to mimic the increased weight that the fuel and other systems could provide to the tanks while hopefully not changing the mechanical characteristics to net an acceptable result. The acceleration is measured at the same location where the peak acceleration occurred for the drop test analysis of LHP, which is the tank head at the +Y side of the bottom middle tank. The results are shown below in Table 6.10.

Table 6.10: Acceleration comparison over increased weight for LHP.

Mass (kg)	LHP Original	Previous load	Heavier
Total mass	1104	1447	1595.2
Fuselage	248	248	248
Tank and fuel	686.8	1029.8	1178
support	169.2	169.2	169.2
Acceleration	1571.529g	778.8g	1002.859g
Occurred time	72ms	72ms	90ms

The peak acceleration is taken at the same location, at the tank in the middle of the fuselage, on the lower tanks, and on the +Y side. It can be observed that the peak acceleration was the lowest at around the design load. The peak acceleration occurred for the two lighter designs at 72ms. This is the timing of the formation of the plastic hinge under the strut, while for the heaviest analysis, the peak acceleration occurs at 90ms, which is the time mark when the fuselage fully rebounds on the floor when the struts make full contact with the floor. The shift in the acceleration time mark could be attributed to the lack of plastic deformation capabilities. The fuselage is not able to dissipate the energy purely through the crash sequence.

For LCP, the sensitivity study confirms that the friction energy dissipation mechanism would still be triggered despite the increased input energy. After increasing the total weight to 1387 kg, the final total energy is 58 kJ. The friction energy dissipation now increases to 15.9 kJ, which is higher in terms of the percentage of total energy dissipated. This is despite the formation of plastic hinges at the lower strut and the activation of struts and transverse floor beams as energy-dissipating components. Even at a higher weight, the friction dissipation still takes approximately the same in terms of the fraction of total energy. It is, therefore, concluded that the failure mechanism of LCP would work even though the input energy is higher.

Table 6.11: Acceleration and friction energy dissipation over increased weight for LCP.

	LCP original	Previous load	Heavier load
Total weight (kg)	1192.6	1458	1586.32
KE (J)	4.98E+04	5.80E+04	6.63E+04
Fuselage weight (kg)	248	248	248
Tank + fuel weight (kg)	786.6	1052	1180.32
Support weight (kg)	158	158	158
Acceleration (g)	130.6	91.3	85.4
Friction energy (J)	1.26E+04	1.59E+04	1.81E+04
Friction/Kinetic	25%	27%	27%

6.6.2. Retrofit of the struts

The primary load-bearing structure is assumed to be non-retrofittable due to the extensive certification requirements involved in such a retrofit. However, if we relax this assumption and allow for alterations to the primary load-bearing structure, the struts would be the components to be retrofitted. This is because the struts are often installed at the final steps of the assembly sequence, therefore being easily disassembled.

By reducing the thickness of the struts, it is possible to decrease the acceleration of designs that are typically underloaded. As the stiffness of the struts decreases, it becomes easier for them to form plastic hinges and plastically deform to absorb energy.

A study was conducted on the strut thickness, comparing the original thickness of 1.8 mm to a minimum thickness of 0.5 mm, which is still manufacturable. The results of this study are presented in the table below.

Table 6.12: Acceleration and plastic deformation over decreased strut thickness.

Thickness (mm)	1.8	1.7	1.6	1.5	1.4	1.3	1.2
Acceleration (g)	1571.53	511.13	1237.86	462.26	837.03	521.73	603.66
Time (s)	0.072	0.087	0.078	0.090	0.078	0.093	0.144
Struts PD (J)	2.28E+02	3.08E+02	3.35E+02	4.40E+02	5.47E+02	6.40E+02	1.45E+03
Total PD (J)	3.46E+04	3.46E+04	3.46E+04	3.46E+04	3.46E+04	3.45E+04	3.3E+04
Percentage	0.66%	0.89%	0.97%	1.27%	1.58%	1.85%	4.40%
PEEQ	0.7465	0.7703	0.7506	0.764	0.7323	0.6939	0.5185
Thickness (mm)	1.1	1	0.9	0.8	0.7	0.6	0.5
Acceleration (g)	573.66	477.96	557.74	436.45	372.64	566.38	459.96
Time (s)	0.126	0.144	0.084	0.090	0.090	0.144	0.087
Struts PD (J)	1.33E+03	1.25E+03	1.25E+03	1.14E+03	8.98E+02	9.64E+02	9.23E+02
Total PD (J)	3.29E+04	3.27E+04	3.27E+04	3.25E+04	3.23E+04	3.21E+04	3.26E+04
Percentage	4.05%	3.82%	3.82%	3.51%	2.78%	3.00%	2.83%
PEEQ	0.5075	0.5672	0.4964	0.5036	0.5131	0.4717	0.4502

In general, as the thickness of the struts decreases, the plastic dissipation (PD) increases, and it increases suddenly after the thickness is reduced down to 1.3 mm. This sudden increase is due to the struts transitioning from pure plastic deformation to buckling failure mode, leading to a mixed mode failure. This results in a high acceleration around the 140 ms mark, which is when the fuselage leaves the ground and the beams are fully extended.

In the case of buckling failure mode for the struts, as the strut thickness decreases, the plastic dissipation actually decreases. This is because buckling is a local failure that can be purely elastic, and as the strut thickness decreases, the second moment of inertia also decreases, leading to decreased plastic energy dissipation.

The peak acceleration generally decreases as the strut thickness decreases. However, the acceleration

stops decreasing after the strut thickness reaches 1.3 mm, coinciding with the point when the struts start to experience buckling failure.

It's also worth noting that no obvious plastic hinges form under the struts despite the decrease in thickness. Although there is a notable increase in plastic dissipation from the struts, the plastic dissipation for the struts is still significantly lower compared to LSP [5]. The decreased thickness actually contributes to the decrease in plastic equivalent strain (PEEQ) under the struts, meaning less plastic deformation occurs. This is because decreasing the strut thickness decreases the local stiffness at the lower end of the struts, causing less stress to accumulate.

Based on the analysis, it seems that a thickness of 1.3 mm is the best choice for ensuring crashworthiness for a payload weight of 865 kg of LHP. At this thickness, the total plastic energy dissipation did not decrease due to mass loss, the crash sequence remained undisturbed, and the acceleration decreased significantly.

[5] Struts PD of LSP, is around 5255 J

7
Discussion

7.1. Range estimation

Range is a crucial factor when it comes to retrofitting aircraft. Despite having a higher gravimetric density, the total fuel weight on board is reduced due to its low volumetric density. The range of each design varies depending on the volumes contained within the tanks. Breguet's equation is used to estimate the range [13]. The $\sqrt{\frac{2}{\rho S}}\frac{C_L^{\frac{1}{2}}}{C_D}$ parameter in the equation is assumed to be constant and calculated using the parameters of the F28 using the same equation for the maximum payload range of 1705 km [89]. The specific fuel consumption (SFC) for the engine of the F28, Rolls-Royce Spey Mk 555-15, is 0.75 lb/lbf hr (0.0765 kg/N h) [90]. W_0 for the maximum payload range is MTOW, while the W_1 is the OEM plus the maximum payload weight. Thus, the $\sqrt{\frac{2}{\rho S}}\frac{C_L^{\frac{1}{2}}}{C_D}$ parameter is calculated to be 4.56.

$$R = \frac{2}{\text{SFC}}\sqrt{\frac{2}{\rho S}}\frac{C_L^{\frac{1}{2}}}{C_D}\left(W_0^{\frac{1}{2}} - W_1^{\frac{1}{2}}\right) \tag{7.1}$$

The specific fuel consumption (SFC) for a liquid hydrogen engine at cruise is estimated to be 0.202 lb/lbf hr (0.0206 kg/N h) [62]. However, since the weight of the payload configuration is unknown, the range is estimated using the maximum range. In this estimation, W_0 represents the operational empty weight (OEM) plus the fuel weight, support weight, and tank weight, while W_1 represents the OEM plus the support weight and tank weight. The graph below depicts the range and shows a non-linear but nearly linear relationship between the range and retrofitted length. This almost linear behaviour is due to the low weight of the fuel resulting from the density of hydrogen fuel. The original fuel load of the retrofitted aircraft using Jet A fuel is approximately 10480 kg while using liquefied hydrogen ranges from a few hundred kilograms to thousands of kilograms. Using the nearly linear range estimate, the range per meter of retrofitted fuselage is calculated, and the results are displayed in Table 7.1.

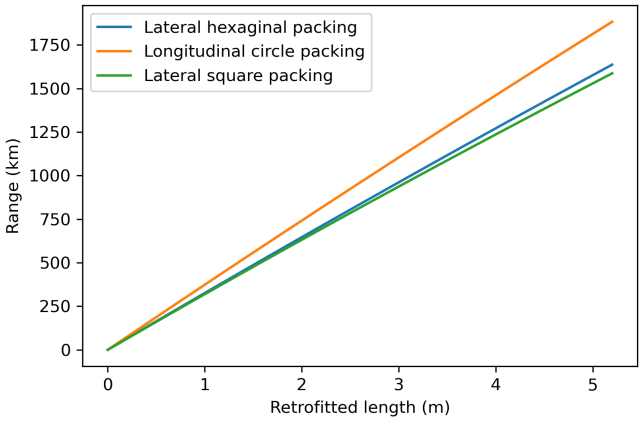

Figure 7.1: Range of the retrofitted aircraft.

Table 7.1: Range estimation per meter of fuselage retrofitted for hydrogen tanks

	LCP	LHP	LSP
Fuel weight per meter of fuselage retrofitted (kg)	216.1	188.7	185.5
Range per meter of fuselage retrofitted (km)	362.02	314.72	305.12

The difference in tank support weight will not be considered as it is already accounted for in the original equipment manufacturer (OEM) specifications for the aircraft's range estimate. Even if the tank support weight is considered, the added mass should have a negligible effect on the range estimate.

7.2. Continue airworthiness

The inspection of an aircraft is crucial for ensuring its continuous airworthiness. Inspecting fuel tanks is necessary for the design to be certified, and it's important to compare the design based on fuel tank inspectability. This is especially important when considering the use of composite materials for liquid hydrogen fuel tanks, which require more frequent inspections. As per the recommendation of API 620 [37], the inspector should have access to the tanks. The tanks should allow access to the interior through manholes on two of the sides, each with a diameter of 20 inches (508 mm).

Catwalks must be designed to allow the inspector to approach the tanks. However, this thesis assumes no detailed design will be conducted, and catwalks will not be modelled. Therefore, the general accessibility of the tanks is determined based on the remaining volume not filled with the tanks. This volume is used for fuel systems, and EWIS is required for liquid hydrogen fuel systems and catwalks or manholes to allow access to the tanks for inspection and repairs.

The configuration of the tanks and connectors also influences this metric, as the tanks' design and support structures will impact their accessibility. Assessing the accessibility of tanks involves checking if they are obstructed by other tanks or tank supports. The tank support designs are designed so that the tank heads always remain accessible so that the tanks can be connected to the fuel systems, thus ensuring that no tanks are completely cut off from access. However, if the tank body is blocked in by other components, it is considered inaccessible and thus requires removal from the fuselage to be inspected.

Table 7.2: The inspectability comparison of the three designs.

	LCP	LHP	LSP
Volume (%)	56.79	49.57	48.73
Volume (L)	8028	7008	6889
Remaining volume (L)	6109	7129	7248
Accessible tanks	7 out of 7	12 out of 14	0 out of 15
Accessibility for inspection/ repair	Do not require removal of the tanks	Requires removal of the tanks from aircraft	Require removal since the tank and support will constantly be removed for swapping

This is only an estimation of the inspectability as the designs of the supports presented in this thesis are conservative and mainly serve to provide support for the tanks and to allow load transfer from the tanks to the fuselage.

7.3. Retrofitting cost estimation

The estimation of retrofitting costs is often ambiguous, and there is currently no unified model for this estimation. Vecchia et al. proposed a method based on the cost estimation of developing new aircraft, and the methodology is detailed in Appendix A. The cost is divided into three categories: development costs, equipment costs, conversion costs, and capital costs. It is assumed that nonrecurring costs, such as development and capital costs, are similar for the three designs because the technology level for the three designs will be the same. It is also assumed that the capital investment into the infrastructure and production line will also be the same. Therefore, the estimated cost of retrofitting is mainly based on recurring costs, which involve equipment and conversion costs. To estimate the cost of equipment, an estimation of fleet size would need to be performed. The fleet size is set at 20.

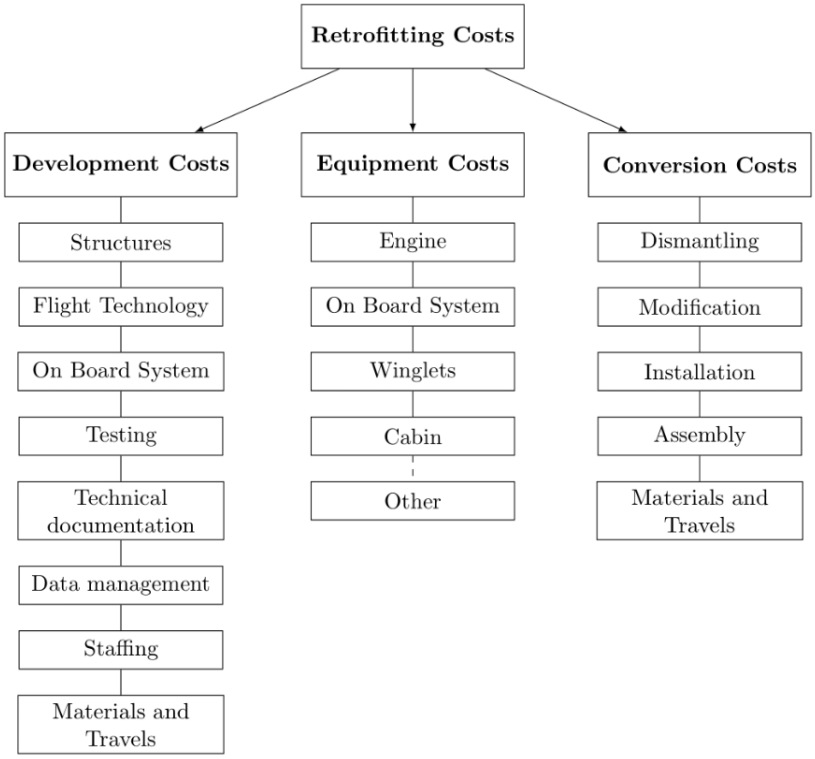

Figure 7.2: General representation of the retrofitting cost breakdown [16].

7.3.1. Equipment cost

Regarding equipment costs, the retrofitting components are the tank supports and the tanks themselves, along with the liquefied hydrogen system, which is not included in this thesis. Due to the secret nature of equipment costs, it is difficult to give an accurate estimation. However, traditional cost approximation methods can estimate the cost of equipment based on weight. This method is only applicable if the technology level for the cost comparison is the same for all of the comparison cases. As shown in Equation A.5, the number of tanks would decrease the cost of the tanks due to the discount effect. Vecchia et al. estimated the discount to be 5% per 50 pieces of equipment.

Using the weight per tank, with the fleet size of 20 retrofitted aircraft and the retrofitted length of six frames, the total weight of the tanks is calculated below. The obtained discounted tank weight could be used as a baseline for liquefied hydrogen tank equipment cost estimation.

Table 7.3: Equipment cost: hydrogen fuel tank estimation.

	LCP	LHP	LSP
Total tank weight (kg)	224.74	196.23	192.89
Tank weight per (kg)	32.11	14.02	12.86
Number of tanks	7	14	15
N for 20	140	280	300
Discount	10%	25%	30%
Discounted tanks weight (kg)	4045.371	2943.429	2700.4

The same process is carried out for the tank supports. The number of tank supports is calculated based on each individual, self-contained box-shaped support or plate. In the case of LCP, the six supports secured on the frames are counted separately. For LHP and LSP, both designs feature box-shaped supports, so each box is counted individually. The total weight of discounted tank supports is then calculated using the number of individual tank supports for each design.

Table 7.4: Equipment cost: tank support estimation.

	LCP	LHP	LSP
Total support weight (kg)	158	169.2	548.4
Number of support (kg)	6	2	5
Weight per support (kg)	26.33	84.6	109.68
N for 20	120	40	100
Discount	10%	0%	10%
Discounted support weight (kg)	2844	3384	9871.2

We can use the two estimates and the cost per kilogram of each component to estimate the equipment cost for all three designs. However, this estimation does not include the cost of the hydrogen fuel systems outside of the fuel tanks, which should scale with the number of tanks. Unfortunately, due to the constraints of this thesis, this part of the cost estimation has been omitted. Additionally, for LSP, the fuselage would require extra retrofitting equipment to allow tank swapping.

7.3.2. Conversion cost

The conversion cost is associated with the process of dismantling the components inside the fuselage, modifying the typical fuselage with the retrofitting components, and assembling the said components. Assuming the learning curve effect is consistent throughout, the conversion cost can be assessed based on the retrofit of one aircraft.

The conversion cost takes into consideration the working hours of the workers for each operation needed for the retrofit. Retrofitting the fuselage with hydrogen tanks involves several operations. Firstly, the seats and floors need to be disassembled, followed by the assembly and installation of the fuel systems. After that, the tank supports and tanks can be assembled and installed inside the fuselage. For LSP, the tanks and supports can be assembled outside of the fuselage.

Each operation is considered separately, and the total conversion cost is the combined cost of all the operations. The disassembly of the fuselage should cost the same amount of work for the three designs as long as the retrofitted aircraft and length are the same. For the retrofitting of the fuel systems, the more tanks there are, the more operations are required. Thus, the installation of fuel systems is related to the number of tanks in each design. The installation of the fuel tanks to supports is calculated based on the number of flanges that the tank supports have since each flange represents a connection between the supports and the tanks and thus would need to be operated on.

Table 7.5: Conversion cost estimation.

Operation	LCP	LHP	LSP
Number of tanks	7	14	15
Number of supports	6	2	5
Installation of fuel systems	7	14	15
Installation of supports	6	2	0
Installation of tanks to support	42	56	30

The total conversion cost needs to be calculated by multiplying the number of man-hours required for each operation by the cost of the man-hours. This calculation provides only a rough estimate of the actual conversion cost based solely on the number of tanks and supports in the design. It does not take into account the actual difficulty involved in installing tank supports, such as the LCP, which is suspended and installed on thin frames. The complexity of these operations could be quantified in working hours, but determining an accurate estimate is challenging without the required expertise in this field.

7.4. Crashworthiness

In comparing the crashworthiness of the three designs, the results are listed in the table below. While all designs passed the crashworthiness criteria for the fuel systems, indicating that there should be no damage shown on the tanks due to scraping, the crashworthiness of the three designs still varies tremendously.

Table 7.6: Crashworthiness comparison.

	LCP	LHP	LSP
Inertia loading PEEQ	0	0	0
Dynamic loading PEEQ	0	0	0
Peak DRI	70.43	278.17	91
Median acceleration (g)	123.55	501.69	111.81
Peak acceleration (g)	131	1571.53	671
Peak strain energy (%)	16	17.2	17.4
Conversion time (ms)	N/A	15	21
Friction energy (%)	24.53	20	14.08
Energy dissipation (%)	95.8	95.2	95.4

In both the quasi-static and dynamic crash tests, no plastic deformation was observed on the tank's outer wall. As a result, the tank should be certified.

Among the three designs, LSP exhibited the lowest median acceleration at its measured locations. However, at one specific location, there was a large peak acceleration due to an imbalance during the drop test. Other than that, the acceleration was quite similar across the measured locations.

Looking at the DRI, which could be related to passenger survivability, LCP and LSP again show similar results, while LSP is slightly lower.

LHP ranks among the worst for all aspects of crashworthiness, primarily on the lower tanks within the

designs.

Despite differences in acceleration, the total energy dissipated was found to be relatively similar. What varied was the percentage of friction energy dissipation and the time taken for strain energy conversion. It was observed that LCP releases strain energy slowly over the entire analysis time post-crash, with most of the strain energy dissipated through friction.

7.5. Other consideration

A notable design feature of LCP is its adaptability to payload weight. As shown in Table 6.11, the peak acceleration at the design's load and the baseline aircraft's load showed similar peak acceleration, while the heavier test case exhibited decreased peak acceleration. By suspending the tanks in the fuselage, this design also provides a larger crash zone and distances itself from the point of impact, resulting in improved crashworthiness.

However, this design makes day-to-day tank support more challenging due to its being secured on thinner frames and not supported by the main vertical load-bearing component, thus making it more likely to suffer fatigue damage. The suspension of the tanks also makes conversion operations more difficult, though this cannot be judged in the conversion cost estimation.

LSP shows the most promise in terms of post-retrofit operation due to the tank-swapping capability built into the design. The tank supports do not require installation and are designed to be easily swappable. This reduces the turnaround time and also allows easy inspection or repair of the tanks and fuel system. If the current problem in refuelling persists, the swapping of the tanks may be the only method to achieve a reasonable turnaround time for the aircraft operators.

7.6. Trade off

After evaluating the tradeoffs in range, inspectability, cost, and crashworthiness, it is concluded that LCP is the best choice for retrofitting. This design offers the longest range and allows for easy inspection within the fuselage. In terms of cost, it has the highest tank equipment costs but the lowest tank support equipment costs, which are directly related to the total volume of the tanks calculated from the volume fraction. The lower tank support cost is due to the tanks being supported by the frames, eliminating the need for stiffer support to compensate for the rotational moment.

LCP demonstrated the best performance in terms of crashworthiness. It showcased the low DRI, lowest peak acceleration on the tanks, lowest peak strain energy during the drop test, and highest friction energy dissipation. This design allows the cross beams to deform and rotate freely, facilitating easier conversion of strain energy to friction energy.

Part III

Conclusions and Recommendation

8

Conclusions

The European Commission aims to achieve net-zero greenhouse gas emissions within Europe by 2050. However, this goal poses a significant challenge for the aviation sector, as decarbonizing the energy source is extremely difficult. Hydrogen fuel is seen as a key solution to enable this transition. Although the development of fully hydrogen-powered aircraft is not expected to be completed until 2035 and 2040, retrofitting existing aircraft with hydrogen tanks is a viable interim solution to bridge the gap.

This thesis proposes the retrofitting of hydrogen tanks within a typical fuselage using packing solutions. Three packing solutions, each with two orientations of tank placement, have been selected to fill the internal volume of the fuselage with hydrogen tanks to about 50% to 56% of the total volume. Tank supports have been designed to prevent scraping against the fuselage, sustain the load under normal operation, and protect the tanks from direct impact on the ground. These designs have been created and modelled using 3DEXPERIENCE software and then analyzed with Abaqus FEA software.

All three packaging designs have successfully passed the crashworthiness certification requirements despite experiencing higher Dynamic Response Index (DRI) and peak acceleration than conditions considered survivable for humans. This was expected since the survivable conditions for humans are determined under different acceleration measuring environments, often using ATDs secured on padded seats, which significantly dampens the acceleration.

No plastic damage was observed on the outer tank wall of the tanks in any of the three designs in any of the five loading conditions. Therefore, it can be concluded that the section carrying a typical fuselage could be certified for all three designs.

The crashworthiness of the three designs has been compared, with each design showcasing different energy dissipation methods. LCP allows the transverse cross beams to bend freely, which allows for significant energy dissipation through friction. LHP absorbs part of the energy through strain energy but releases this energy through kinetic energy over a short period of time, resulting in heightened acceleration on the tanks. On top of that, due to the proximity and the packing density of the tanks, the tanks are clustered and constrained, which leads to even higher acceleration. LSP showed the most plastic deformation in the lower fuselage, leading to the highest plastic energy dissipation. This is due to its similarity to the originally designed weight of the fuselage, which should be optimised for this specific energy dissipation capacity.

The LHP's high acceleration could be reduced by adding more weight through the fuel systems and the electrical wiring interconnecting system. This would increase the flexibility of the lower fuselage, thereby lowering the peak acceleration. However, this can only be done if the replacement of the struts underneath the cabin cross beams is permitted.

A trade-off study has been conducted to compare the designs based on range estimation, continued airworthiness, preliminary retrofitting cost estimation, and crashworthiness. The study concludes that

the LCP design showed the best potential for retrofitting for the baseline aircraft due to its upside in crashworthiness and range, an important aspect during the operation of the post-retrofit aircraft.

9

Recommendation for future work

The primary focus of this thesis was to provide a preliminary design methodology for the simpler retrofit of the fuselage to accommodate hydrogen tanks without altering the primary loading structure, all while ensuring crashworthiness. Due to time constraints, it was not feasible to thoroughly explore and implement every idea. Therefore, these ideas and framework limitations can be considered as recommendations for future work. By addressing these points, the design methodology developed in this thesis can evolve into a more practical and comprehensive approach:

- Optimisation of the designs can enhance respectability, retrofit feasibility, and manufacturability.
- This study omits hydrodynamic forces during the analysis, though due to the extremely low density of the liquefied hydrogen, the total added force acting upon the structures wouldn't be too significant. However, it might still affect the designs, and possibly significantly in some cases.
- Detail designs for each component are essential for the overall design. This encompasses detailed designs of the tanks, tank supports, and the connecting mechanism between the tanks and their supports, which are not within the scope of this study. One possible mechanism could involve hooks and holes, as observed in some hydrogen-powered trucks. Further exploration and detailed designs will be required for the connection design and tank components.
- Computational packing could be implemented among all orientations and all packing methods to increase packing density if the resulting designs are deemed manufacturable
- The cost analysis conducted in this study is still very preliminary and mainly uses traditional cost estimation based on weight, as the technology level is similar among the three designs. An actual cost analysis should be carried out with more precise numbers, particularly for conversion costs. Currently, only the number of operations required for the retrofit operations is used as a rough estimate, without considering the difference in man-hours for each operation among the designs.
- The devised designs, though, do not transport humans; there are no indications on how the heightened acceleration would have on connecting, possibly human carrying, fuselage.
- In an effort to simplify the designs, the retrofit process examined in this thesis aims to avoid retrofitting the primary loading structure of the aircraft. It is important to note that this approach significantly limits the available retrofitting options for the aircraft, as it alters which components can be retrofitted. While the design method using packing methods remains applicable, the tank support design would need to be reconsidered.
- LCP itself did not limit the design height; this is because the hypotenuse of the door on the baseline aircraft could almost fit in the entire height of the DV, and the tank support itself is in a plate design. This will incur a problem if the fuselage diameter is higher or the cross beam is higher. However, this will only incur problems during the conversion since the tank requires more assembly steps.
- Water landing is not considered in this thesis. Water landing should be considered during a full certification analysis.
- Stability of the retrofitted aircraft should be carefully considered.

Overall, the technology related to hydrogen aircraft still requires maturation, and developing a retrofit methodology for hydrogen tanks is only the first step in making hydrogen aviation a more feasible transition.

References

[1] Saullo G. P. Castro. *The CrashProof Knowledge Centre (CrashProofLab). Zenodo. Published on 2022-Nov-01. Update 2024-Jun-06.* Version 2024-Jun-06. June 2024. DOI: 10.5281/zenodo.11500722.

[2] Robert Thomson and Uwe Weichenhain. *Hydrogen: A future fuel for aviation?* en. Tech. rep. Roland Berger, 2020.

[3] *Towards a Sustainable Air Transport System*. en. White Paper. TU Delft, NLR, Feb. 2021.

[4] Rodolfo Taccani et al. "High energy density storage of gaseous marine fuels: An innovative concept and its application to a hydrogen powered ferry". en. In: *International Shipbuilding Progress* 67.1 (July 2020). Ed. by Klaas Visser, Francesco Baldi, and Lindert Van Biert, pp. 33–56. ISSN: 15662829, 0020868X. DOI: 10.3233/ISP-190274.

[5] K. Seeckt and D. Scholz. "Jet Versus Prop, Hydrogen Versus Kerosene for a Regional Freighter Aircraft". en. In: (2009).

[6] AIRBUS. *ZEROe-Towards the world's first hydrogen-powered commercial aircraft*. URL: https://www.airbus.com/en/innovation/low-carbon-aviation/hydrogen/zeroe (visited on 06/22/2023).

[7] Embraer. *Future Aircraft Concepts*. URL: https://embraercommercialaviationsustainability.com/concepts/ (visited on 06/22/2023).

[8] Universal Hydrogen. *Product*. URL: https://hydrogen.aero/product/ (visited on 06/22/2023).

[9] Heinz G. Klug and Reinhard Faass. "CRYOPLANE: hydrogen fuelled aircraft — status and challenges". en. In: *Air & Space Europe* 3.3-4 (May 2001), pp. 252–254. ISSN: 12900958. DOI: 10.1016/S1290-0958(01)90110-8.

[10] G. Onorato, P. Proesmans, and M. F. M. Hoogreef. "Assessment of hydrogen transport aircraft: Effects of fuel tank integration". en. In: *CEAS Aeronautical Journal* 13.4 (Oct. 2022), pp. 813–845. ISSN: 1869-5582, 1869-5590. DOI: 10.1007/s13272-022-00601-6.

[11] G. D. Brewer et al. *Study of fuel systems for LH2-fueled subsonic transport aircraft, volume 1*. Tech. rep. NASA Langley Research Center, July 1978.

[12] D. Verstraete et al. "Hydrogen fuel tanks for subsonic transport aircraft". en. In: *International Journal of Hydrogen Energy* 35.20 (Oct. 2010), pp. 11085–11098. ISSN: 03603199. DOI: 10.1016/j.ijhydene.2010.06.060.

[13] Arturo Gomez and Howard Smith. "Liquid hydrogen fuel tanks for commercial aviation: Structural sizing and stress analysis". en. In: *Aerospace Science and Technology* 95 (Dec. 2019), p. 105438. ISSN: 12709638. DOI: 10.1016/j.ast.2019.105438.

[14] Sebastian Nicolay et al. "Conceptual design and optimization of a general aviation aircraft with fuel cells and hydrogen". en. In: *International Journal of Hydrogen Energy* 46.64 (Sept. 2021), pp. 32676–32694. ISSN: 03603199. DOI: 10.1016/j.ijhydene.2021.07.127.

[15] Massimo Mandorino et al. "Regional jet retrofitting through multidisciplinary aircraft design". en. In: *IOP Conference Series: Materials Science and Engineering* 1226.1 (Feb. 2022), p. 012047. ISSN: 1757-8981, 1757-899X. DOI: 10.1088/1757-899X/1226/1/012047.

[16] Pierluigi Della Vecchia et al. "Retrofitting Cost Modeling in Aircraft Design". en. In: *Aerospace* 9.7 (June 2022), p. 349. ISSN: 2226-4310. DOI: 10.3390/aerospace9070349.

[17] Elisabeth Martin. *Statistical Summary of Commercial Jet Airplane Accidents*. Tech. rep. Boeing, Aug. 2022.

[18] Matthias Waimer. "Development of a Kinematics Model for the Assessment of Global Crash Scenarios of a Composite Transport Aircraft Fuselage". PhD thesis. Deutsches Zentrum für Luft- und Raumfahrt, Sept. 2013.

[19] Dries Verstraete. "Long range transport aircraft using hydrogen fuel". en. In: *International Journal of Hydrogen Energy* 38.34 (Nov. 2013), pp. 14824–14831. ISSN: 03603199. DOI: 10.1016/j.ijhydene.2013.09.021.

[20] *HYDROGEN AIRCRAFT POWERTRAIN AND STORAGE SYSTEMS (HAPSS)*. Feb. 2024. URL: https://luchtvaartintransitie.nl/en/project-item/hydrogen-aircraft-powertrain-and-storage-systems/ (visited on 03/07/2024).

[21] *ABOUT AVIATION IN TRANSITION*. 2023. URL: https://luchtvaartintransitie.nl/en/about-aviation-in-transition/ (visited on 03/07/2024).

[22] Salvador M. Aceves et al. "High-density automotive hydrogen storage with cryogenic capable pressure vessels". en. In: *International Journal of Hydrogen Energy* 35.3 (Feb. 2010), pp. 1219–1226. ISSN: 03603199. DOI: 10.1016/j.ijhydene.2009.11.069.

[23] S. Bruce et al. *Opportunities for hydrogen in commercial aviation*. en. 2020.

[24] Oscar Serpell et al. *Ammonia's Role in a Net-zero Hydrogen Economy*. en. Tech. rep. Kleinman Center for Energy Policy, Mar. 2023.

[25] Subodh K. Mital et al. *Review of Current State of the Art and Key Design Issues With Potential Solutions for Liquid Hydrogen Cryogenic Storage Tank Structures for Aircraft Applications*. en. Tech. rep. National Aeronautics and Space Administration, Oct. 2006.

[26] S. Sherif. "Liquid hydrogen: Potential, problems, and a proposed research program". en. In: *International Journal of Hydrogen Energy* 22.7 (July 1997), pp. 683–688. ISSN: 03603199. DOI: 10.1016/S0360-3199(96)00201-7.

[27] Maria Chiara Massaro et al. "Potential and technical challenges of on-board hydrogen storage technologies coupled with fuel cell systems for aircraft electrification". en. In: *Journal of Power Sources* 555 (Jan. 2023), p. 232397. ISSN: 03787753. DOI: 10.1016/j.jpowsour.2022.232397.

[28] Olga Anatol'evna Boeva et al. "Low-temperature ortho–para hydrogen conversion catalyzed by gold nanoparticles: Particle size does not affect the rate". en. In: *International Journal of Hydrogen Energy* 42.36 (Sept. 2017), pp. 22897–22902. ISSN: 03603199. DOI: 10.1016/j.ijhydene.2017.07.187.

[29] Joachim Wolf. *Liquid-Hydrogen Technology for Vehicles*. en. Sept. 2002.

[30] Stephen Rondinelli et al. "Benefits and challenges of liquid hydrogen fuels in commercial aviation". en. In: *International Journal of Sustainable Aviation* 3.3 (2017), p. 200. ISSN: 2050-0467, 2050-0475. DOI: 10.1504/IJSA.2017.086845.

[31] Véronique Dias et al. "Energy and Economic Costs of Chemical Storage". en. In: *Frontiers in Mechanical Engineering* 6 (May 2020), p. 21. ISSN: 2297-3079. DOI: 10.3389/fmech.2020.00021.

[32] NASA spinoff technologies. *Making Visible the Invisible*. 1999. (Visited on 06/13/2023).

[33] *14 CFR Part 25 Airworthiness Standards: Transport Category Airplanes, Subpart C Structure*. Mar. 2023.

[34] Ali Bahrami. *Special Conditions: Boeing Model 787-8 Airplane; Crashworthiness*. Sept. 2007.

[35] Jeffrey E. Duven. *Airbus A350–900 Airplane; Crashworthiness, Emergency Landing Conditions*. July 2014.

[36] Zhan Liu et al. "Fluid sloshing dynamic performance in a liquid hydrogen tank". en. In: *International Journal of Hydrogen Energy* 44.26 (May 2019), pp. 13885–13894. ISSN: 03603199. DOI: 10.1016/j.ijhydene.2019.04.014.

[37] *Design and Construction of Large, Welded, Low-Pressure Storage Tanks*. en. Feb. 2002.

[38] *Standard for the Storage, Use, and Handling of Compressed Gases and Cryogenic Fluids in Portable and Stationary Containers, Cy* Feb. 2005.

[39] Gerardo Olivares, Luis Gomez, and Armando De Abreu. *List of Occupant Injury Criteria*. en. Tech. rep. Office of Aerospace Medicine, Federal Aviation Administration, Feb. 2018.

[40] Marius Lützenburger. "Studies about the Utilisation of the Aircraft Cargo Compartment as Additional Passenger Cabin by Use of Numerical Crash Simulation". en. In: (2007).

[41] A. Martin Eiband. *Human Tolerance to Rapidly Applied Accelerations: a Summary of the Literature*. Tech. rep. NASA Lewis Research Center Cleveland, OH United State, June 1959.

[42] Joseph A Pellettiere, David Moorcroft, and Gerardo Olivares. "Anthropomorphic Test Dummy Lumbar Load Variation". en. In: Washington DC, Aug. 2018.

[43] Robert T Lynch, Daniel M McDonough, and Timothy Keon. "An update to the Dynamic Response Index (DRI) model for use in assessing seat performance in military ground vehicles". en. In: (Oct. 2012).

[44] Ernest L. Stech and Peter R. Payne. *Dynamic Models of The Human Body*. en. Dec. 1969.

[45] James W. Brinkley and John T. Shaffer. *Dynamic Simulation Techniques for the Design of Escape Systems: Current Applications and Future Air Force Requirement*. en. Dec. 1971.

[46] *Certification Specifications and Acceptable Means of Compliance for Large Aeroplanes (CS-25)*. Nov. 2021.

[47] Rolf Eppinger et al. *Development of Improved Injury Criteria for the Assessment of Advanced Automotive Restraint Systems - II*. en. Nov. 1999.

[48] Michael Kaszycki. *Special Conditions: TIMCO Aerosystems, Boeing Model 777300ER Series Airplanes; Dynamic Test Requirements for Single-Occupant, Oblique (Side-Facing) Seats with Airbag Devices*. Washington, DC, Nov. 2015.

[49] F. Caputo et al. "Experimental and Numerical Crashworthiness Study of a Full-Scale Composite Fuselage Section". en. In: *AIAA Journal* 59.2 (Feb. 2021), pp. 700–718. ISSN: 0001-1452, 1533-385X. DOI: 10.2514/1.J059216.

[50] Y. Ren and J. Xiang. "Energy absorption structures design of civil aircraft to improve crashworthiness". en. In: *The Aeronautical Journal* 118.1202 (Apr. 2014), pp. 383–398. ISSN: 0001-9240, 2059-6464. DOI: 10.1017/S0001924000009180.

[51] M. Waimer et al. "Crash concepts for CFRP transport aircraft – comparison of the traditional bend frame concept versus the developments in a tension absorbers concept". en. In: *International Journal of Crashworthiness* 23.2 (Mar. 2018), pp. 193–218. ISSN: 1358-8265, 1754-2111. DOI: 10.1080/13588265.2017.1341279.

[52] Navid Mehreganian and Arash Soleiman Fallah. "Blast loading effects on aircraft fuselage". en. In: *Multiphysics Simulations in Automotive and Aerospace Applications*. Elsevier, 2021, pp. 239–285. ISBN: 978-0-12-817899-7. DOI: 10.1016/B978-0-12-817899-7.00004-6.

[53] *Getting Started with ABAQUS/Explicit: Keywords Version*. URL: https://classes.engineering.wustl.edu/2009/spring/mase5513/abaqus/docs/v6.5/books/gsx/default.htm?startat=ch03s07.html (visited on 05/04/2024).

[54] M. Waimer et al. "Contribution to an improved crash design for a composite transport aircraft fuselage—development of a kinematics model and an experimental component test setup". en. In: *CEAS Aeronautical Journal* 4.3 (Sept. 2013), pp. 265–275. ISSN: 1869-5582, 1869-5590. DOI: 10.1007/s13272-013-0070-3.

[55] Allan Abromowitz, Timothy G. Smith, and Tong Vu. *Vertical Drop test of a Narrow-Body Transport Fuselage Section with a Conformable Auxiliary Fuel Tank Onboard*. en. Tech. rep. DOT/FAA/AR-00/56. Federal Aviation Administration, Sept. 2000.

[56] P. Xue et al. "Crashworthiness study of a civil aircraft fuselage section". In: *Latin American Journal of Solids and Structures* 11.9 (2014), pp. 1615–1627. ISSN: 1679-7825. DOI: 10.1590/S1679-78252014000900007.

[57] Karen E. Jackson et al. "Finite Element Simulations of Two Vertical Drop Tests of F-28 Fuselage Sections". en. In: (Feb. 2018).

[58] Justin D. Littell. "A Summary of Results from Two Full-Scale Fokker F28 Fuselage Section Drop Tests". en. In: NASA/TM–2018-219829 (May 2018).

[59] Karen E. Jackson and Edwin L. Fasanella. *Crash Simulation of Vertical Drop Tests of Two Boeing 737 Fuselage Sections*. Tech. rep. DOT/FAA/AR-02/62. U.S. Army Research Laboratory Vehicle Technology Directorate, Aug. 2002.

[60] NI Solutions. *CFC Filters*. Apr. 2023. URL: https://www.ni.com/docs/en-US/bundle/diadem/page/crash/misc_cfc.html (visited on 06/28/2023).

[61] Pieter-Jan Proesmans et al. "Aircraft Design Optimization Considering Network Demand and Future Aviation Fuels". en. In: *AIAA AVIATION 2023 Forum*. San Diego, CA and Online: American Institute of Aeronautics and Astronautics, June 2023. ISBN: 978-1-62410-704-7. DOI: 10.2514/6.2023-4300.

[62] G. D. Brewer. *Hydrogen aircraft technology*. eng. Boca Raton: CRC, 1991. ISBN: 978-0-8493-5838-8.

[63] Jon Huete and Pericles Pilidis. "Parametric study on tank integration for hydrogen civil aviation propulsion". en. In: *International Journal of Hydrogen Energy* 46.74 (Oct. 2021), pp. 37049–37062. ISSN: 03603199. DOI: 10.1016/j.ijhydene.2021.08.194.

[64] William J. Brown et al. *SAFETY STANDARD FOR HYDROGEN AND HYDROGEN SYSTEMS Guidelines for Hydrogen System Design, Materials Selection, Operations, Storage, and Transportation*. July 2005.

[65] G. W. Davis and I. F. Sakata. *Design Considerations for Composite Fuselage Structure of Commercial Transport Aircraft*. en. Tech. rep. Langley Research Center, Mar. 1981.

[66] Ramin Moradi and Katrina M. Groth. "Hydrogen storage and delivery: Review of the state of the art technologies and risk and reliability analysis". en. In: *International Journal of Hydrogen Energy* 44.23 (May 2019), pp. 12254–12269. ISSN: 03603199. DOI: 10.1016/j.ijhydene.2019.03.041.

[67] Marco Desiderio. "Flying-V Crashworthiness: a Preliminary Assessment". en. MA thesis. Technische Universiteit Delft, Mar. 2023.

[68] Marco Desiderio. *Data set: Fokker F-28 Fellowship typical fuselage surface model for crashworthiness*. Mar. 2023. DOI: 10.5281/zenodo.7724227. URL: https://doi.org/10.5281/zenodo.7724227.

[69] Karen H. Lyle, Alan E. Stockwell, and Robin C. Hardy. "Application of Probability Methods to Assess Airframe Crash Modeling Uncertainty". en. In: *Journal of Aircraft* 44.5 (Sept. 2007), pp. 1568–1573. ISSN: 0021-8669, 1533-3868. DOI: 10.2514/1.27722.

[70] Derek I. Gransden and René Alderliesten. "Development of a finite element model for comparing metal and composite fuselage section drop testing". en. In: *International Journal of Crashworthiness* 22.4 (July 2017), pp. 401–414. ISSN: 1358-8265, 1754-2111. DOI: 10.1080/13588265.2016.1273987.

[71] Paul van Weezepoel. *Fokker F.28 Fellowship, Fokker's first jet plane*. URL: http://www.dutch-aviation.nl/index5/Civil/index5-2%20F28.html (visited on 03/11/2024).

[72] Eric W. Weisstein. *Circle Packing*. URL: https://mathworld.wolfram.com/CirclePacking.html.

[73] Jianrong Zhou et al. *Geometric Batch Optimization for the Packing Equal Circles in a Circle Problem on Large Scale*. en. Mar. 2023. URL: http://arxiv.org/abs/2303.02650 (visited on 04/02/2024).

[74] E. Specht. *The best known packings of equal circles in a circle (complete up to N = 2600)*. Mar. 2023. URL: http://hydra.nat.uni-magdeburg.de/packing/cci/ (visited on 04/03/2024).

[75] Ferenc Fodor. "The Densest Packing of 12 Congruent Circles in a Circle". In: *Beiträge zur Algebra und Geometrie* 41.No. 2 (2000), pp. 401–409.

[76] László Fejes Tóth. *Lagerungen in der Ebene auf der Kugel und im Raum*. eng. Springer Berlin Heidelberg, 1972.

[77] E. Specht. "High density packings of equal circles in rectangles with variable aspect ratio". en. In: *Computers & Operations Research* 40.1 (Jan. 2013), pp. 58–69. ISSN: 03050548. DOI: 10.1016/j.cor.2012.05.011.

[78] Gregory Kay. *Failure Modeling of Titanium 6Al-4V and Aluminum 2024-T3 With the Johnson-Cook Material Model*. Technical Report DOT/FAA/AR-03/57. Lawrence Livermore National Laboratory, Sept. 2003.

[79] Mohanraj Murugesan and Dong Jung. "Johnson Cook Material and Failure Model Parameters Estimation of AISI-1045 Medium Carbon Steel for Metal Forming Applications". en. In: *Materials* 12.4 (Feb. 2019), p. 609. ISSN: 1996-1944. DOI: 10.3390/ma12040609.

[80] Amin Bassiri Nia et al. "Dynamic response of aluminium sheet 2024-T3 subjected to close-range shock wave: experimental and numerical studies". en. In: *Journal of Materials Research and Technology* 10 (Jan. 2021), pp. 349–362. ISSN: 22387854. DOI: 10.1016/j.jmrt.2020.12.029.

[81] European Aviation Safety Agency. *Type-certificate Data Sheet for Fokker F28*. Tech. rep. EASA.A.037. EASA, Sept. 2018.

[82] *Transport Aircraft Crashworthiness and Ditching Working Group Report to FAA Report to FAA*. Sept. 2018.

[83] Edwin L. Fasanella and Karen E Jackson. *Best Practices for Crash Modeling and Simulation*. en. Tech. rep. NASA/TM-2002-211944. NASA Langley Research Center, Oct. 2002.

[84] Yi Yang Tay, Paulo Flores, and Hamid Lankarani. "Crashworthiness analysis of an aircraft fuselage section with an auxiliary fuel tank using a hybrid multibody/plastic hinge approach". en. In: *International Journal of Crashworthiness* 25.1 (Jan. 2020), pp. 95–105. ISSN: 1358-8265, 1754-2111. DOI: 10.1080/13588265.2018.1524547.

[85] M. Manzo et al. "A crashworthiness optimisation procedure for the design of full-composite fuselage section". en. In: *IOP Conference Series: Materials Science and Engineering* 1038.1 (Feb. 2021), p. 012058. ISSN: 1757-8981, 1757-899X. DOI: 10.1088/1757-899X/1038/1/012058.

[86] L. Di Palma et al. "Vertical Drop Test of Composite Fuselage Section of a Regional Aircraft". en. In: *AIAA Journal* 58.1 (Jan. 2020), pp. 474–487. ISSN: 0001-1452, 1533-385X. DOI: 10.2514/1.J058517.

[87] J. D. Littell. "Full-Scale Drop Test of a Fokker F28 Wingbox Fuselage Section". en. In: *Earth and Space 2018*. Cleveland, Ohio: American Society of Civil Engineers, Nov. 2018, pp. 702–714. ISBN: 978-0-7844-8189-9. DOI: 10.1061/9780784481899.067.

[88] Murray Mackay. "The increasing importance of the biomechanics of impact trauma". en. In: *Sadhana* 32.4 (Aug. 2007), pp. 397–408. ISSN: 0256-2499, 0973-7677. DOI: 10.1007/s12046-007-0031-9.

[89] Modern Airliners. *Fokker F28 Fellowship.* 2023. URL: https://www.modernairliners.com/fokker-f28-fellowship?expand_article=1&utm_content=cmp-true (visited on 04/23/2024).

[90] Philip P. Walsh and Paul Fletcher. *Gas Turbine Performance*. en. 1st ed. Wiley, Mar. 2004. ISBN: 978-0-632-06434-2 978-0-470-77453-3. DOI: 10.1002/9780470774533.

[91] Ilaria Sorrentino. "Cost Modelling in Collaborative Aircraft Design: A Retrofitting Cost Estimation Methodology". PhD thesis. Scuola Politecnica e delle Scienze Di Base, 2023.

A

Retrofitting Cost

Aircraft retrofitting involves upgrading existing aircraft systems and structures to improve their performance, efficiency, and safety. This can include installing new avionics systems, upgrading engines, making structural modifications, and integrating new technologies. In the context of this thesis, retrofitting involves replacing part of the passenger cabin with hydrogen tanks, along with the necessary piping, fuel systems, new engine(s), and any required structural modifications to accommodate the hydrogen tanks.

Retrofitting isn't limited to ageing or out-of-production aircraft. It also goes beyond maintenance repair and overhaul (MRO) activities, as it involves modifying aircraft with innovative components. Performance Improvement Packages (PIPs) programs, which are typically carried out by the engine and/or airframe OEMs, could also be developed as a viable option for developed aircraft [16].

Retrofitting is a complex and multifaceted process that involves numerous technical, economic, and regulatory challenges. Despite these challenges, retrofitting is often a more cost-effective solution than purchasing or developing new aircraft. This chapter aims to provide an overview of aircraft retrofitting. It will delve into how the challenges and cost of retrofitting could serve as a balancing factor to the designs later developed in this thesis so that the designs are not overly complicated and the systems not overly complicated.

A.1. Methodology

Cost is frequently the primary barrier for airlines and OEMs to consider when investing in a retrofitting package or PIPs. Accurately estimating the cost of a retrofitting package is crucial. However, there is currently no unified cost theory on which these models are based.

Typically, industries focus on estimating the individual costs of each retrofit operation or component rather than implementing a comprehensive and holistic cost-modelling approach that can take all cost components into account. However, this approach does not consider the causal relationship between costs and parameters, leading to a limited estimation approach. Consequently, cost estimation tends to rely more on experience rather than a systematic approach, while traditional methods for estimating design, development, certification, and operational costs often rely on statistical data and sometimes outright experience.

Vecchia et al. [16] developed a parametric method based on causal cost relationships and using bottom-up classical methods. This method estimation is made using the number of hours and the corresponding costs that the development and conversion activities will require during the aircraft retrofit, as well as the cost of each piece of equipment needed. This method is developed from a general aircraft unit cost, which is divided into recurring costs and nonrecurring costs. These two types are then separated into three main categories:

- Recurring costs. These costs occur throughout a programme's life and arise due to the repetitive

nature of production costs. Examples of recurring costs include the cost of raw materials, tool maintenance, and labour costs, as well as the acquisition of components not produced in-house. Additionally, it covers the labour costs for integrating these components into a completed aircraft. It must be pointed out that the recurring costs per product unit should reduce with the production quantity increasing [91].

  - Equipment costs. These costs include acquiring raw materials, major components, and subassemblies that are not developed and manufactured in-house, as well as the cost of integrating all of the equipment into the aircraft.
  - Conversion costs. This cost is related to the labour and tooling required to conduct all the activities required for the retrofit, such as the cost of logistics, packaging, transporting, storing, and moving.

- Non-recurring costs. These costs include expenses for research, development, testing, and certification. A non-recurring cost is typically a one-time capital expenditure that is incurred before the first unit of production and occurs only once during the life cycle of a project. Examples of non-recurring costs can include pre-production activities, tool development, engineering models built for testing purposes, and capital investments in production lines and equipment needed for retrofitting.

$$C_{Retrofit} = C_{DEV} + C_{CONV} + C_{EQUIP} \tag{A.1}$$

A.1.1. Development cost

The aircraft OEM will need to invest in activities related to design and preparation for conversion. This is a one-time capital cost at the beginning of the retrofitting activity. This category includes costs such as producing flight manuals, research and development, testing, and all types of engineering efforts. The methodology involves determining the total development cost by starting from the required activities, establishing the time needed to complete them in hours, and calculating the cost of each activity based on hourly costs.

To estimate development costs for an aircraft upgrade, consider all activities involved in the design process, including studies on structure, flight technology, and onboard systems. Costs of testing, certification, technical documentation, data management, material acquisition, travel, and engineering activities must be factored in. Multiply total hours by hourly cost to calculate the total development cost.

$$C_{DEV} = Ch_E \sum_{i=1}^{N} \left(Eh_i \cdot Ep_i\right) + \sum_{j=1}^{M} \left(Ch_{T_j} \cdot Th_j\right) + C_{ODEV} \tag{A.2}$$

Eh_i and Th_j represent the hours needed for each engineering and testing activity. Eh_i indicates the engineering hours for one employee; this number is then multiplied by Ep_i, the number of people needed for that activity. N is the number of engineering operations needed, and M represents the number of test and certification activities that are required to certify the retrofit. CODEV represents all other costs associated with complementary development activities or those expenses for which it makes no sense to specify an operational time.

$$C_{ODEV} = C_{DOC} + C_{DATA} + C_{STAF} + C_{TRDEV} \tag{A.3}$$

CDOC represents the cost of documentation, CDATA is the cost of data management, CSTAF includes the cost of all personnel not covered in the previous categories, and CTRDEV represents travel costs. CTRDEV specifically accounts for travel costs related to development activities, with an additional charge of 2.25 euros per hour per staff member, as recommended by Leonardo Company.

$$C_{\text{TRDEV}} = 2.25 \sum_{i=1}^{N} \left(Eh_i \cdot Ep_i\right) \tag{A.4}$$

A.1.2. Equipment cost

The retrofitter will need to cover the costs of purchasing equipment for the retrofit. Estimating the total cost of the equipment presents a challenge due to the confidential nature of purchase prices for individual aircraft components. Traditional estimation cost approximation methods can estimate the cost of equipment based on weight. This is especially useful if a cost comparison needs to be made between similar technologies. However, this method will not be able to account for advances or differences in technology levels. For instance, it is impractical to estimate the cost of composite tanks based on the cost of metal tanks cost estimation.

Additionally, the equipment manufacturer may discount the aircraft retrofit performer based on the quantity of items ordered. The discount amount can vary depending on factors such as time, equipment manufacturer, and other variables, making it challenging to estimate. The presented methodology allows for reduced equipment acquisition costs by simulating a manufacturer-supplier agreement.

$$C_{EQUIP} = [1 - DISC \cdot (Q/N_{DISC})] \cdot \sum_{l=1}^{E} C_{EQUIP_l} \quad \text{with } (Q/N_{DISC}) \in Z \tag{A.5}$$

with Q representing the amount of aircraft retrofitted and C_{EQUIP_l} representing the equipment cost to retrofit a single aircraft. E represents the number of equipment items to be purchased. In this case, (Q/NDISC) represents the division without a remainder. Vecchia et al. [16] estimate that, for every 50 aircraft to be retrofitted, a 5% discount on one type of equipment could be obtained, with a maximum discount of 50%.

A.1.3. Conversion cost

The cost of converting an aircraft depends on the practical activities involved and the time required to complete them. The major expenses in this category include labour, manufacturing, and logistics costs. Conversion costs, unlike development costs, are expenses that must be sustained for the activities that take place on every single aircraft. This method employs a learning curve to display these costs, considering the phenomenon of increasing productivity as the number of items produced accumulates.

To calculate the total conversion cost in terms of labour, we need to multiply the number of hours required by the number of workers involved and the hourly labour rate. It's important to note that $C_{\text{CONV 1}}$ represents the cost of converting a single aircraft. $N_p k$ and $O_h k$ denote the number of workers and the time required to perform a single conversion activity by one employee. The index k represents the kth operation that is accounted for, and P is the number of operations considered. The cost of each operation per hour is denoted by Ch_O.

$$C_{\text{CONV 1}} = \text{Ch}_\text{O} \sum_{k=1}^{P} \left(Np_k \cdot Oh_k\right) + C_{\text{OCONV}} \tag{A.6}$$

The variable C_{OCONV} includes all the additional costs associated with complementary conversion activities or expenses for which it doesn't make sense to specify an operational time. This includes material costs (C_{MAT}), travelling costs related to aircraft conversion activity, calculated in the same way as other travel costs (C_{TRCONV}), and costs related to reception, painting, and delivery (C_{RDP}).

$$C_{OCONV} = C_{MAT} + C_{TRCONV} + C_{RDP} \tag{A.7}$$

The cost of retrofitting an aircraft is affected by the labour-learning effect. As more aircraft are retrofitted, the time required for retrofitting decreases, resulting in a lower cost. This can be expressed using the following equation: the total cost of retrofitting the Xth aircraft, denoted as C_{CONV_X}, is equal to the cost of retrofitting the first aircraft, denoted as C_{CONV_1}, multiplied by a logarithmic variable based on the labour learning rate (LR).

$$C_{\text{CONV}_X} = C_{\text{CONV}_1} \cdot X^{\log(LR)/\log(2)} \tag{A.8}$$

C_{CONV} can be calculated with the following equation to find the mean conversion cost over all of the operations, where P is the number of operations.

$$C_{CONV} = \frac{\sum_{X=1}^{P} C_{\text{CONVX}}}{P} \tag{A.9}$$

A.2. Takeaways

Cost modelling of a complex project such as retrofit is near impossible without relying on component-based estimation and often lacks the holistic view of the entire project. Traditionally, component-based estimations are often based on the weight of the component, this is only useful when there are no dramatic technology differences. Vecchia et al. present a retrofit cost estimation methodology based on new aircraft development cost methods. These methods mainly separate the costs into recurring costs and non-recurring costs [91]. Non-recurring costs are mainly associated with costs related to the cost of development and recurring costs related to equipment costs and conversion costs.

Nonrecurring costs require an estimation of the total fleet size, as the development of the retrofitting method requires the same amount of cost for a large fleet. Using Vecchia et al.'s engine retrofitting case as an example, on average, with seven different retrofitting configurations, the development cost will be extensively lessened, with the cost, as a percentage, decreased from 89.5% to 31.2% of the total cost with only 20 aircraft considered as its fleet size.

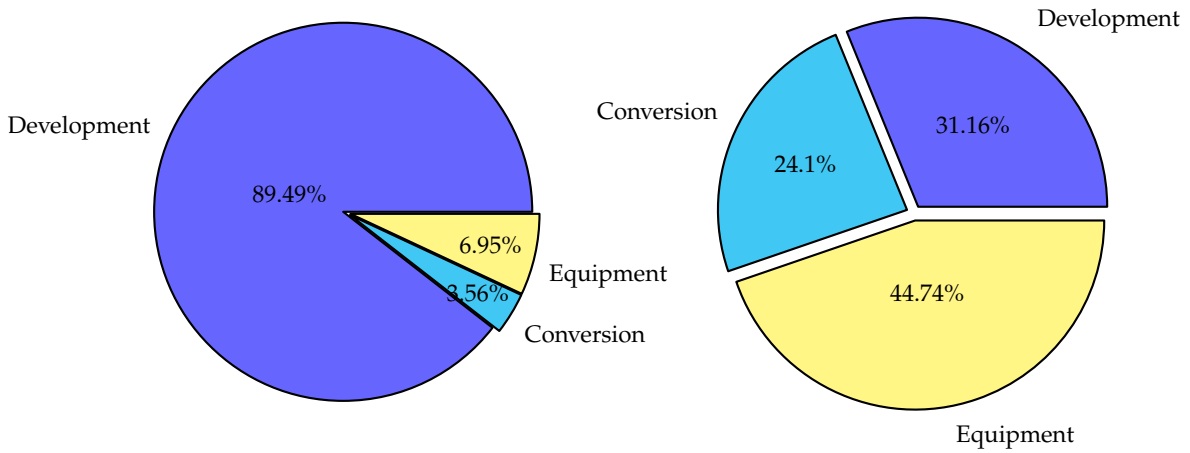

Figure A.1: Cost in terms of percentage for one aircraft retrofitted vs twenty aircraft for an engine upgrade, adapted with the data provided from [16].

Conversion cost considers the operation required for the retrofit to be completed. A more complex system requires more conversion costs due to the number of operations required to make the conversion. More operations also entail more hours required for the operations, which would increase the total labour cost. However, the conversion cost would slowly decrease over time due to the learning effect. Equipment costs will also decrease as the fleet size increases due to the discounts offered by component manufacturers.

B

Acceleration data

Accelerations in g (9.81 m/s).

B.1. Longitudinal circle packing

Time (ms)	Tank 1 +x	Tank 1 -x	Tank 2 +x	Tank 2 -x	Tank 3 +x	Tank 3 -x	Tank 4 +x	Tank 4 -x
0	-1.0	-1.0	-1.0	-1.0	-1.0	-1.0	-1.0	-1.0
3	-1.1	-1.0	-0.9	-0.9	-1.0	-0.9	-0.9	-0.9
6	12.9	11.9	2.7	13.8	-12.1	11.0	-11.5	29.2
9	-11.3	113.1	13.7	-25.3	38.7	15.4	44.7	9.5
12	52.3	-20.4	3.1	-24.1	-9.3	-49.0	-33.1	3.2
15	5.2	32.3	21.3	28.1	5.4	49.0	68.2	99.9
18	-15.7	-23.4	61.8	3.8	-33.9	15.9	-9.8	-16.0
21	56.2	-24.1	-12.0	24.9	19.6	-40.3	87.3	76.1
24	17.0	99.8	-45.2	-37.5	-38.6	32.6	-38.1	52.2
27	-86.0	-37.5	39.6	62.1	35.9	20.4	-0.8	20.6
30	-72.7	-46.7	-50.7	35.2	-22.4	13.1	2.2	125.6
33	-66.2	10.7	57.1	-28.3	12.0	30.6	-33.5	-21.6
36	-21.8	-99.4	21.5	13.5	-14.9	-21.0	25.5	-48.7
39	0.5	-47.8	-70.8	38.8	81.0	42.0	71.4	-19.1
42	-54.6	-79.0	7.4	30.1	-0.3	-8.4	-41.3	44.9
45	43.0	-81.1	34.3	3.9	-5.2	-13.6	42.8	11.5
48	4.8	-77.8	33.2	18.9	21.7	75.3	-51.7	52.1
51	82.0	69.9	29.6	5.0	0.6	-29.1	27.1	50.6
54	8.3	37.3	48.1	107.2	-39.8	2.0	51.0	-10.8
57	-34.2	-57.2	-90.5	41.9	1.5	-8.3	76.2	10.7
60	-109.2	92.9	-54.1	0.4	-18.5	54.8	57.6	86.2
63	-76.1	126.7	-21.6	-16.3	54.1	11.8	59.9	68.3

Continued on next page

(Continued)

66	55.2	25.5	-101.6	130.6	66.4	-13.8	0.8	43.9
69	91.1	64.7	-57.3	54.2	19.2	47.3	-4.9	-5.9
72	39.8	43.6	11.8	15.2	61.0	10.4	130.3	-54.6
75	28.3	-74.6	121.5	11.9	71.9	27.9	99.7	-11.1
78	-6.7	39.3	3.5	-25.3	-13.6	-28.7	24.2	-37.7
81	-3.3	82.8	-7.7	-51.2	3.1	7.8	12.6	20.6
84	-11.1	43.5	49.1	46.4	0.8	59.3	1.1	-53.6
87	84.2	45.5	-0.5	114.4	-21.8	49.5	9.9	9.5
90	83.0	109.1	13.8	29.2	-32.1	-52.7	17.0	21.1
93	69.7	-21.4	-21.8	42.3	-80.2	3.0	4.6	13.8
96	-31.9	-8.1	-1.6	19.9	21.4	23.7	19.9	-17.3
99	-3.3	48.0	2.6	66.3	2.8	70.3	2.6	3.0
102	31.5	65.2	-9.8	-42.9	-42.3	17.4	36.5	-50.4
105	17.7	87.8	40.8	-10.7	-11.3	11.5	-40.4	-13.0
108	78.7	16.8	-1.7	3.8	13.0	-29.5	-37.4	31.5
111	12.7	14.3	-51.6	-8.0	4.7	-23.9	31.7	35.1
114	-52.3	26.8	62.2	33.3	44.6	-8.8	-58.3	-17.1
117	17.7	-32.0	10.9	-2.6	29.0	-18.3	8.7	0.4
120	-32.9	23.4	57.9	12.8	8.3	-20.7	36.9	-7.0
123	14.5	11.1	-13.1	26.4	2.3	18.2	15.2	29.0
126	13.7	7.1	-18.5	-7.5	-15.1	-11.0	7.1	-18.5
129	-48.3	5.6	3.0	-6.1	-8.5	4.8	46.6	21.3
132	26.7	-21.4	21.2	3.6	4.2	5.7	-10.2	19.0
135	-12.7	-11.0	19.7	-4.2	-4.3	-1.0	9.8	-4.1
138	34.0	-41.8	-0.8	-0.1	10.6	25.1	14.0	-1.2
141	-5.6	-14.0	-17.8	15.7	16.1	-22.7	-11.0	26.5
144	19.9	7.6	-0.7	10.0	-24.4	20.7	-27.5	6.3
147	-14.1	-26.8	13.1	12.0	-15.2	8.2	-19.6	10.5
150	42.8	-8.1	11.2	-6.1	-17.8	-7.3	10.9	-6.0

B.2. Lateral hexagonal packing

Time (ms)	Tank X=1 Y=1 -y side	Tank X=1 Y=1 +y side	Tank X=3 Y=1 -y side	Tank X=3 Y=1 +y side	Tank X=5 Y=1 -y side	Tank X=5 Y=1 +y side	Tank X=1 Y=3 -yside	Tank X=1 Y=3 +y side	Tank X=3 Y=3 -y side	Tank X=3 Y=3 +y side	Tank X=5 Y=3 -y side	Tank X=5 Y=3 +y side
0	-1.0	-1.0	-1.0	-1.0	-1.0	-1.0	-1.0	-1.0	-1.0	-1.0	-1.0	-1.0
3	22.3	-25.2	-33.8	0.3	55.8	-32.8	-24.4	2.3	-8.4	3.6	-32.2	12.9

Continued on next page

(Continued)

6	43.0	18.6	22.3	-33.9	5.6	16.0	-16.9	-16.4	8.7	3.1	-40.7	-71.0
9	-61.4	3.4	-42.8	-30.9	-134.5	51.7	91.9	61.6	-10.2	-35.4	-26.7	7.5
12	53.6	107.3	9.0	-44.1	-23.8	224.5	114.5	-58.8	-16.3	22.1	1.5	-18.7
15	231.1	2.9	-76.1	55.6	-95.6	276.8	-11.3	-15.0	-8.9	19.6	44.8	-15.9
18	94.6	-84.7	57.6	66.7	-59.1	16.4	36.9	-39.7	12.3	76.8	-103.1	18.1
21	103.9	21.5	-46.8	58.0	-31.9	291.6	76.2	50.7	2.2	9.8	-92.5	-34.3
24	-39.8	-5.8	-82.0	-46.1	36.6	-54.0	-53.3	23.5	0.0	14.3	16.5	40.0
27	-95.3	-102.3	61.1	72.5	-122.6	100.0	9.9	-27.1	37.8	1.4	-38.5	8.5
30	-50.8	220.6	-1.5	165.9	5.8	33.8	22.9	18.1	8.5	5.1	-49.6	22.1
33	-412.8	3.6	-165.1	55.8	261.7	138.2	11.8	37.8	38.6	-18.5	15.1	26.1
36	227.4	-32.3	194.5	279.3	232.2	139.3	38.0	24.3	45.2	16.1	14.7	60.9
39	-43.0	-89.3	87.8	189.1	62.5	60.8	94.3	20.1	5.0	1.2	34.2	-2.1
42	-80.3	261.4	-98.7	76.0	-112.2	1.4	24.0	-0.3	33.2	-38.5	-13.0	35.2
45	-15.2	-91.5	34.2	44.4	-40.4	-84.0	4.4	-46.3	-43.3	-1.3	56.4	-7.8
48	-169.2	-128.8	-43.4	-38.7	51.2	-169.8	-4.7	77.1	2.3	-27.1	33.1	84.4
51	-229.0	195.7	-129.5	137.2	-42.1	-76.5	8.7	-67.7	29.8	48.4	9.0	-13.3
54	21.3	-195.7	-17.5	-139.3	-169.0	-532.8	2.7	-102.5	-78.9	-20.4	-85.1	3.2
57	-261.6	1.1	82.0	-188.9	-6.0	42.1	14.7	1.4	-43.3	-22.1	-97.9	-25.3
60	-397.5	-448.9	-55.7	-227.3	384.6	-332.3	77.9	141.7	-35.3	36.4	76.7	-75.5
63	107.4	546.9	44.2	631.8	-408.0	366.1	18.1	-18.4	-16.4	13.4	-15.6	-84.9
66	284.7	-254.7	-25.4	-451.1	-80.1	243.0	89.1	-18.7	28.8	-34.6	-16.2	133.1
69	432.4	-346.0	89.2	-495.9	1089.7	380.6	44.7	47.5	53.5	-112.4	82.4	-7.0
72	-1051.9	-263.2	-113.7	1571.5	-282.5	509.4	-21.6	34.8	54.8	-13.1	-32.3	67.8
75	173.6	-470.0	1134.4	616.5	-740.1	-128.3	41.0	-97.6	66.4	-17.6	-29.1	11.1
78	1272.0	241.8	808.0	-716.8	268.9	37.5	-29.4	35.4	102.8	-7.8	-59.8	27.8
81	-565.8	-263.9	908.7	691.4	415.5	736.2	-19.0	6.7	105.8	-0.3	13.0	-91.9
84	-41.9	832.0	21.2	-783.7	-502.6	-75.9	201.2	-35.1	47.7	101.2	143.2	152.2
87	621.5	532.5	-244.1	-272.8	362.4	802.2	-41.9	25.1	70.2	0.6	146.0	165.0
90	105.3	7.1	-526.2	-1047.6	-421.3	-605.8	32.5	-20.9	-69.6	77.1	-96.3	18.9
93	312.2	-202.5	-29.9	4.6	352.4	-32.5	-37.3	-107.5	19.5	14.5	-34.4	-68.5
96	-153.3	-346.5	330.2	985.6	-446.4	41.3	-92.9	-146.6	21.2	-33.9	-36.8	9.1
99	-82.8	223.4	107.6	-356.3	156.7	-102.3	76.8	138.5	-12.7	6.7	67.4	-1.3
102	-126.4	117.3	-48.9	42.0	183.7	-64.4	94.7	27.5	69.8	-11.3	-40.7	-51.1
105	192.8	199.4	-81.6	-47.5	12.5	-12.2	-45.4	7.0	18.3	-64.0	43.3	-18.3
108	9.9	-481.6	353.4	71.3	282.0	-91.6	-17.3	-58.2	42.0	26.4	2.8	-66.2
111	511.1	-214.8	256.3	-139.1	-632.2	-161.7	-45.9	-3.3	-28.2	7.0	-25.6	-26.8
114	-50.0	465.3	-249.4	95.0	769.1	136.4	-86.1	-2.1	-13.8	-17.9	27.5	-47.9
117	-9.1	-131.2	43.6	680.5	-196.3	610.2	-16.8	-23.7	-7.1	-9.2	-43.5	128.0
120	237.2	-176.9	-135.0	333.6	-381.6	-128.5	54.6	-66.9	-18.5	16.7	-50.0	100.1

Continued on next page

(Continued)

123	537.1	245.7	-122.6	119.6	-204.6	-21.1	-9.3	79.2	7.3	42.3	-1.0	-110.7
126	-245.1	-523.6	-424.7	-22.2	585.3	-408.7	-37.7	7.4	38.9	0.6	60.7	9.7
129	592.0	-88.1	136.4	-151.5	-252.0	234.6	-2.9	84.4	3.7	-18.4	-86.0	-41.5
132	-83.4	138.6	-108.8	200.6	1032.7	3.0	-25.8	84.8	-23.3	-1.1	-26.4	-16.7
135	50.4	270.2	-98.2	-43.4	-290.9	264.0	47.5	38.2	-83.1	-11.1	-51.0	-112.7
138	261.2	-66.0	-117.7	-84.4	76.0	-157.6	-68.8	17.0	-16.2	-5.4	-69.0	17.9
141	0.8	-247.5	62.3	-18.4	-197.6	-10.7	60.0	39.6	41.8	23.3	54.4	-48.4
144	215.9	-66.0	-44.1	-152.1	-226.8	93.6	-28.5	-44.6	-50.5	-13.7	23.2	-5.9
147	-154.7	16.1	125.7	17.5	97.1	235.5	-13.5	-3.1	-48.3	13.5	64.9	-39.5
150	32.4	207.6	75.8	4.0	20.0	17.9	-5.7	13.2	6.1	17.1	30.8	-22.2

B.3. Lateral square packing

Time (ms)	Tank X=1 Y=1 -y side	Tank X=1 Y=1 +y side	Tank X=3 Y=1 -y side	Tank X=3 Y=1 +y side	Tank X=5 Y=1 -y side	Tank X=5 Y=1 +y side	Tank X=1 Y=3 -yside	Tank X=1 Y=3 +y side	Tank X=3 Y=3 -y side	Tank X=3 Y=3 +y side	Tank X=5 Y=3 -y side	Tank X=5 Y=3 +y side
0	-1.0	-1.0	-1.0	-1.0	-1.0	-1.0	-1.0	-1.0	-1.0	-1.0	-1.0	-1.0
3	0.8	-13.3	8.8	-27.8	-27.0	-3.4	9.7	-22.5	-4.3	-2.3	2.6	5.4
6	-26.1	-32.7	16.0	66.6	13.4	9.3	7.1	17.1	21.0	26.2	1.5	1.7
9	31.6	16.0	-2.7	14.4	13.6	77.3	3.1	-48.6	30.8	39.0	33.1	-16.8
12	-21.0	92.4	25.8	134.9	-49.8	-45.0	38.6	30.9	-9.1	5.3	4.1	31.7
15	-12.5	66.1	28.1	19.0	16.2	-10.7	42.0	18.8	-1.0	-7.7	43.2	23.8
18	106.2	5.4	-44.5	21.1	52.9	-9.1	-54.1	34.7	-35.1	-0.3	-13.8	-33.7
21	-4.6	-58.3	9.9	-7.7	-50.4	36.1	11.3	-11.1	-7.1	-48.5	-34.3	-35.3
24	7.3	-23.5	9.3	50.1	10.3	-22.7	-4.1	10.5	5.1	-34.9	-93.1	32.1
27	116.3	49.0	31.9	-12.2	37.7	-31.1	5.4	34.7	16.0	-26.2	-29.0	-30.2
30	-30.4	142.9	11.1	-11.7	48.6	-60.6	3.9	53.1	-40.0	62.8	30.1	-10.9
33	89.3	53.5	20.1	53.3	13.2	63.1	-56.9	-38.4	57.3	-21.4	-7.3	36.0
36	22.8	34.2	20.1	28.1	80.3	44.6	-42.9	-0.2	15.4	-65.8	-34.6	16.8
39	31.5	-37.0	48.4	-65.1	5.5	33.0	-3.4	-15.2	-13.4	-51.6	3.0	-8.4
42	-18.8	-32.7	-55.8	32.7	21.9	1.5	-18.5	-3.3	10.4	-8.7	13.5	6.0
45	28.6	14.5	-20.3	14.6	-63.2	-100.6	19.3	-0.7	-4.5	25.2	-14.7	44.8
48	-42.7	-55.6	11.2	9.3	62.4	-138.9	-13.7	29.3	-14.7	-31.5	22.7	43.0
51	43.1	-6.9	-5.6	35.2	-118.8	-147.7	-40.3	21.9	19.9	-38.9	-24.1	40.3
54	13.0	3.3	-21.1	-6.3	115.1	19.4	23.6	20.8	7.8	-36.0	42.5	-39.3
57	-20.9	-3.2	-14.7	46.1	13.4	0.4	67.4	35.5	-14.7	-13.7	-38.3	18.0

Continued on next page

(Continued)

60	34.9	27.1	54.7	-2.0	-27.8	108.6	22.8	36.0	12.2	19.1	-52.4	29.7
63	89.0	-8.4	25.4	-26.4	49.3	74.9	-49.1	9.4	-0.4	32.6	-19.5	30.3
66	-25.0	-24.3	64.4	1.1	-12.2	51.9	17.1	34.1	-1.7	47.7	-37.0	25.5
69	-8.4	80.6	42.7	90.1	79.8	98.5	17.3	27.5	71.2	25.0	-17.2	85.4
72	48.0	-92.1	55.1	2.9	67.4	42.7	17.3	42.5	50.1	70.5	-2.3	158.1
75	-15.0	64.6	28.9	3.6	51.9	79.5	2.9	41.4	67.8	64.0	64.4	19.9
78	-13.1	1.4	0.2	51.0	0.3	30.2	-12.1	19.8	71.4	18.8	45.0	3.4
81	99.5	90.2	-22.4	3.2	49.0	24.0	62.5	-58.0	4.6	-22.8	5.0	-19.0
84	-20.1	-1.0	32.6	18.2	-45.0	-44.9	-19.0	-4.5	15.4	51.9	11.6	-2.8
87	50.2	93.0	-49.3	75.8	52.8	74.9	-21.6	-24.9	-25.8	31.7	76.1	-11.8
90	-87.8	68.7	81.0	96.3	43.6	-19.0	-25.2	41.0	-89.4	19.9	-32.2	38.8
93	-9.4	47.1	21.7	-5.9	64.6	6.3	55.0	-20.9	-6.6	5.0	-12.5	8.6
96	45.6	-11.2	34.8	-32.8	14.9	92.9	-7.4	5.3	-15.4	37.0	0.8	10.5
99	-46.3	4.9	-22.9	41.9	46.7	38.5	2.8	32.5	14.4	6.7	31.2	9.0
102	-111.3	3.9	-9.7	35.6	-24.9	-136.0	-53.8	-39.3	-27.3	14.8	-9.2	-21.1
105	-25.7	36.0	26.8	-42.1	20.4	673.5	13.8	-46.6	-26.8	-1.5	11.6	-39.9
108	3.1	-5.1	-46.7	1.8	-91.4	-224.1	-11.6	12.7	-12.6	-15.9	23.9	-18.5
111	-4.6	38.4	-21.5	-24.8	-58.8	108.0	-5.9	-13.2	11.2	19.6	-7.1	50.4
114	-17.7	-0.9	-8.7	-42.0	5.9	73.9	-5.3	-0.2	-1.9	8.0	-0.8	35.2
117	11.1	52.3	-4.3	21.5	57.6	-27.8	-19.6	-36.6	-28.4	-20.1	55.1	36.7
120	25.5	41.1	4.2	26.5	92.2	12.3	20.2	-36.8	-10.8	47.4	27.2	33.7
123	-26.0	-2.3	16.5	27.5	7.1	7.1	-7.7	39.0	7.5	7.3	-16.6	3.8
126	-31.7	18.8	-7.3	-56.9	5.5	70.3	-22.3	-26.8	-4.3	62.5	-2.4	-5.6
129	16.2	-13.1	22.5	41.4	36.1	0.7	-38.0	1.6	37.1	-12.6	37.5	64.7
132	-16.6	-16.8	-7.1	-34.2	7.6	-31.3	0.9	7.5	-5.7	35.2	14.8	-40.7
135	25.8	-23.9	-5.4	-7.7	-13.8	35.7	-13.2	0.3	10.1	-81.7	-44.1	181.9
138	38.4	-6.8	-54.8	12.1	19.9	0.6	-15.9	-10.9	10.9	103.6	56.4	-105.2
141	20.1	-36.4	19.3	14.3	7.7	9.4	-34.7	-11.7	-30.0	-20.2	107.3	-32.1
144	55.2	-40.5	-17.0	-23.8	3.0	2.0	-13.8	0.2	-31.6	66.4	37.4	26.3
147	-5.9	25.0	10.1	-16.8	-21.0	-12.7	10.3	38.8	-5.2	18.0	18.3	5.7
150	48.7	26.2	8.4	13.5	0.5	-2.6	-9.8	-10.7	12.4	-15.1	-1.5	-0.6